CHARACTERIZATION OF MAGNETITE THIN FILMS PRODUCED BY SOL-GEL PROCESSING

A THESIS SUBMITTED TO
THE GRADUATE SCHOOL OF NATURAL AND APPLIED SCIENCES
OF
MIDDLE EAST TECHNICAL UNIVERSITY

BY

ALİ ERDEM EKEN

IN PARTIAL FULFILLMENT OF THE REQUIREMENTS
FOR
THE DEGREE OF MASTER OF SCIENCE
IN
METALLURGICAL AND MATERIALS ENGINEERING

FEBRUARY 2008

Approval of the thesis:

CHARACTERIZATION OF MAGNETITE THIN FILMS PRODUCED BY SOL-GEL PROCESSING

Submitted by **ALİ ERDEM EKEN** in partial fulfillment of the requirements for the degree of **Master of Science in Metallurgical and Materials Engineering Department, Middle East Technical University** by,

Prof. Dr. Canan Özgen ___________
Dean, Graduate School of **Natural and Applied Sciences**

Prof. Dr. Tayfur Öztürk ___________
Head of Department, **Metallurgical and Materials Engineering**

Prof. Dr. Macit Özenbaş ___________
Supervisor, **Metallurgical and Materials Engineering Dept., METU**

Examining Committee Members:

Prof. Dr. Muharrem TİMUÇİN _______________
Metallurgical and Materials Engineering Dept., METU

Prof. Dr. Macit ÖZENBAŞ _______________
Metallurgical and Materials Engineering Dept., METU

Prof. Dr. Mehmet PARLAK _______________
Physics Department, METU

Prof. Dr. Ali KALKANLI _______________
Metallurgical and Materials Engineering Dept., METU

Asst. Prof. Dr. Caner DURUCAN _______________
Metallurgical and Materials Engineering Dept., METU

Date: 06.02.2008

I hereby declare that all information in this document has been obtained and presented accordance with the academic rules and ethical conduct. I also declare that, as required by these rules and conduct, I have fully cited and referenced all material and results that are not original to this work.

Name, Last name : Ali Erdem Eken

Signature :

ABSTRACT

CHARACTERIZATION OF MAGNETITE THIN FILMS PRODUCED BY SOL-GEL PROCESSING

Eken, Ali Erdem
M.Sc., Department of Metallurgical and Materials Engineering
Supervisor: Prof. Dr. Macit Özenbaş

February 2008, 113 pages

Magnetite (Fe_3O_4) thin films were prepared by a sol-gel process in which, a solution of iron (III) nitrate dissolved in ethylene glycol was applied on glass substrates by spin coating. Xerogel films were obtained by drying the coated films at 110 °C. The films were sintered between 300 °C and 450 °C in order to observe the phases existing in the films at different temperatures. Coating solution showed Newtonian behaviour and viscosity was found as 0.0215 Pa.s. DTA analysis showed that, sintering temperature should be selected between 291 °C and 350 °C in order to produce magnetite thin films. Prepared magnetite thin films were characterized by XRD, SEM, AFM, TEM, VSM and UV-Vis spectrometer. In-plane grazing angle diffraction studies showed that magnetite phase was present upon sintering the films at 300 °C. From the SEM studies, it was shown that films with defect free surfaces were obtained and by cross section studies, thickness of the films was found as ~10-200 nm. AFM images showed that no cracks or any other defects on the film surface were present. TEM results proved the existence of single phase magnetite in the produced films. UV-Vis spectrum results showed that transmittance of the films increases with decreasing sintering temperature and increasing spinning rate. Up to 96% transmittance was observed between the wavelengths of 900-1100 nm.

Magnetic properties of magnetite thin films were also examined by VSM (Vibrating Sample Magnetometer) and ferromagnetic behaviour was shown using VSM data.

Keywords: Iron oxide, magnetite, sol-gel, thin film.

ÖZ

SOL-JEL YÖNTEMİYLE HAZIRLANAN MANYETİT İNCE FİLMLERİN KARAKTERİZASYONU

Eken, Ali Erdem
Y. Lisans, Metalurji ve Malzeme Mühendisliği Bölümü
Tez Yöneticisi: Prof. Dr. Macit Özenbaş

Şubat 2008, 113 sayfa

Manyetit ince filmler, demir (III) nitratın etilen glikol içinde çözünmesiyle elde edilen solüsyonun cam altlıklara uygulanmasıyla elde edilmişlerdir. Kaplanan filmler 110°C de kurutulmuştur. Kurutulan numuneler, değişik sıcaklıklardaki ince filmlerin fazlarını gözlemlemek için 300°C ile 450°C arasında azot atmosferinde ısıl işleme tabi tutulmuşlardır. Çözeltinin akışkanlığı 0.0215 Pa.s olarak bulunmuştur. DTA analizi sonucu ısıl işlem sıcaklıklarının 291°C ile 350°C arasında olması gerektiği görülmüştür. Hazırlanan manyetit ince filmler XRD, SEM, AFM, TEM, VSM ve UV-Vis spektrofotometresi yöntemleri kullanılarak karakterize edilmiştir. X-ışınlarıyla inceleme sonunda 300°C' de manyetit ince filmlerin oluştuğu gösterilmiştir. SEM çalışmaları sonucu ince filmlerin yüzeylerinin oldukça düzgün olduğu gözlenmiş ve kesit çalışmalarından filmlerin kalınlığının yaklaşık 10-200 nm arası olduğu bulunmuştur. AFM çalışmaları film yüzeyinde herhangi bir çatlak ya da hata olmadığını göstermiştir. TEM sonuçları üretilen filmlerde yanlızca manyetit fazı olduğunu kanıtlamıştır. UV-Vis sonuçları filmlerin geçirgenliklerinin azalan ısıl işlem sıcaklıklarıyla ve artan döndürme hızlarıyla arttığını ve 900-1100 nm dalga boyları arasında %96 a kadar yükselen geçirgenlik değerlerine erişildiğini göstermiştir. Manyetit ince filmlerin manyetik özellikleri VSM ile ölçülmüştür ve VSM sonuçlarından manyetit ince filmlerin ferromanyetik davranış gösterdiği gözlenmiştir.

Anahtar Sözcükler: Demir oksit, ince film, manyetit, sol-jel

To my family,

ACKNOWLEDGEMENTS

I would like to express my gratitude to my supervisor Prof. Dr. Macit Özenbaş for his supervision, guidance, support and encouragement during the study. Without his knowledge and support I would not complete this study.

I am grateful to all the stuff of the Department of Metallurgical and Materials Engineering. I must thank my dear labmates Özge Acarbaş, Volkan Kayasü, Halil İbrahim Yavuz and Aylin Karakuşcu for their valuable supports and also for their invaluable friendships.

I would like to express my sincere thanks to Dr. Süleyman Tarı from İYTE for VSM analysis, Prof. Dr. Kerim Allahverdi and Dr. Özgür Duygulu from TÜBİTAK for TEM analysis and Alp Yürüm from METU Chemical Engineering Department for AFM analysis. I am also grateful to METU Central Laboratory for viscosity, DTA and FE-SEM analysis and METE Electromagnetic Materials Laboratory for their help in the measurement of optical properties.

I must also express my special thanks to Erdem Erişen, Görkem Demircioğlu, Alican Tabakçı, Arda İskenderoğlu and Hakan Karabulut for being always there for me. I am also thankful to my colleagues Evren Tan, Sıla Süer, Yankı Başaran, Güher Kotan, Doruk Doğu, Alper Kınacı and Fatih Şen for their helps and supports.

Finally I want to express my great thanks to my family who gave their endless love and support during my life. I am thankful to my mother, Habibe Eken and my father, Sabri Eken. I would like to specially thank to my brother, Alper Eken for his great help, support and guidance through my life.

TABLE OF CONTENTS

CHAPTER

LIST OF TABLES

LIST OF FIGURES

CHAPTER 1

INTRODUCTION

Presently iron oxides are extensively used in many technological applications. Especially nanocrystalline iron oxides are widely used in the fields of electronics and optics and they are the most used metal oxides in scientific and industrial fields [1]. They are also used in magnetic recording, photoelectrochemistry, energy storage, electrochromism, catalysis and sensors [2].

There are three stoichiometric forms of iron oxide at room temperature. These are magnetite (Fe_3O_4), maghemite (γ-Fe_2O_3) and hematite (α-Fe_2O_3). Iron cations exist in Fe^{3+} state in maghemite and hematite, whereas in magnetite both Fe^{3+} and Fe^{2+} ions exist together [3].

Maghemite (γ-Fe_2O_3) is known to have a cubic spinel structure and known to be ferrimagnetic [4]. Maghemite films are used in high-density magnetic recording devices and magneto-optic recording [5], whereas hematite (α-Fe_2O_3), which is antiferromagnetic, films are used as a red-pigment, an anticorrosive agent, in electrochromic devices, gas sensors [1] and in photocatalytic applications [6]. Magnetite (Fe_3O_4) is ferrimagnetic and has spinel structure just like maghemite. Thin films of magnetite are used for magnetic recording applications [5], tunnel magnetoresistance (TMR) devices [7], in magnetic sensor technology [8] and room temperature giant magnetoresistance (GMR) applications [9].

Magnetic elements have been used in electronic recording devices since the late 1940's. Its moderate cost and chemical stability make maghemite the principal magnetic pigment. Even though it displays high magnetization and coercivity, magnetite is less suitable for recording devices owing, to its magnetic instability

[10]. But magnetite thin films have recently received considerable attention on account of the potential industrial applications. These films can be oxidized to give maghemite for use as a magnetic recording medium and magnetic multilayers involving magnetite can also be used to fabricate thin film systems with desirable magnetic properties [11].

Iron oxide thin films have numerous advantages over their bulk forms. As Mathur et al. [12] suggested when the particle size decreases to nanometer size, iron oxides exhibits unique properties such as high coercivity, superparamagnetism, enhanced surface sensitivity etc. and these properties cannot be seen in their bulk forms.

In the discovery of magnetism; magnetite has played a crucial role and for many applications in technology, it is an attractive candidate [13]. Studying magnetite is important because it can lead to a better understanding of complex ferrites [14].

Magnetite has Curie Temperature (T_C) of 850 K. It has a rather high Curie Temperature when compared to other half-metallic materials. It is a mixed valence compound. Ferric ions fully occupy the tetrahedral (A) sublattices. Half of the octahedral (B) sublattices are occupied by Fe^{2+} ions and other half are occupied by Fe^{3+} ions. Below T_C, A-site magnetic moments are aligned antiparallel to the B-site magnetic moments [15].

In Fe_3O_4 at the Fermi Level, only spin down electrons exist. This indicates the half metallicity of Fe_3O_4. It acts as a metal for one spin orientation and as an insulator for the opposite orientation. From the calculations; it was found that the spin polarization of Fe_3O_4 is 100% [15].

Half metallic materials are extensively studied in recent years. Materials such as LSMO ($La_{1-x}Sr_xMnO_3$) (T_C = 360 K), CrO_2 (T_C = 395K), Mn based Heusler alloys, doped manganites and double perovskites are suitable candidates for spintronic device applications because of their 100% spin polarization. Among these materials

Fe_3O_4 has the highest T_C and high conductivity of magnetite let rapid electron hopping between Fe^{2+} and Fe^{3+} ions under the room temperature. So, much attention should be paid to fabrication, microstructure and magnetic properties of Fe_3O_4 [16]. Other half-metallic ferromagnets cannot be used in magnetoelectronic applications in a wide range of temperature due to their low Curie Temperature [17].

Applications such as magnetoresistive random access memory and magnetoresistance head devices are related to the tunnel magnetoresistance (TMR) and TMR is related to the spin polarization of conduction electrons in ferromagnetic electrodes of tunnel junction. Half metallic ferromagnets can induce TMR because of their 100% spin polarization and among half metallic ferromagnets, magnetite is expected to induce a large TMR [18].

Magnetite thin films have been produced by many different production methods such as molecular beam epitaxy [19, 20], rf-sputtering [7, 15, 21-23], reactive evaporation [24], hydrothermal processes [25], ferrite plating [26, 27], pulsed laser deposition [20], solid reactions [8], sol-gel method [9, 28-34], liquid phase epitaxy, metal-organic chemical vapor deposition and plasma spray [9]. Among other techniques sol-gel method became one of the successful techniques for preparing iron oxide thin films. Sol-gel process has many advantages over physical techniques. One of them is the ability to control the film microstructure. Highly uniform films can be prepared satisfactorily [35]. Large areas at any shape can be coated easily by sol-gel method. High temperatures or vacuum is not needed in this method [29].

In sol-gel film processing, firstly a gel-precursor solution, or sol, is synthesized, then it is applied to a substrate by using spin-on or dip-coating techniques. A gel layer is formed after this step and then it is heated to obtain ceramic film. Generally this process is carried out in two stages. In drying step, by employing a hot plate, heat treatment is done at a temperature like 100 °C. It is followed by an sintering step, which is the final heat treatment, at temperatures between 300 °C and 500 °C [36].

Transition metal oxides are considered to be promising nonlinear optical materials. Magnetite is a promising candidate for this type of materials [33]. Nonlinear optics (NLO) is an attractive research field because of its role in ultrafast optical processing of information. Nonlinear optical phenomena include the ability to alter the frequency of light and to amplify one source of light with another, or to switch it and to alter its transmission characteristics through medium, depending on its intensity. Taking into account the nonlinear optical device applications as waveguide, thin film on substrate is also an important form. So preparation of these films on transparent substrates as NLO samples is important [34].

The glass substrate disks produced by IBM are much stiffer and more robust than other substrates. Therefore, potentially they provide much higher reliability than traditional disks. Improved uniformity of the magnetic films surface, reduction in overall surface defects which reduce read/write errors, greater fly-height margin and ability to withstand shock and damage makes these substrates greatly important [37].

The aim of this study was to produce magnetite thin films on glass substrates by sol-gel process and characterize them with several methods. Magnetite thin films are important for applications in many different types of devices and for their possible future applications. Glass substrates are used because they have many benefits over other substrates that were previously used for preparing magnetite thin films. Sol-gel process which has many advantages on thin film formation was chosen for the film deposition process. During the study, magnetite phase was observed at sintering temperatures of 300-350 °C. Increasing sintering temperature leads to phase transformations.

This report begins with a literature survey of magnetite thin films. First, a general description of data storage is given followed by a description of iron oxide phases to explain the terms that were used during characterization. Their crystal structures and magnetic properties are given. In the last part of Chapter 2, production of magnetite thin films by sol-gel process was explained with details of this process. Third chapter includes the experimental procedure consisting of solution preparation, coating procedure of thin films and characterization of them. In the fourth chapter, results of experiments and discussion on these results on solution preparation, film deposition and sintering procedure were given. Characterization of the solution by thermal analysis using DTA (Differential Thermal Analysis) and viscosity measurements were explained. In addition, microstructural characterization of thin films by XRD (X-ray diffraction), film microstructure and morphology characterization by SEM (scanning electron microscopy), AFM (atomic force microscopy) and TEM (transmission electron microscopy), optical characterization by UV-Vis and magnetic characterization by VSM (vibrating sample magnetometer) were also explained in this part. Finally, the last chapter includes the conclusion and further suggestions related to the present work.

CHAPTER 2

LITERATURE SURVEY

2.1. Data Storage

As Agarwal et al. [38] described in his/her thesis, in the present age, information technology (IT) has been significantly revolutionized. The unlimited imaginary and hunger of the humankind for the knowledge led them to improve methods to gather and store information. Because of this, the way information is created, acquired, processed and stored has been completely changed during the past decade. The amount of worldwide market for IT and electronics is more than trillion dollars. For sustaining, improving and continuing this market, fundamentals of data storage technology must be understood better than before. Increasing the density of data storage and scaling down further are musts for the data storage technology. So, new technologies are needed.

Human memory is the earliest form of storing information. This was not a reliable way to store and transfer information from one place and time to another. Sun-dried clay tablets were the next step for the information storage but still they could not meet the portable means of information transfer. Before the development of paper, animal hides and river reeds were used. Paper was an effective way of storing data because it could last longer than most of the alternatives. 1725 is a milestone in data storage; punch cards were introduced. Perforated paper loop was used to store patterns that were to be used on cloth. The first patent for the data storage was dated 23 September 1884 and it was used for nearly 100 years. Punched tapes were introduced in 1846 by Bain and with this method; information was recorded by punching holes into the paper or cardboard medium. The information was read by sensing whether a particular location on the medium is solid or holed. This paper tape significantly increased the amount of data stored. The Williams tube, which was developed in 1946, used cathode ray tube to store electronic data. At the same time Selectron tubes were introduced by RCA. These tubes can be counted as the early form of computer memory. The largest Selectron tube was 10 inches and it could store 4096 bits. But these tubes were expensive.

In the 1950s, IBM firstly used the magnetic tapes for the data storage. The next step in the evolution of the data storage was the introduction of the compact cassettes. They were introduced by Phillips in 1963 and it could store 700 kilo-bytes (KB) to 1 mega-byte (MB) of data on each side. In 1969, the earliest version of floppy-disk was introduced which could store 80 KB of data on an 8-inch read-only disk. An improved version which could store 256 KB of data and could be re-writable, was introduced in 1973. First hard-disk drive which could store 4.4 MB of data, was introduced by IBM and it was called IBM 350 Disk File. It was introduced by IBM 305 computer in 1955. Its inventor was Reynold Johnson.

The hard-disk-drives (HDD) have been improved over years, their storage capacities improved but still they were large and complicated devices and also they need special protective environments. So they cannot meet the demand of portable means of data transfer. Over time, there have been vast improvements in the design and capacities of these drives.

Today, there are several different alternatives for storing information. Compact discs (CDs) and Digital Video Discs (DVDs), which use optical recording, are used for storing audio-video tracks and other files also in digital format. Semiconductor flash memories are another form of memory devices and they are popular due to their compactness, reliability, robustness and inexpensive price.

The future of the data storage industry will be worth of wondering by looking at the options available today and the evolution during the time. Due to the capacity, ultrahigh density storage, durability over millions of read-write cycles, reliable performance under challenging environments and ever reducing cost to the user in terms of price per bit of stored data, magnetic data storage might eventually predominate over other competing media [38].

2.2. Iron Oxides

Iron oxides are very common compounds and they are widespread in nature and readily synthesized in laboratory. As shown in Figure 2.1, in almost everywhere of the global system; athmosphere, biosphere, hydrosphere and lithosphere, iron oxides present [10].

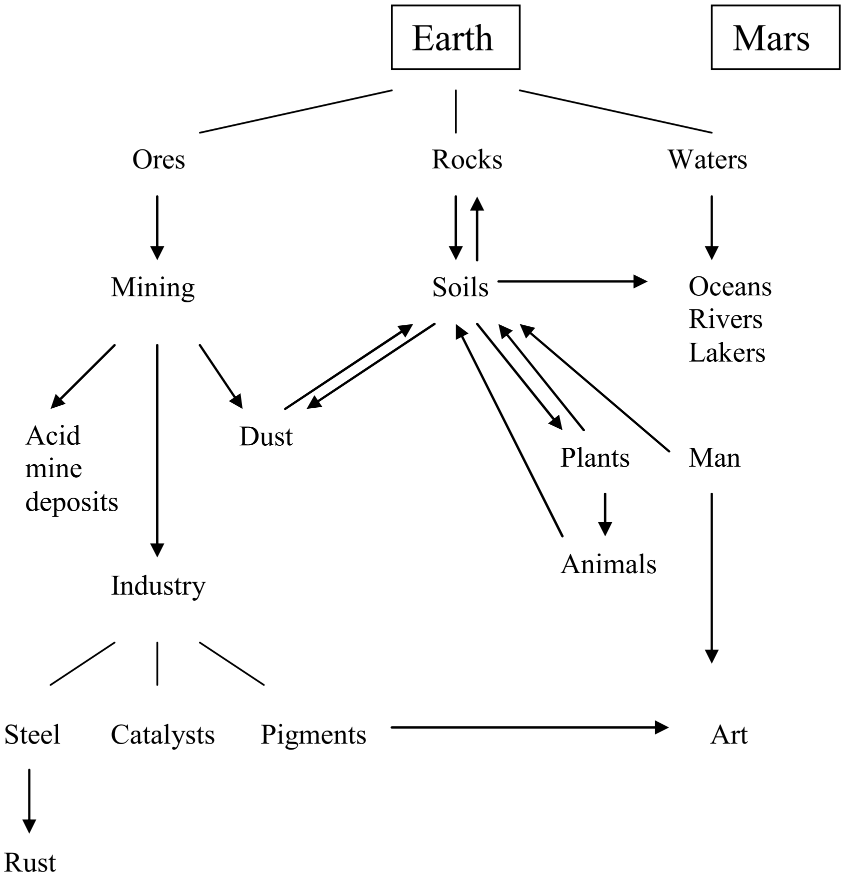

Figure 2.1 Iron oxides in the global system [10].

In a variety of disciplines such as corrosion science, pure chemistry, medicine, industrial chemistry and soil science, iron oxides play important role. These iron oxides are needed to be prepared in laboratory in order to be investigated for their own particular properties or as a starting material or catalyst for other processes. There are several types of iron oxides with different crystal structures and compositions, but most important ones are hematite (α-Fe_2O_3), magnetite (Fe_3O_4) and maghemite (γ-Fe_2O_3) [39]. As shown in Figure 2.2 many different scientific disciplines interest in iron oxides [10].

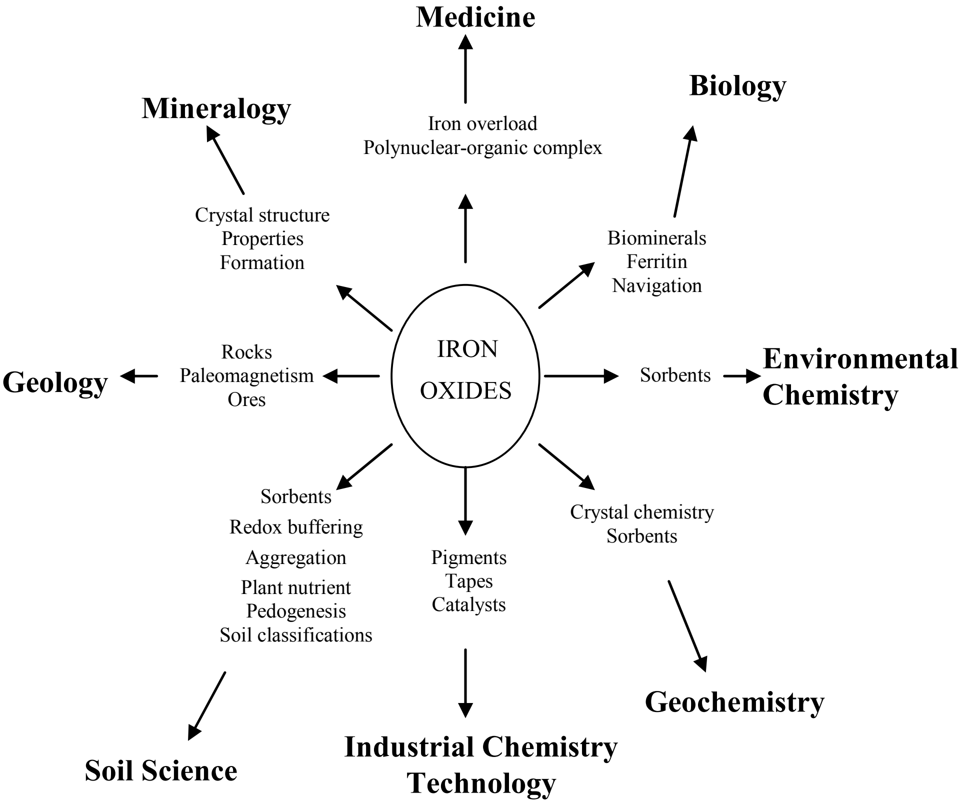

Figure 2.2 The multidisciplinary nature of iron oxide research [10].

Some selected properties of iron oxides are listed in Table 2.1.

Table 2.1 General properties of iron oxides [10].

Mineral Name	**Goethite**	**Hematite**	**Magnetite**	**Maghemite**
	orthorhombic	Rhombohedral Hexagonal	Cubic	Cubic or Tetragonal
Cell Dimensions (nm)	a=0.9956 b=0.30215 c=0.4608	a=0.50356 c=1.37489	a=0.8396	a=0.83474
Formula Units, per unit cell, Z	4	6	8	8
Density (g/cm^3)	4.26	5.26	5.18	4.87
Octahedral occupancy	1/2	2/3	-	-
Colour	Yellow brown	Red	Black	Reddish-brown
Type of magnetism	Antiferromag.	Weakly ferromag. or antiferromag.	Ferrimag.	Ferrimag.
Néel or Curie temperature (K)	400	956	850	820-986
Standard free energy of formation ΔG_f^0 (kJ mol^{-1})	-488.6	-742.7	-1012.6	-711.1
Solubility product (pFe+3pOH)	40-44	42.2-43.3	35.7	40.4

2.2.1. Hematite

Hematite, α-Fe_2O_3, is the oldest known iron oxide, and can be widespread found in rocks and soils. If it is finely divided, its color is blood red and if it is coarsely crystalline, its color is sparkling gray or black. It is extremely stable and mostly it is the end product of transformations of other iron oxides [10].

Hematite has a same structure with corundum. Its unit cell is hexagonal with a=0.503 nm and c=1.375 nm. Hematite can also be indexed in rhombohedral system. For rhombohedral unit cell, a_{rh}=0.5427 nm and α=55.3°.

Structure of hematite consists of hcp arrays of oxygen stacked along [001] direction. Fe^{3+} ions occupy the two thirds of the sites. They are arranged regularly with two filled sites followed by one vacant site in the (001) plane.

The cation arrangement produces pairs of $Fe(O)_6$ octahedra. In the same plane, each octahedron shares edges with three different octahedra and in an adjacent plane, each octahedron shares one face with an octahedron. Face sharing occurs in c-axis. Because of this face sharing, the cation sublattice is distorted from ideal packing. This can be explained by repelling of Fe atoms in the octahedra which share faces, along the direction normal to [001], which causes the cations to shift closer to the unshared faces. The O-O distances along the shared face are shorter than the distance along the unshared edge, so the octahedron is trigonally distorted. The $Fe-O_3-Fe$ triplet structure influences the magnetic properties of the oxide.

2.2.2. Magnetite

Magnetite, Fe_3O_4, is black colored and it is a ferrimagnetic mineral which contains both Fe^{2+} and Fe^{3+} ions together. Its structure is inverse spinel [10].

Structure of magnetite is shown in Figure 2.3. Magnetite has a face-centered cubic unit cell based on 32 O^{2-} ions which are regularly cubic close packed along the [111]. The unit cell edge length is a=0.839 nm.

Magnetite is different from most other iron oxides because it contains both divalent and trivalent iron. Its formula can be written as $Y[XY]O_4$ where $X=Fe^{2+}$, $Y=Fe^{3+}$ and the brackets denote the octahedral sites. Eight tetrahedral sites are distributed between Fe^{2+} and Fe^{3+} ions, i.e trivalent ions occupy both tetrahedral and octahedral sites. In the magnetite structure, there exist octahedral and mixed tetrahedral/octahedral layers stacked along [111].

The Fe^{2+} and Fe^{3+} ratio is 0.5 in stoichiometric magnetite. The divalent ion can be replaced by other divalent atoms because of the flexibility of the oxygen framework which can expand or contact to accommodate cations which are sizely different from Fe^{2+}.

Magnetite can be slightly metal deficient with vacancies on the octahedral sites. It is both an n and p type semiconductor. The band gap is small (0.1 eV), therefore magnetite has the lowest resistivity of any oxide. Its conductivity is 10^2-10^3 Ω^{-1} cm^{-1} which shows that magnetite is almost metallic. In edge sharing octahedral, the Fe^{2+} and Fe^{3+} ions on the octahedral sites are close together and as a result, the holes can migrate easily from Fe^{2+} and Fe^{3+} and this accounts for the good conductivity.

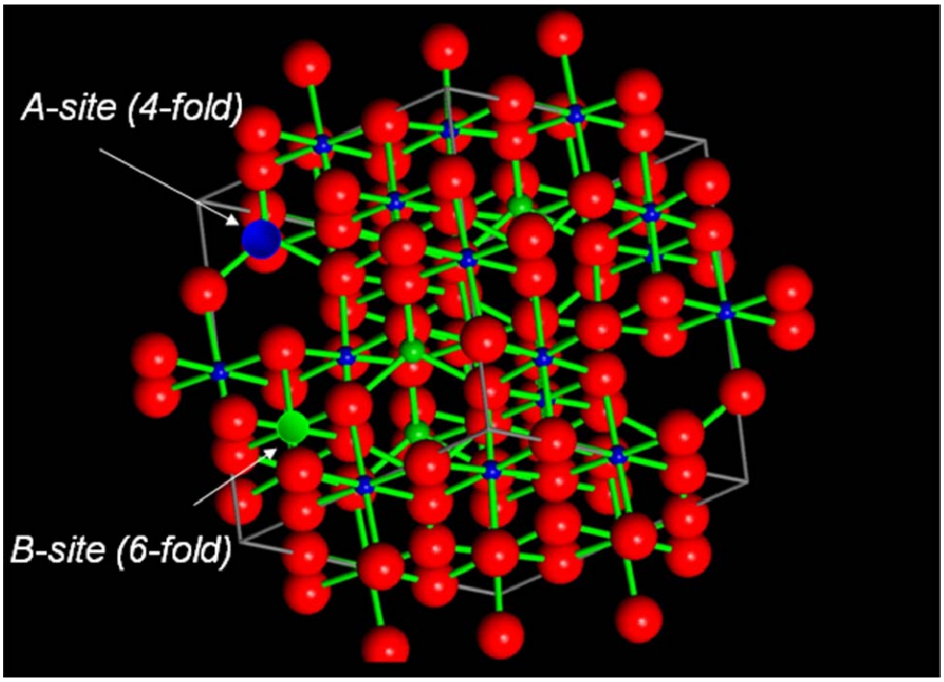

Figure 2.3 Representation of structure of magnetite [40].

2.2.3. Maghemite

Maghemite (γ-Fe_2O_3), which is red-brown colored, is a ferrimagnetic material and it has the same structure with magnetite but cation sites are deficient. Maghemite is an important magnetic material.

The difference between the maghemite and magnetite is that most of or all of the iron ions are in the trivalent state. The oxidation of the Fe^{2+} ions can be compensated by cation vacancies.

Maghemite has a unit cell length of a=0.834 nm and each of the cell has 32 O^{2-} ions, $21^1/_3$ Fe^{3+} ions and $2^1/_3$ vacancies. Eight of the cations are in the tetrahedral sites and others are distributed randomly over the octahedral sites. Vacancies are restricted to the octahedral sites [10].

2.3. Magnetic Properties of Iron Oxides

The magnetic properties of the materials depend on the electrons of the atoms, which have magnetic moments. There are two types of electron motions which are spin motion and orbital motion. Each of them has a magnetic moment related to itself [41]. These two motions are the reasons of the macroscopic magnetic phenomena in materials. It can be thought that each electron spin around an axis of itself which makes the spin moment. The other magnetic moment comes from the electronic spin which is originated along the orbit around nucleus of atom. The net magnetic moment is the sum of these two moments [42].

There are mainly three types of magnetism. These are diamagnetism, paramagnetism and ferromagnetism. Antiferromagnetism and ferrimagnetism can be considered as the subclasses of ferromagnetism. All materials exhibit at least one of these types. Materials are classified depending on how they behave in magnetic fields [42]. Figure 2.4 shows a schematic representation of different types of arrangements of magnetic dipoles.

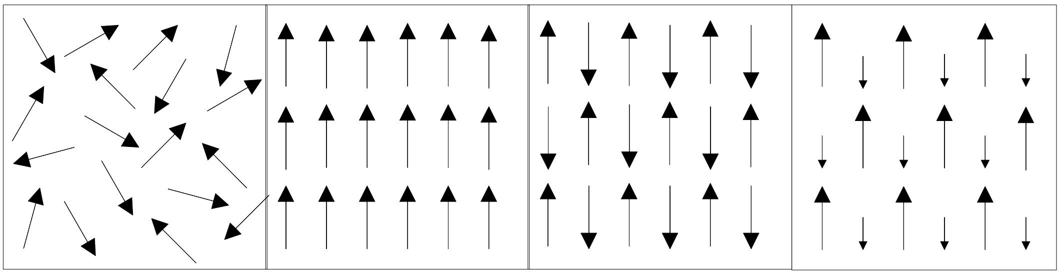

Figure 2.4 Different orientations of magnetic dipoles: (a) paramagnetic (b) ferromagnetic (c) antiferromagnetic and (d) ferrimagnetic [35].

2.3.1. Diamagnetism

As Poudyal et al. [42] described; diamagnetism is the basic property of all matter and it is very weak. The origin of this behavior comes from the non-cooperative behavior of orbiting electrons when they are exposed to an applied magnetic field. The atoms of materials, which show diamagnetism, have no net magnetic moments. The orbiting electrons either accelerate or decelerate when they are exposed to a field, so that their magnetic moments aligned to the opposite direction from the external field. When external field is removed, diamagnetic materials lose their magnetization.

The magnetic susceptibility of a diamagnetic material is very small ($\sim 10^{-6}$) and it does not depend on temperature [10].

2.3.2. Paramagnetism

In the paramagnetic material some of the atoms or ions have a net magnetic moment. This comes from the unpaired electrons in partially filled orbitals. When the field is removed, the net magnetization is zero just like the diamagnetism and the individual magnetic moments do not interact magnetically. There is a partial alignment of magnetic moments in the presence of a field. The direction of the moment is the same with the direction of the field. This results in a net positive magnetization [42]. The magnetic susceptibility, χ_M is positive and small (0 to 0.01) [10].

The temperature effect can randomize the moments, and it opposes the efficiency of the field which aligns the moments [42].

Its behavior is described by Curie-Weiss law by Cornell et al. [10],

$$\chi_{\mathrm{M}} = \frac{C_M}{T - T_C} \qquad \text{Eq. [2.1]}$$

C_M is the Curie constant, T_C is the Curie temperature and T is the temperature. From the equation, it can be concluded that if the temperature rises χ_{M} decreases because thermal vibrations opposes the increased alignment of the magnetic moments in the material.

Below a certain temperature (Nèel or Curie) iron oxides goes through a transition and they become magnetically ordered (ferromagnetic, antiferromagnetic or ferrimagnetic). For ferromagnetic and ferrimagnetic materials, transition temperature is called Curie temperature but for antiferromagnetic materials, it is the Nèel temperature.

2.3.3. Ferromagnetism

These materials show permanent net magnetic moments which leads to a large net magnetization even if there is no magnetic field. Overall contribution of electron spin and orbital magnetic moments are the origin of these permanent net magnetic moments. Magnetic ordering temperature and their spontaneous magnetization are the two main characteristics of ferromagnetic materials. The spontaneous magnetization can be defined as the net magnetization of a volume in the absence of a field.

A block of ferromagnetic substance has many magnetic domains which are spontaneously magnetized. Since the magnetization is different along the domains, sometimes no net magnetization can be obtained and if there is a net magnetization, its value is the resultant magnetization of the magnetic domains. Saturation magnetization is the maximum possible magnetization that can be obtained in a magnetic field and if further increase is impossible. Saturation magnetization depends on temperature but does not depend on particle size [42].

2.3.4. Antiferromagnetism

In antiferromagnetic materials, all moments are antiparallel to each other, and it is totally opposite to ferromagnetic ordering [41]. The magnetic moments which are opposing each other, cancel one another and results in zero net magnetization in material [42].

2.3.5. Ferrimagnetism

Just like antiferromagnetic materials, ferrimagnetic materials have the same antiparallel alignment of magnetic moments. But the magnitude of the magnetic moments differs in opposite direction. Hence in the absence of a magnetic moment, there remains a net magnetic moment [41]. Fe_3O_4 can be given as the best example for the ferrimagnetic materials, because in magnetite, iron exists both in divalent and trivalent forms. The two trivalent ions have opposite magnetic moments hence they cancel each other and net magnetization arise from divalent ions. Ferromagnetism and ferrimagnetism have similarities such as spontaneous magnetization, Curie temperatures, hysteresis and remanence. But they have very different magnetic ordering [42].

In Ferrimagnetism, the exchange energy, J, in many ionic crystals, between the two neighbouring atom spins is negative. This is because of the spin of the shared electron from metal ions with the oxygen follows Pauli principle. Therefore, if the metal ion has an outer shell less than half occupied, all the spins will be aligned parallel inside the shell and antiparallel with respect to the other metal ion. Therefore antiparallel alignment is the lowest energy alignment [43].

In the spinel ferrites, metal ions arranged into two sublattices which are A and B. A corresponds to tetrahedral positions and B corresponds to octahedral positions. In the spinel ferrites, the unit cell contains 8 tetrahedral and 16 octahedral positions. There are two types of spinel ferrites which were shown by neutron diffraction studies. These are normal and inverse type. Studies also showed that normal spinel ferrites are paramagnetic and inverse spinel ferrites are ferrimagnetic. In the normal spinel ferrites, divalent ions are in the sublattice A and trivalent ions are located in the sublattice B. In the inverse spinel ferrites, half of the trivalent ions occupy the sublattice A and other half of the trivalent ions occupy the B lattice together with divalent metal ions.

Metallic ions are separated by O^{2-} ion in the spinel iron oxides. Because of the large distance between the metallic ions, it is assumed that there is a super exchange between the metallic ions through the oxygen ion [43].

2.3.6. Superparamagnetism

Magnetic materials which behave like paramagnetic materials at temperatures below Curie or Nèel temperature show superparamagnetism. This fact occurs when materials consist of very small crystallites (<10 nm). Thermal energy is sufficient to overcome the coupling forces and the direction of the magnetization changes in the entire crystallite. Average magnetic field becomes zero as the fluctuations in the magnetization direction occur. It is a similar phenomenon with paramagnetism, but each individual atom behaves independently in the presence of an external magnetic field. Therefore, entire crystallite aligns with magnetic field. [42].

Superparamagnetism arises as a result of magnetic anisotropy, i.e. the existence of preferred crystallographic directions along which the electron spins are most readily aligned and the substance most easily magnetized. The preferred direction for easy magnetization is along some crystallographic axis or set of axes. If sufficient energy is supplied, magnetism can be reversed along these axes. The time required for spin reversal, the relaxation time, τ depends on the height of the energy barrier between the forward and reverse spin states and the temperature, according to

$$\tau \propto \exp\left(\frac{K_{eff}V}{kT}\right) \qquad \text{Eq. [2.2]}$$

The height of the energy barrier between the forward and reverse states is the product of the particle volume, V, and the anisotropy constant K_{eff} (which is, to some extent, a function of particle size). Superparamagnetic relaxation occurs when the thermal energy of the particles exceeds the activation energy barrier between the spin states and so allows rapid, spontaneous fluctuations between these states. The effect of these spin reversals is that the observed magnetic field is reduced or even absent.

Because the appearance of the superparamagnetic effect depends on the particle size and on the anisotropy constant, it is often displayed at room temperature by iron oxides <10 nm in size, for example, soil iron oxides. Superparamagnetic relaxation may be counteracted by lowering the temperature and thereby increasing τ. Superparamagnetic particles will usually be ordered below a blocking temperature, T_B, which is:

$$T_B = \frac{K_{eff}V}{25k} \qquad \text{Eq. [2.3]}$$

In the hysteresis loops shown in Figure 2.5, various forms of magnetism are shown. M_S is the saturation magnetization (all the spins are aligned with the magnetic field), H_C is the coercive field (internal magnetic field of material), M_R is the remanent magnetization (magnetization retained by the material). From the figure it can be seen that superparamagnetic and paramagnetic materials do not show hysteresis loop.

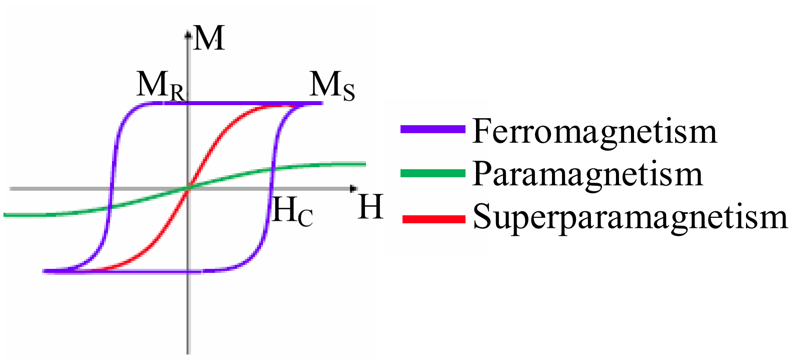

Figure 2.5 Magnetization (M) vs. applied field (H) for ferromagnetic, paramagnetic and superparamagnetic materials [35].

2.4. Sol-Gel Processing of Thin Films

Many techniques have been used for the preparation of magnetite thin films. Different production techniques used to prepare magnetite thin films are given in Table 2.2.

Table 2.2 Different production techniques which were used to prepare magnetite thin films.

Production Method	Precursor/Target	Experimental Details	Substrate
MBE [19]			MgO and $MgAl_2O_4$
Sputtering [7, 15, 21-23]	99.95 % Fe Fe_3O_4 and Fe_2O_3	Oxygen flow rate is between 0-2 sccm Argon flow rate=50 sccm Base pressure=$3x10^{-7}$ Torr Deposition pressure=4 mTorr Substrate temperature= RT and 400 °C Substrate rotation=120 rpm Sputtering power=300 W Deposition rate=350-400 Å/min	Amorphous SiO_2 Glass
Ferrite Plating [26, 27]	Ammonium acetate $FeCl_2 \cdot 4H_2O$ $NaNO_2$	$FeCl_2 \cdot 4H_2O$ and $NaNO_2$ were seperately added to ammonium acetate Solutions were supplied to reaction vessel at a flow rate of 6,4 ml/min Ultrasound wave (20 kHz, 750 W) applied to substrate Reaction temperature=70-85 °C Films were sintered at 250 °C-350 °C in air	Glass
Reactive Evaporation [24]	Metallic iron	Iron metal was evaporated by resistive heating in oxygen atmosphere Chamber was baked and evacuated below $2x10^{-8}$ Torr Pressure during evaporation is between $1x10^{-6}$ and $1x10^{-5}$ Torr	Glass and Kapton

Table 2.2. (Continued) Different production techniques which were used to prepare magnetite thin films.

Hydrothermal Growth [25]	$FeSO_4 \cdot 7H_2O$ $N_2H_4 \cdot H_2O$	150°C for 8 h and cooled normally to room temperature Obtained film was dried at 50 °C for 2h	Nickel
PLD (Pulsed Laser Deposition) [44-47]	Commercial sintered Fe_3O_4	KrF excimer laser beam under an incidence 45° with a repetition rate of 5Hz and fluence of 2 $J.cm^{-2}$ Films were grown at 483 °C Working pressure is either $5x10^{-1}$ or $7,8x10^{-2}$ Pa	Si (100)
Solid State Reactions [8]		Glass/Fe_2O_3/Fe, Si/Fe_2O_3/Fe and Si/Fe/Fe_2O_3 multilayers were sintered at 450 °C temperature during 120 min at vacuum (10^{-4} Pa)	Glass and Si(100)

As described by Sakka et al. [48], sol–gel technology is quite important for processing important materials. Since it is one of the technologies for producing materials, application of this technology is valuable only when a better material can be made, a target material can be produced with much lower cost and only this method is available for making the target material. The sol–gel method has proved to be quite versatile as a result of intensive and extensive fundamental researches for these three decades. The type of materials processed by this method covers metallic, inorganic, organic and hybrid materials. The use of the materials covered by this method ranges from highly advanced materials to materials for general use. The areas of technology covered by this method ranges from photonics to biology. These indicate that the sol–gel method can be applied for processing of extremely much kind of materials.

Sol-gel process is attractive for the replacement of other deposition methods for many reasons such as low temperature synthesis, equipments for deposition is much simpler than the equipments used in other methods, thin film formability and so on. Capability of coating materials of different shapes and/or large areas, controlling the composition for obtaining homogenous solutions and controlling concentration with relatively cheap equipments; makes the sol-gel process a very useful technique for film deposition. Also, whole process can be conducted in ambient pressure [49].

For the preparation of thin films and coating, sol-gel method is suitable. Room temperature usage of the solution is an advantage, but theoretically, if preparations of multicomponent homogenous liquid solutions are available, than any crystalline or non-crystalline films or coatings can be applied to much type of substrates. For the large monolithic samples, sol-gel method is costly and difficult because of raw materials, porosity and large shrinkages but for the thin films, the process is free from these problems [50].

As Yıldırım et al. said [51], the sol-gel process covers the preparation of homogenous solution which contains the precursor; the deposition of the thin films on the substrate which produces amorphous film by simultaneous hydrolysis and polycondensation during deposition, and then heating the amorphous film until it crystallizes. In modern ceramic and device technology, materials must be produced with high purity and control over composition and microstructure must be provided. In sol-gel processing, chemical reactants can be purified by distillation and crystallization, hence by this method high purity films can be fabricated.

In sol-gel process, high degree of homogeneity is obtained because of the molecular level mixing of the starting materials in the solution. Also, control on thickness and lateral homogeneity is possible. Sol-gel derived ceramics can be obtained at low temperatures because, the pores in the dried gels are extremely small and components of the gel are well mixed. These are important in the structures which have any phases, transform to undesired phases or have volatile components. Adjusting the microstructure and improving the film properties can also be provided by introducing tracing elements into the structure by adding these elements into the solution.

Properties like viscosity, surface tension and concentration of the organometallic polymeric solution can be easily adjusted. Film geometry allows the escape of the oxidation products during firing.

As Karakuşcu et al. [35] briefly explained, many variations can be brought to the sol-gel synthesis of ceramics. In fact, sol-gel processing does not only designate a unique technique, but a very broad type of procedures that centralizes around a single scheme as presented in Figure 2.6. The first step of any sol-gel process always consists of selecting the precursors of the required materials. It is the precursor that, by its chemistry, leads the reaction towards the formation of either colloidal particles or polymeric gels. When the future material is composed of several components (i.e., when several oxides are mixed together), then the use of a combination of different precursors and procedures enhances different chemical synthesis and hence different products. The colloidal particles obtained can then be precipitated and treated according to one of the conventional processing techniques, such as cold pressing, hot-pressing and sintering, in order to produce the desired ceramic. Sols and gels can also be drawn into fiber form or transformed through one of other various techniques into a coating material. If a gel powder for melting purposes is required, than the gel may be dried and no special cares need. On the other hand, controlled gelation and drying leads to the formation of monosized droplets which can reach several hundred micrometers in diameter. Furthermore, the size of pores can also be controlled by supercritical drying or by the use of surfactants.

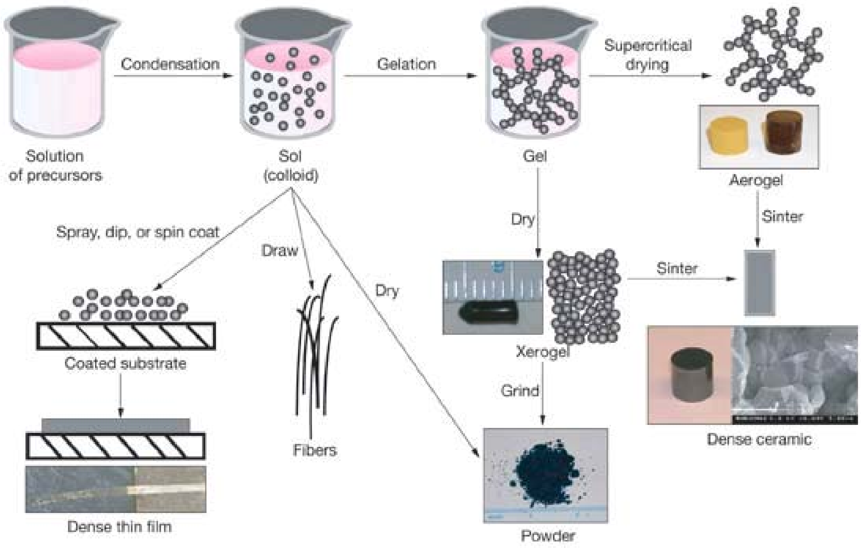

Figure 2.6 The chart of sol-gel process [52].

2.4.1. Process Chemistry

This part was briefly discussed by Yıldırım et al. [51]. Most processes can be categorized in one of three general approaches, which are drawn schematically in Figure 2.6.

In the first approach, a colloidal sol is prepared, and powders are precipitated from the sol. Obtained powders are dried and processed by using traditional ceramic processing techniques. In the second approach, a porous ceramic is formed firstly by drying gel which is formed by linking the particles in the colloidal sol. This ceramic is fired to crystallize and/or densify the material. In the third approach, by polymerizing the individual oligonomeric units, a gel is formed. The gelation of a solution is the formation of a network in the solution. The hydrolysis and polycondensation of organometallic compounds such as alkoxides leads to gelation.

Second and third approaches are convenient ways of film coating. Because, they can be cast, spun, dip coated, or sprayed onto substrates prior to gelation. The vast majority of applications of sol-gel coatings come from applying solutions to substrates prior to gelation. This type of sol-gel processing technique is called “Chemical Solution Deposition”. The solution completely transforms into a xerogel during the spin coating process. The organic precursor constituents of the dried precursor film decompose upon heat treatment resulting in mixing of the cations on a scale close to that of the sol-gel approaches.

As Karakuşcu et al. [35] told, a “colloid” is a suspension in which the dispersed phase is so small that gravitational forces are negligible and interactions are dominated by short-range forces, such as van der Waals attractions and surface charges. The inertia of dispersed phase is so small enough that it exhibits Brownian motion, a random walk driven by momentum imported by molecules of the suspending medium. A “sol” is a colloidal suspension of solid particles in a liquid.

Metal oxides are members of the family of metallorganic compounds, which have an organic ligand attached to a metal or metalloid atom. Organometallic compounds are defined as having direct metal-carbon bonds, not metal-oxygen-carbon linkages as in metal alkoxides; thus alkoxides are not organometallic compounds, although that usage turns up frequently in the literature. Metal oxides; are popular precursors because they react with water. The reaction is called hydrolysis, because a hydroxyl ion becomes attached to the metal atom

$$M(OR)_x + H_2O \rightarrow M(OH)_x + xROH \qquad \text{Eq. [2.4]}$$

Two partially hydrolyzed molecules can link together in a condensation, such as

$$(OR)_{x-1}M - OH + HO - M(OR)_{x-1} \rightarrow (OR)_{x-1}M - O - M(OR)_{x-1} + H_2O \quad \text{Eq. [2.5]}$$

or

$$(OR)_{x-1}M - OR + HO - M(OR)_{x-1} \rightarrow (OR)_{x-1}M - O - M(OR)_{x-1} + ROH \qquad \text{Eq. [2.6]}$$

These reactions cause the formation of a metal-oxygen-metal bridge, which constitutes the backbone of any oxide ceramic structure. Continued condensation leads to an increase in the density of metal-oxygen-metal crosslinks until eventually gelation or precipitation occurs.

The basic principle of the sol-gel process is to form a solution of the elements of the desired compounds in an organic solvent, polymerize the solution to form a gel, and dry and fire this gel to displace the organic components and form a final inorganic oxide.

Important and typical precursors for making sol-gel solutions are alkoxides of the general composition $M(O\text{-}R)_n$, where R is an alkyl radical (CH_3, C_2H_5, etc.). Their properties and reactions affect the preparation process and determine the product features. Inorganic and organic salts can also be used for introducing some oxides into multicomponent systems. The precursors are dissolved in a suitable organic solvent to form the solution. In order to get the solution with a high concentration of necessary components and proper viscosity, surface tension and boiling point, the solvent must be carefully selected.

In order to obtain a suitable solution for making films, various properties of solution are adjusted. Different alkoxides of different elements show a wide range of reactivity toward H_2O which makes the preparation of multicomponent homogeneous systems difficult and also presents difficulties with premature gelation during film processing. This can be overcome by adding a chelating organic ligand into the solution to control the hydrolysis rates of highly reactive alkoxide. The gelation of a solution means the formation of a network in the solution.

The hydrolysis and polycondensation of organometallic compounds such as alkoxides leads gelation. During the drying stage the wet coating is converted to a relatively dry, harder coating and considerable shrinkage of the coating occurs. At this stage problems related to film cracking and surface smoothness in the final film become most acute.

The sintering step converts the gel coating into a densified complex oxide film. This process includes the removal of residual –OH or –OR groups by polycondensation reactions, pyrolysis of the organic compounds or groups left in the film into carbon, oxidation of the carbon and gradual densification of the film.

Table 2.3 summarizes the details of the sol-gel processes which were used to produce magnetite thin films taken from the literature.

Table 2.3 The literature survey of the sol-gel processes which were used to produce magnetite thin films.

Formed phases	**Solvent and precursors**	**Experimental details**	**Drying time and temperature**	**Sintering time and temperature**	**Substrate**	**One-layer thickness**	**Ref. no**
Fe_3O_4	Hydrated iron (III) nitrate DMAB	pH of the solution= 3.5 0.01 mol/L hydrated iron(III) nitrate and 0.03 mol/L DMAB T=Room Temp.			Glass	2 µm	[53]
Fe_3O_4	Iron (III) nitrate 2-methoxyethanol 2,4-pentanedione	T=30 °C for 2 h 1:20:2 molar ratio	800 °C for 10 min	600 °C 5 h under N_2 (Fe_3O_4)	SiO_2 glass	-	[33]
Fe_3O_4	Iron (III) nitrate Ethylene glycol 2-methoxyethanol Polyethylene glycol	Concentration is 12 wt %	100 °C for 10 min and 350 °C in nitrogen atmosphere	600 °C for 2 h in a flow of gas mixture of H_2 and N_2	Fused quartz substrates	300 nm	[32]

Table 2.3 (Continued) The literature survey of the sol-gel processes which were used to produce magnetite thin films.

Fe_3O_4	Iron (II) lactate Iron (III) nitrate Ethylene glycol Citric acid monohydrate Ethanol	Mole ratio of iron(II)/iron(III)=1/2 10 h stirring	Vacuum drying at 40 °C for 1 h	450 °C for 3 h under nitrogen atmosphere	Quartz	120 nm	[30]
Fe_3O_4	$FeCl_2 \cdot 4H_2O$ Citric acid monohydrate Ascorbic acid Ethanol absolute N, DMF	Stirred for 30 min at 60 °C	100 °C	300 °C for 30 min	Silica-glass		[28]
Fe_3O_4	Tris(acetylacetonato)iron(III) $Fe(acac)_3$ CH_3COOH HNO_3	Stirred 4 h at room temperature	940 °C for 10 min in air	510 °C -630 °C for 5 h	Silica-glass		[29]

Table 2.3 (Continued) The literature survey of the sol-gel processes which were used to produce magnetite thin films.

Fe_3O_4	Iron (III) nitrate nonahydrate Ethylene glycol Ethanol	Molar ratio of ethylene glycol/iron nitrate nonahydrate=15:1 0.3M sol was prepared	80 °C for 10 min	300 °C – 1000 °C	Quartz		[9]

2.4.2. Coating Process for Depositing Sol-Gel Films

The deposition parameters are important for the final properties of the film. There are two common techniques for the deposition of the films from the solution. These are dip coating and spin coating techniques.

2.4.2.1. Dip Coating

It is the most common and easiest way to deposit a film on a substrate by sol-gel method (Figure 2.7). The substrate geometry may differ; it could be flat panel, cylinder or in a complex geometry. Square meter sized areas can be easily coated by this technique. It can also operate in either continuous or batch modes. In the batch dip coating process, there exists five stages. These are immersion, start up, deposition, drainage and evaporation. For a coating sol containing volatile solvent, evaporation goes along with start up, drainage and the deposition stages to form a gel film in a relatively short time. The thickness of the film is affected by six different forces during deposition; (1) viscous drag upward on the liquid by the moving substrate, (2) gravitational force, (3) net force of the surface tension in the concavely curved meniscus, (4) inertial force of the boundary liquid layer which comes at the deposition region, (5) surface tension gradient and (6) the disjoining or conjoining pressure which is important for the films thicker than 1μm [54].

If the substrate speed and liquid viscosity are not high, the thickness of the film can be expressed by the relationship;

$$h = \frac{0.94 * (\eta . U)^{2/3}}{{\gamma_{LV}}^{1/6} * (\rho g)^{1/2}} \qquad \text{Eq. [2.7]}$$

where η is the sol viscosity, U is the substrate withdrawal speed, ρ is the density of sol, and γ_{LV} is the liquid-vapor surface tension. In this equation, Newtonian fluid behavior is assumed and evaporation is ignored [54].

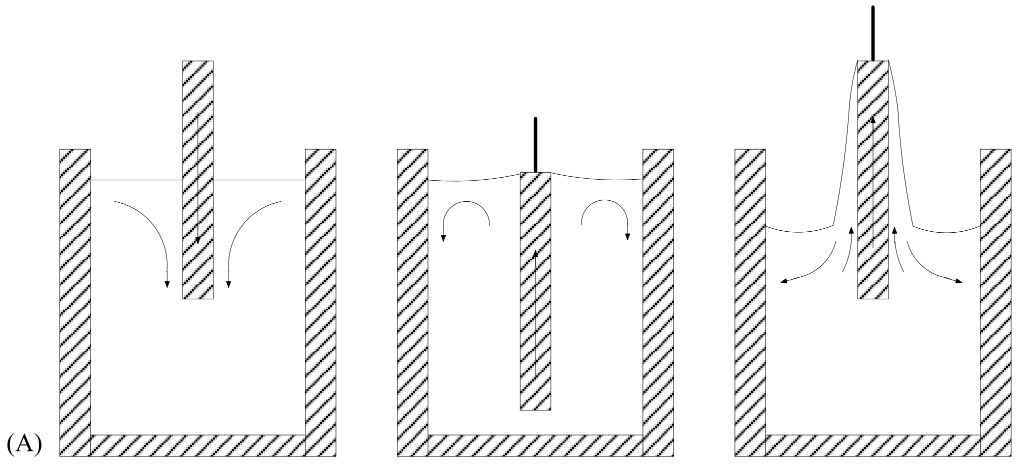

IMMERSION
(a)

START-UP
(b)

DEPOSITION & DRAINAGE
(c)

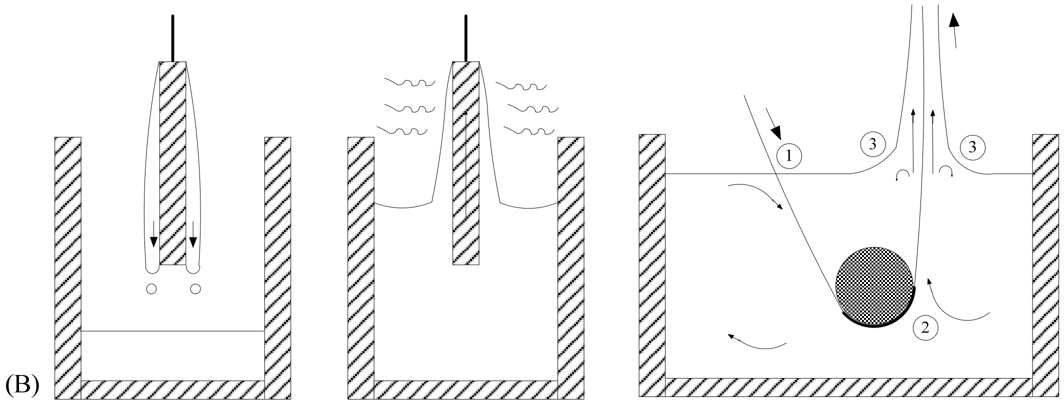

DRAINAGE
(d)

EVAPORATION
(e)

CONTINUOUS
(f)

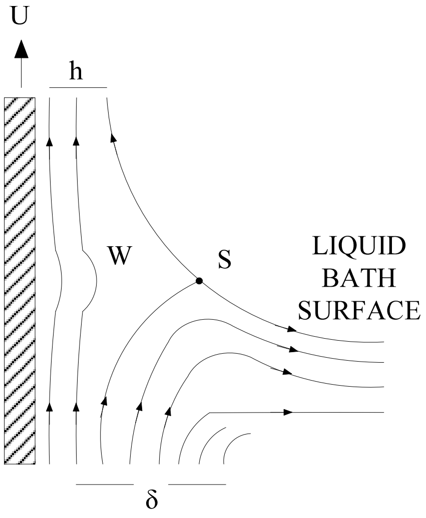

Figure 2.7 Stages of dip coating process [54].

2.4.2.2. Spin Coating

Spin coating is an inherent batch process to produce thin films on rigid flat or slightly curved substrates. The substrates for this process must be small because at very high rotational speeds, i.e. 1000-4000 rpm, they can be held down steadily. Spin coating can be divided into four stages: deposition, spin up, spin off, and evaporation (Figure 2.8). First three stages are consecutive while the fourth one proceeds throughout the coating process [55].

In the first stage, while the substrate is at rest or slowly spinning, excess amount of liquid is poured to the substrate. In the second stage, by the rotating substrate, a centrifugal force is obtained and by this force and the liquid flows radially outward. In this stage, substrate begins to spinning and reaches to a maximum speed. In the third stage, excess liquid on the substrate flows to the perimeter. Flow of the remaining liquid slows down as the film gets thinner. In the fourth stage, further thinning of the film occurs by evaporation and it generally continues after the spin off has totally stopped by solidification brought about by the concentrating of non-volatile solutes and particulates. Deposition and spin up minimally affect the final thickness of the film. Spin off stage is the key stage of the spin coating process. Thickness of the film from liquid tends to become uniform and it thins by spin off and remains so as it gets thinner further. This provides that, liquid’s viscosity is insensitive to shear and it does not vary all over the substrate surface. The rotation induced centrifugal force, which is radially outward flow, and the resisting viscous force, which is radially inward, are the two counteracting forces which results to film uniformity [54].

The thickness of film is the result of the delicate transition by which evaporation takes over from spin off. Nonvolatile constituents can leave the substrate solely by flow. Whatever quantities of them are left when the film becomes so thin and viscous that flow stops, must remain as the coating after all the volatile species have evaporated [54].

The disadvantage of this process is that, it is less economical than dipping because excess solution is lost during the deposition and it is not a continuous process. This technique is suitable for small disk and lens coatings [56].

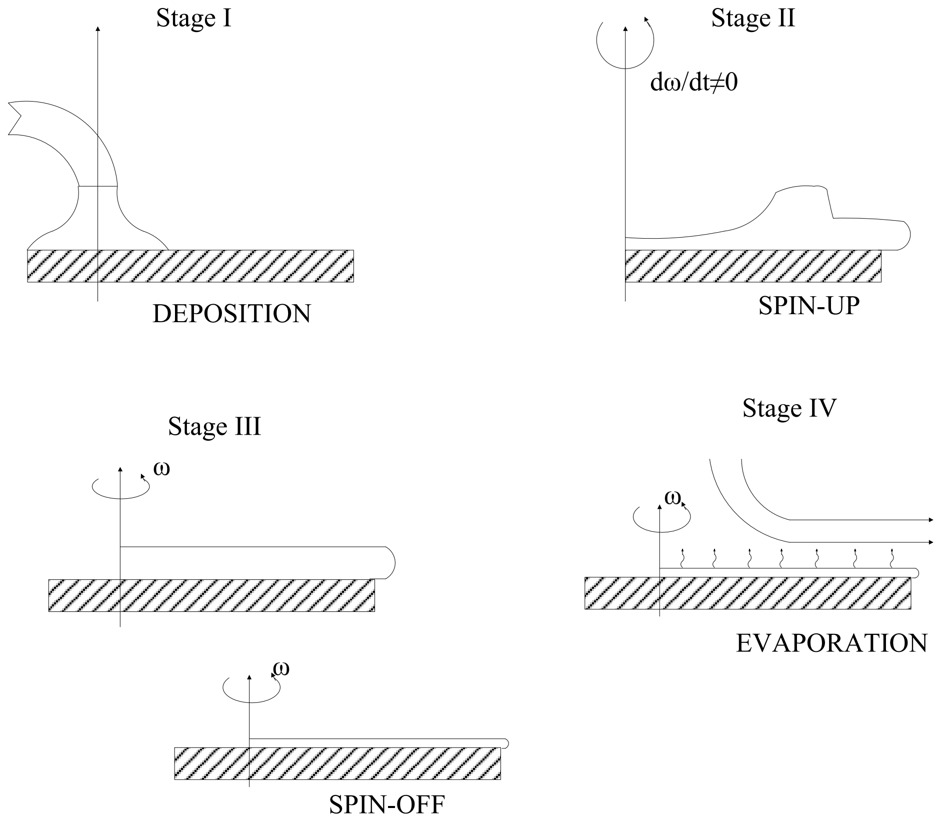

Figure 2.8 Stages of the spin coating process [55].

2.4.3. Thermal Treatment

Forming the ceramic phase is the final stage in the ceramic film processing. Drying and heating the deposited material are the steps of this process. At that stage, transformation reactions and the interactions of amorphous film with the substrate takes place [56].

2.4.3.1. Drying

When the solution is applied to the substrate a sol-gel system is by no means stagnant. The oxide and solvent phases are intimately mixed and the high solid/liquid surface area makes the network to shrink, which is known as syneresis. Condensation reactions between hydroxyl groups also continue to take place, resulting in further shrinkage [54].

During the drying stage, evaporation of alcohol, combustion and carbonization of the organic compounds occur. Crack formation appears at that stage and films is in the amorphous stage after this stage (Figure 2.9) [54].

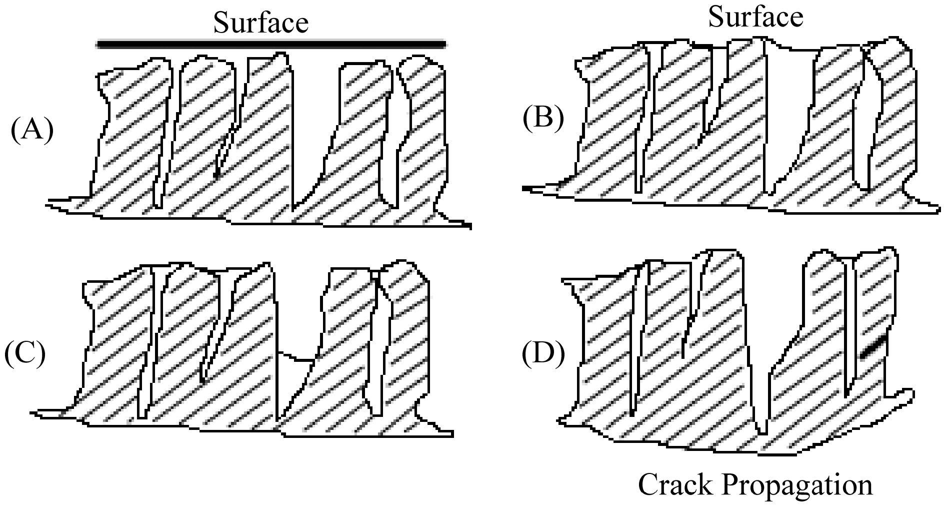

Figure 2.9 Stages in the drying of a gel [56].

Thermal mismatch of the film and the substrate result to the internal stresses in the film. These large stresses cause the crack formation. If there is a little difference between the thermal expansion coefficients of the substrate and the film, there will be no considerable amount of stress. If the adhesion of the film to the substrate is very strong, during the heat treatment all of the internal stresses will be relaxed and this will yield a film having minimum amount of cracks [54].

2.4.3.2. Sintering

Aim of this step is to obtain densified ceramic oxide. The heat treatment step affects the crystal structure, grain size, the amount of crystallization and film cracking [54].

2.4.4. Advantages of Sol-Gel Synthesis

There are numerous advantages of sol-gel synthesis. They can be listed as [57];

1. The temperatures required for all stages apart from densification are low, frequently close to room temperature. Thus thermal degradation of both the material itself and any entrapped species is minimized, and high purity and stoichiometry can be achieved.
2. Precursors such as metal alkoxides and mixed alkyl/alkoxides are frequently volatile and easily purified to very high levels (e.g. by distillation or sublimation) using techniques developed for the microelectronics industry. This further contributes to high-purity products.
3. Since organometallic precursors involving different metals are frequently miscible, homogenous controlled doping is easy to achieve.
4. The chemical conditions are mild. Hydrolysis and condensation are catalyzed by acids and bases, but extreme pH conditions may easily be avoided, especially by the use of "two step" methods in which acid catalyzed hydrolysis is followed by rapid neutralization or buffering. In this way pH sensitive organic species and even biological species including enzymes and whole cells may be entrapped and still retain their functions.
5. Highly porous materials and nanocrystalline materials may be prepared in this way.

6. By appropriate chemical modification of the precursors, control may be achieved over the rates of hydrolysis and condensation over colloid particle size and the pore size, porosity and pore wall chemistry of the final material.
7. Using functionalized precursors, covalent attachment of organic and biological species to porous silicate glass structures is possible.
8. By controlling the ageing and drying conditions, further pore size and mechanical strength control may be achieved.
9. By using organometallic precursors containing polymerisable organic ligands, materials may be produced which contain both inorganic and organic polymer networks.
10. Entrapped organic species may serve as templates for creation of pores with controlled size and shape. Subsequent removal of these species leaves "molecular footprints" with potential as catalytic sites.
11. Since liquid precursors are used it is possible to cast ceramic materials in a range of complex shapes and to produce thin films or fibers as well as monoliths, without the need for machining or melting.
12. The optical quality of the materials is often good, leading to applications for optical components.
13. The low temperature sol-gel process is generally below the crystallization temperature for oxide materials, and this allows the production of unusual amorphous materials.

2.5. Viscosity

Viscosity is a measure of the resistance of a fluid to deform under shear stress. Viscosity describes a fluid's internal resistance to flow and maybe thought of as a measure of fluid friction.

For straight, parallel and uniform flow, the shear stress, τ, between layers is proportional to the velocity gradient, $\partial u / \partial y$, in the direction perpendicular to the layers, in other words, the relative motion of the layers.

$$\tau = \mu \frac{\partial u}{\partial y} \qquad \text{Eq. [2.8]}$$

where the constant μ is known as the coefficient of viscosity, the viscosity, or the dynamic viscosity. Many fluids satisfy Newton's criteria and are known as Newtonian fluids. Non-Newtonian fluids exhibit a more complicated relationship between shear stress and velocity gradient than simple linearity.

Newtonian and non-Newtonian behaviors of fluids are given in Figure 2.10. When the viscosity decreases with increasing shear rate, it is called the fluid shear-thinning. In opposite case where the viscosity increases as fluid is subjected to a higher shear rate, fluid is called shear-thickening [58].

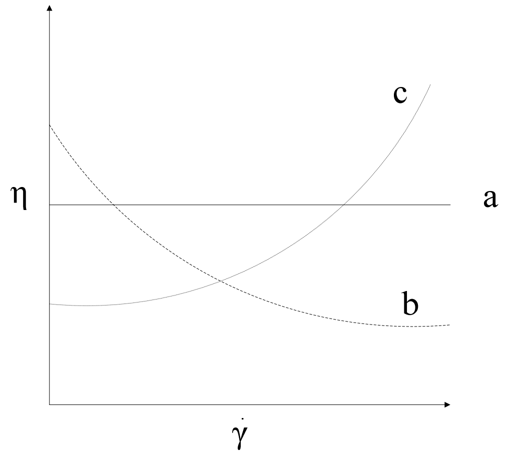

Figure 2.10 (a) Newtonian, **(b)** shear thinning and **(c)** shear thickening non-Newtonian behaviors [58].

The regions where the apparent viscosity is approximately constant are known as Newtonian regions. The behavior between these regions can usually be approximated by a straight line on these axes. It is known as the power-law region. In this region, the behavior can be approximated by

$$\log\eta = a + b\log\dot{\gamma} \qquad \text{Eq. [2.9]}$$

where η is viscosity, $\dot{\gamma}$ is shear rate, *a* is the intersect of the curve and *b* is the slope of the curve. It can be also written as

$$\eta = K\dot{\gamma}^{b} \qquad \text{Eq. [2.10]}$$

where $K = \exp(a)$. Instead of *b*, (*n-1)* is commonly used for the exponent and write result for the apparent viscosity as follows.

$$\eta = K\dot{\gamma}^{n-1} \qquad \text{Eq. [2.11]}$$

Upon using the connection among the shear stress, apparent viscosity, and the shear rate the power-law model is obtained.

$$\tau = K\dot{\gamma}^{n} \qquad \text{Eq. [2.12]}$$

where *n* is called the power-law index. It is an important fact that *n* =1 corresponds to Newtonian behavior. Typically, for shear thinning fluids, it lies between 1/3 and, 1/2 and for shear thickening fluids, it is higher than 2 [58]. Solutions having power law index near 1 (between 1.1- 0.9) can be accepted as Newtonian behavior.

It is well known that non uniform films are expected from spinning non-Newtonian fluids. Non-Newtonian solutions change their viscosities depending on what shear rate is used, thus depending on distance from the center, the shear rate will be different and thus the flow behavior. This can give radial thickness variation that varies rather smoothly in a radial sense.

CHAPTER 3

EXPERIMENTAL PROCEDURE

In this study, magnetite thin films were prepared by spin-coating the solutions on glass substrates. The thickness of the films was adjusted by changing the spinning rate of the spin coater. In order to increase the thickness of the films further, coating step was repeated until the desired thickness is achieved. To obtain magnetite phase in the films, sintering process was performed at different temperatures and for different times. Properties of the solutions were investigated by viscosity measurements and differential thermal analysis (DTA). The characterization of the films was performed by XRD, SEM, FESEM, UV-VIS, VSM, AFM and TEM.

3.1. Solution Preparation

Iron (III) nitrate [$Fe(NO_3)_3 \cdot 9H_2O$] was used as the main precursor in this study. Coating solution was prepared by dissolving iron (III) nitrate ($Fe(NO_3)_3 \cdot 9H_2O$) in ethylene glycol. 14 grams of iron (III) nitrate was dissolved in 55 grams of ethylene glycol in a erlenmeyer flask which was optimized for allow N_2 gas flow. Solution was heated to 80 °C for 2 h in N_2 gas flow under continuous stirring. During stirring, iron nitrate was dissolved in the solvent. This solution is named S1. The flow diagram of the preparation of solution S1 is shown in Figure 3.1.

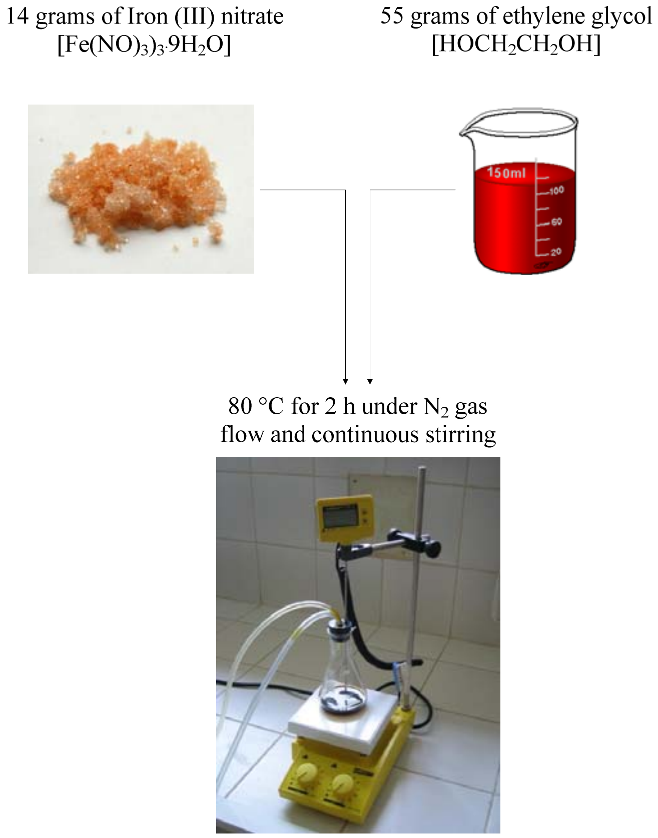

Figure 3.1 The flow diagram of the preparation of solution S1.

For observing the behavior of different starting materials, four different solutions were prepared during the study. In the first one, which will be called S2 from now on, $FeCl_2 \cdot 4H_2O$, citric acid monohydrate, ascorbic acid and ethanol absolute were used as starting materials. In this solution, $FeCl_2 \cdot 4H_2O$ was the raw material and citric acid monohydrate was the chelating reagent. Ascorbic acid and ethanol absolute were used as antioxidant agent and solvent, respectively. For obtaining the coating solution 0.1 mol $FeCl_2 \cdot 4H_2O$, 0.1 mol citric acid monohydrate and 0.1 ml antioxidant agent were dissolved in 100 ml ethanol absolute. This mixture was stirred at 60 ºC for 6 h. Then as a drying chemical control agent, 0.1 ml N, N-dimethylformamide was added to the solution. Finally, solution was stirred for half an h at 60 ºC [28].

Second solution, S3, was obtained by mixing the 0.01 mol $Fe(NO_3)_3 \cdot 9H_2O$, 0.03 mol dimethylamineborane (DMAB) and 100 ml distilled water. The solution was obtained by stirring the solution at room temperature until the color of the solution becomes colorless [53].

For the third solution, S4, 0.005 mol $Fe(NO_3)_3 \cdot 9H_2O$, 0.02 mol citric acid monohydrate and 0.05 mol of ethylene glycol were dissolved in 100 ml of distilled water. The molar ratio of Fe ion: citric acid: ethylene glycol = 1:4:10 in the solution. This solution was stirred and heated until the gas evolution was observed. In the resulting solution, there exists a complex between iron (III) ions and the polyether formed from citric acid and ethylene glycol. Then this complex was dissolved in methanol to obtain a coating solution [59].

For the fourth solution, S5, 0.3 M iron (III) nitrate hydrate was dissolved in a mixture of 2-methoxyethanol (MET) and acetylacetone in a molar ratio of 20:2. Mixture was mixed at room temperature for 2 h prior to obtaining coating solution [60].

In this study only the main solution (S1) was used for obtaining magnetite thin films. Other prepared solutions were not satisfactory in film formation. Adhesion of the films to the substrates was rather weak for the samples prepared by these solutions. Because of this, only the first solution was investigated further.

3.2. Preparation of Magnetite Thin Films

3.2.1. Substrates

In this study, pre-cleaned macroscopic slides (ordinary soda-lime glasses) were used as substrates for the thin films. Substrates such as MgO, $MgAl_2O_4$, quartz and platinum were used for magnetite thin film deposition so far. Glass substrates have many benefits over other substrates used in literature. Being inexpensive, relatively low temperature coating, quick and simple etchings are the advantages of glass substrates. In the near future, digital storage technology is going to use glass substrates for data storage in hard disk drives. Therefore, film deposition on these substrates will be quite important in the near future. For example IBM, introduced new glass substrate design for its industry [37].

To reduce the possibility of disk drive errors, improve data accuracy rates and increase data availability, glass substrates are started to be manufactured for disks. When magnetic films are applied on top of the substrate, film structure follows the same disk surface pattern of microscopic peaks and valleys hence increasing the possibility of minor read-back errors. Better surface finish and increased hardness of glass results in a more rugged disk with better performance and reliability [37].

Another improvement by these substrates is the decreasing fly height margin. Minimizing the interaction between the read/write head and the disk surface can improve the accuracy of drive operation. The physical properties of the disk substrate also have a significant impact on overall disk performance. The disks are part of a dynamic environment involving many materials with different properties of thermal expansion. As the disk rotate in the drive and the internal temperature increases any unpredictable movement of the disk may happen and this increases the potential problems. Using a more rigid disk material such as glass reduces the amount of unpredictable movement of the disk thereby increases drive robustness [37].

3.2.2. Preparation of the Substrates

In this study, it is crucial to obtain crack free and homogenous thin films with smooth surfaces. Magnetic, electronic and optical properties of the films mainly depend on the surface properties of the films. If film surface is homogenous and crack free, optimum properties can be achieved. Also roughness of the boundaries between the film layers affects these properties. The properties and microstructures of the films are affected by the details of coating procedure. Substrate, film material, substrate surface and experimental conditions are the major subjects [35].

As said before, ordinary cover glasses were used as substrates for the thin films. Before cleaning the substrates, they were cut into desired shapes, mostly 2.5x2.5 cm^2 and 1x1 cm^2. But any shape and size can also be coated by sol-gel process.

Because of the importance of the growth and adhesion on the films formation, smooth substrate surfaces must be used in film production. Therefore substrate surface must be prepared before the coating procedure. Two methods were used to clean substrates in this study.

In the first method, which will be called AC method from now on, substrate surfaces were etched by piranha solution. This method is complicated and takes longer times to obtain clean substrates. Substrate surfaces were etched by piranha solution which contains hydrogen peroxide and sulphuric acid with a volume ratio of 1:5. In this method, 1 vol% detergent solution was prepared and formerly cut glass substrates were rinsed into it. Then by an ultrasonic system, 15 min of ultrasonic cleaning was performed. After ultrasonic cleaning, substrates were washed by distilled water. Washed substrates were rinsed in the piranha solution for 24 h. After 24 h, substrates were carefully taken out and washed by distilled water. For the final cleaning; substrates were rinsed into acetone and ultrasonic cleaning step was performed again. In the Figure 3.2, preparation steps can be seen.

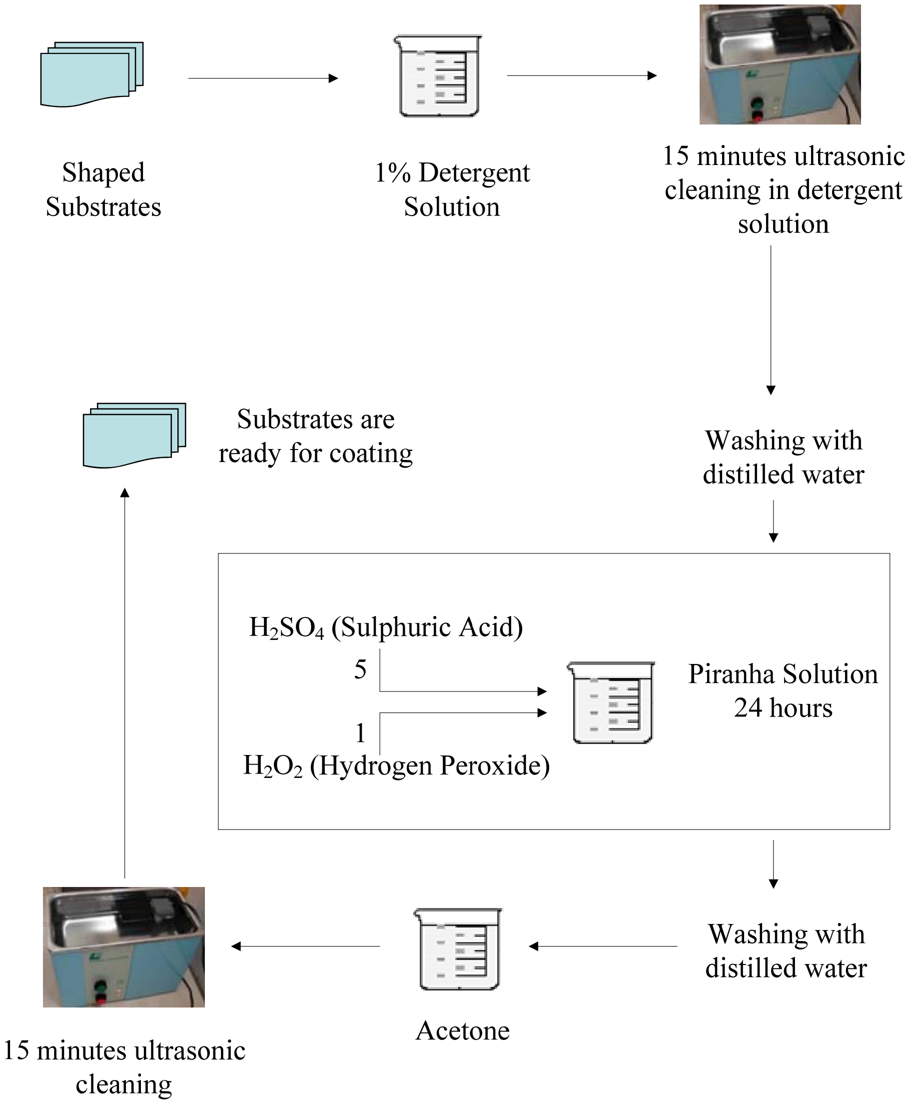

Figure 3.2 Piranha etching method (AC).

In the second method, which will be called DC method from now on, substrates were rinsed in a 5 wt% NaOH solution with distilled water and ultrasonic cleaning procedure was applied. Then substrates were rinsed in distilled water and ultrasonic cleaning was applied again followed by rinsing of the substrates in 1 wt% HCl solution with distilled water and ultrasonic cleaning. Finally substrates were rinsed in distilled water and cleaned ultrasonically. Between each step substrates were washed using distilled water. Substrates can be kept in ethanol absolute prior to use. In the Figure 3.3 preparation steps can be seen.

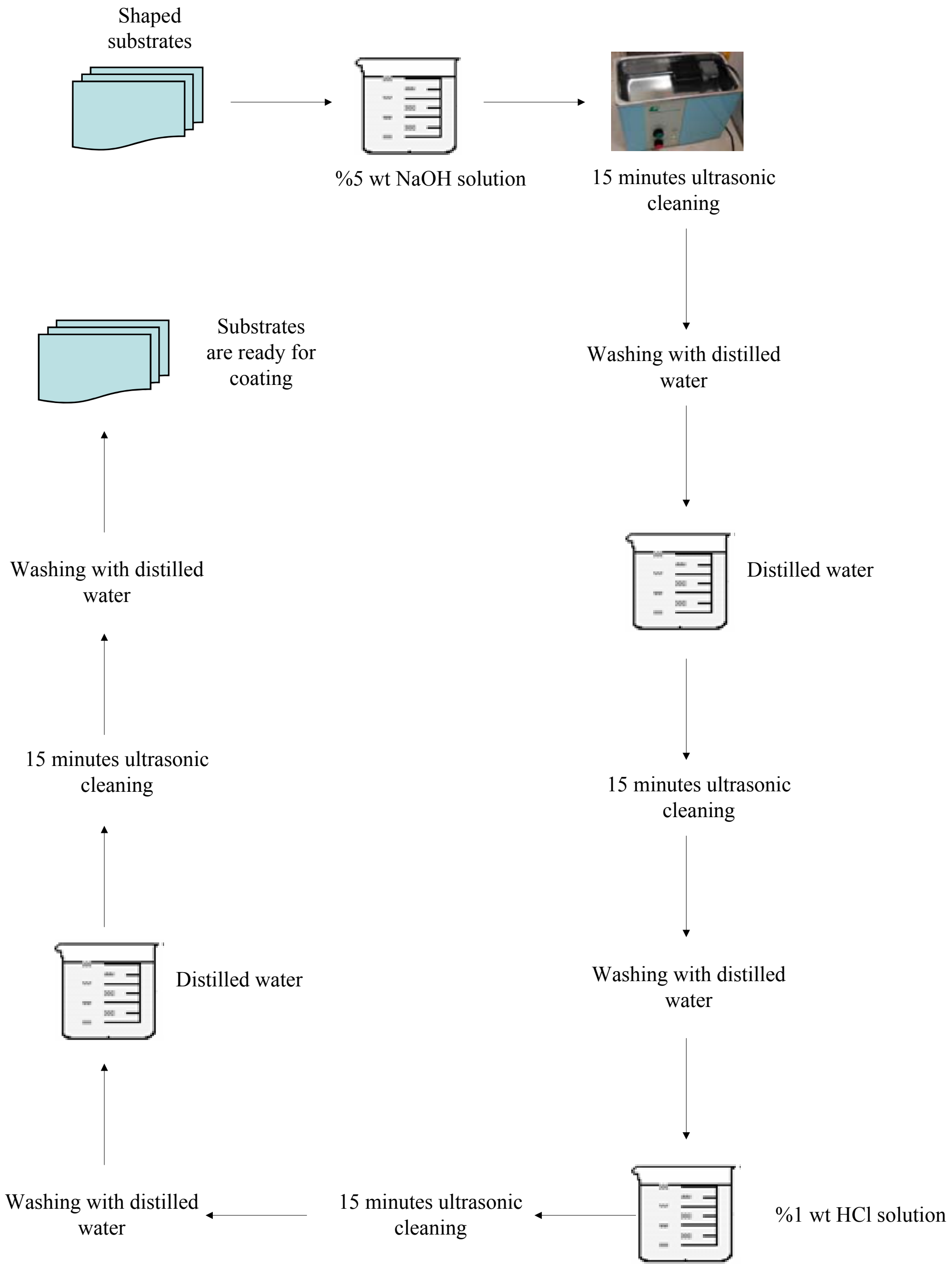

Figure 3.3 DC substrate cleaning method.

3.2.2.1. Piranha Solution

Piranha solution was described in detail by Karakuşcu et al. [35].

Piranha is a trade name for a chemical mixture consisting of sulphuric acid (H_2SO_4) and hydrogen peroxide (H_2O_2). Because the mixture is a strong oxidizer, it will remove most organic matter, and it will also hydroxylate most surfaces, making them extremely hydrophilic. Many different mixture ratios are commonly used and they are all called as piranha.

There are two main applications for piranha solution. Firstly, it is used to remove organic contaminants from the surface of the substrate during cleaning sequences. Secondly, it is used to strip photoresist from the surface of the substrate.

The effectiveness of piranha solution in removing organic residues is due to two distinct processes that operate at noticeably different rates. The first and faster process is the removal of hydrogen and oxygen as units of water by the concentrated sulphuric acid. This occurs because hydration of concentrated sulphuric acid is thermodynamically strongly favorable, with a ΔH of -880 kJ/mol. It is this rapid dehydrating property, rather than acidity itself, that makes both concentrated sulphuric acid, and so piranha solution, very dangerous to handle.

The dehydration process exhibits itself as the rapid carbonisation of common organic materials, especially carbohydrates, when immersed in piranha solution. Piranha solution was named in part for the vigour of this first process, since large quantities of organic residues immersed piranha solution are dehydrated so violently that the process resembles a piranha feeding frenzy. The second and more definitive rationale for the name, however, is the ability of piranha solution to "eat anything," including in particular elemental carbon in the form of soot or char.

This second and far more interesting process can be understood as the sulphuric-acid boosted conversion of hydrogen peroxide from a relatively mild oxidizing agent to dissolve elemental carbon, a material that is notoriously resistant to room temperature aqueous reactions. This transformation can be viewed as the energetically favourable dehydration of hydrogen peroxide to form hydronium ions, bisulfate ions, and, transiently, atomic oxygen.

$$H_2SO_4 + H_2O_2 \longrightarrow H_3O^+ + HSO_{4^-} + O \qquad \text{Eq. [3.1]}$$

It is this extremely reactive atomic oxygen species that allows piranha solution to dissolve elemental carbon. Carbon allotropes are difficult to attack chemically because of the highly stable and typically graphite-like hybridized bonds that surface carbon atoms tend to form with each other. The most likely route by which piranha solution disrupts these stable carbon-to-carbon surface bonds is for an atomic oxygen first to attach directly to a surface carbon to form a carbonyl group.

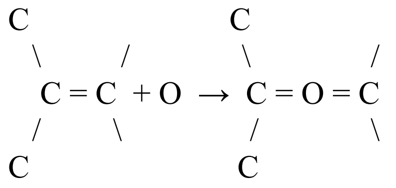

$$\begin{array}{lllllllll} \mathrm{C} & & & & & \mathrm{C} & & & \\ \backslash & & / & & & \backslash & & & / \\ \mathrm{C} & = & \mathrm{C} & + \mathrm{O} & \rightarrow & \mathrm{C} & = \mathrm{O} = & & \mathrm{C} \\ / & & \backslash & & & / & & & \backslash \\ \mathrm{C} & & & & & \mathrm{C} & & & \end{array} \qquad \text{Eq. [3.2]}$$

In the above process, the oxygen atom in effect "steals" an electron bonding pair from the central carbon, forming the carbonyl group and simultaneously disrupting the bonds of the target carbon atom with one or more of its neighbours. The result is a cascading effect in which a single atomic oxygen reaction initiates significant "unraveling" of the local bonding structure, which in turn allows a wide range of aqueous reactions to affect previously impervious carbon atoms. Further oxidation, for example, can convert the initial carbonyl group into carbon dioxide and create a new carbonyl group on the neighbouring carbon whose bonds were disrupted.

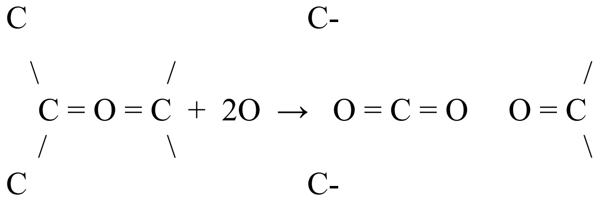

$$\begin{array}{lllll} \mathrm{C} & & \mathrm{C-} & & \\ \;\backslash \quad\quad / & & & & \quad / \\ \mathrm{C=O=C} & + 2\mathrm{O} \rightarrow & \mathrm{O=C=O} & & \mathrm{O=C} \\ \;/ \quad\quad \backslash & & & & \quad \backslash \\ \mathrm{C} & & \mathrm{C-} & & \end{array}$$

Eq. [3.3]

The carbon removed by piranha solution may be either original residues or char from the dehydration step. The oxidation process is slower than the dehydration process, taking place over a period of minutes. The oxidation of carbon exhibits itself as a gradual clearing of suspended soot and carbon char left by the initial dehydration process. In time, piranha solutions in which organic materials have been immersed typically will return to complete clarity, with no visible traces of the original organic materials remaining.

A final minor contribution to the piranha solution cleaning is its high acidity, which dissolves deposits such as metal oxides and carbonates. However, since it is safer and easier to remove such deposits using milder acids, piranha solution is more typically used in situations where high acidity complicates cleaning instead of assisting it. For substrates with low tolerance for acidity, the alkaline oxidising solution known as base piranha can be used instead.

3.2.3. Spin Coating

The spin coating process was performed by using a spin coater (Chemat Technology KW-4A). After solution preparation, spin coating was performed onto cleaned glass substrates. With the help of a double sided tape, cleaned small substrates with different sizes were stuck onto the head of spin coater. Excess amount of solution was poured onto the substrates by using pasteur pipettes.

By changing the spinning rate of the spin coater, thickness of the films can be adjusted. In this study, films were coated at 1500, 4000 and 5000 rpm for 60 seconds. For obtaining crack free and homogenous films, very thin films were prepared. In order to obtain thicker films, individual coating steps were repeated. After each coating step, drying was performed and when desired thickness achieved, sintering was performed as the final step. When the thickness of the films increases and reaches to a critical value, cracks on the film surfaces were observed due to the shrinkage during sintering.

3.2.4. Heat Treatment of Thin Films

Heat treatment of thin films begins with the drying step. Drying temperature was decided according to the boiling temperature of the solvent. Since the boiling temperature of the ethylene glycol is 197 ºC, drying temperature is chosen as 110 ºC which is less than 197 ºC and also enough for the removal of water. The most important part of this process is the shrinkage due to removal of water. In order to reduce the shrinkage, the drying furnace is pre-heated to 110 ºC before drying. Specimens were fired at this temperature for 15 minutes. Between each layer, drying step was performed until the desired thickness is obtained. Figure 3.4 shows the followed route starting from the solution preparation step to heat treatment processes.

Sintering is the final heat treatment procedure. The purpose of sintering is changing the as-dried amorphous thin films into crystalline thin films. Sintering procedure was performed in a tube furnace under N_2 atmosphere with a 3 ºC/min heating rate. Slow heating rate is important to avoid the crack formation during heating.

Another important parameter is the cooling rate. Due to rapid oxidation of magnetite to maghemite at high temperatures, which was discussed by Da Costa et al. [61], samples were allowed to cool slowly inside the tube furnace under N_2 atmosphere.

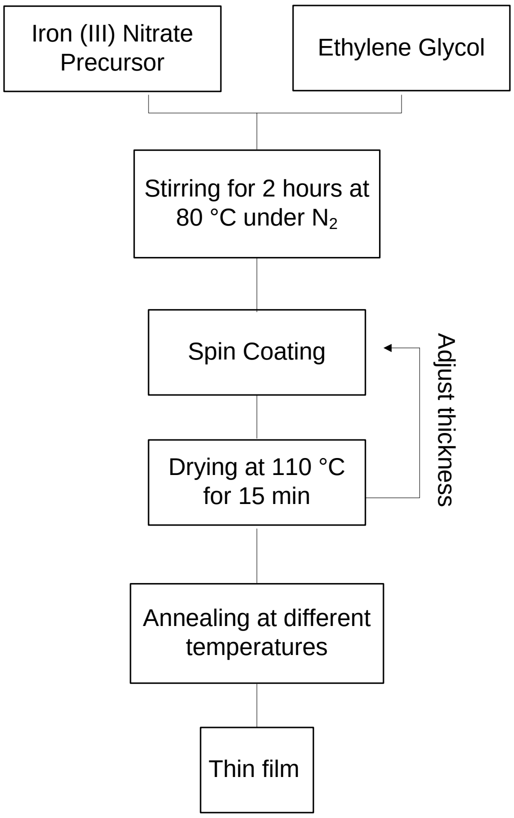

Figure 3.4 The flow chart for the processing of thin films.

For observing the effect of temperature on film formation, five distinct temperatures; 250 ºC, 300 ºC, 350 ºC, 400 ºC, 450 ºC, were used in sintering. Sintering duration was chosen as 2 h and 3.5 h.

The thickness of the magnetite thin films and its effects on the film formation were also observed during this study. Thickness of one layered films was controlled by changing the spinning rate. One to twenty layered thin films were studied to observe the effect of thickness on microstructure and properties of thin films.

For the solution S5, only sintering step was performed and coated substrates were sintered at 300 ºC for 1 h in air atmosphere. Sintering in nitrogen atmosphere was also tried for this solution but film formation was not satisfactory in these experiments. Therefore only air atmosphere was used for sintering thin films obtained from this solution.

3.3. Characterization of Solution

Solution properties should be taken into account for obtaining reliable information on magnetite thin film formation. For this reason viscosity and thermal analysis of the solution was investigated.

3.3.1. Viscosity

Viscosities of the solutions were measured by TA Instruments ARES Rheometer. This instrument provides controlled strain for both oscillatory and steady shear measurement in parallel plate and cone-and plate geometries. In the system, lower plate is driven by a motor, in either steady rotation or oscillation, while the upper plate is connected to a transducer, which measures torque and normal force [62]. Viscosity is an important parameter because homogeneity and smoothness of thin films were determined by viscosity and applied strain relationship.

3.3.2. DTA

Differential thermal analysis (DTA) is a thermal technique and in this technique, heat effects which are related to the physical or chemical changes, are recorded as a function of temperature or time while the substrate is heated at a uniform rate. Heat or enthalpic changes, whether exothermic or endothermic, which are caused by phase transitions, such as crystalline structure inversions, dehydration reactions, dissociation reactions or decomposition reactions and chemical reactions. Phase transitions, dehydration, reduction and some decomposition reactions produce endothermic effects, whereas crystallization, oxidation, and some decomposition reactions produce exothermic effects [54].

DTA studies were conducted by Simultaneous Thermogravimetric Analyser and Differential Thermal Analyser (SETARAM) in Central Laboratory at METU. Main solution (S1) was dried in 110 ºC for 24 h in order to obtain gel powder. DTA analysis was performed from room temperature to 500 ºC with a heating rate of 3 ºC/min.

3.4. Characterization of Magnetite Thin Films

3.4.1. Structural and Morphological Analysis

X-Ray diffraction (XRD) analyses were performed by using Rigaku D/MAX 2200/PC Diffractometer for conventional diffraction and Rigaku TTRAX III Diffractometer for both conventional and in-plane glazing angle diffractions. XRD analysis were performed between angles of 10º-80º (2θ) with Cu(K_α) radiation. Thickness and surface roughness analysis was also made by using Rigaku TTRAX III Diffractometer by reflectivity measurements. Two methods were used for X-ray diffraction analyses. In the first method conventional Bragg-Brentano parafocusing method was used whereas in the second method grazing incidence in-plane XRD method was used. This second technique was done in Rigaku Laboratories in Japan using Rigaku TTRAX III diffractometer.

In the standard diffraction methods such as Bragg-Brentano diffraction method, X-rays penetrate to a certain depth into the sample and it measures the intensities of diffractions from lattice planes which are parallel to the sample surface. However if the sample thickness is extremely small, than no diffraction signal can be measured, because of the complete transmission of X-rays through the sample. In these circumstances in-plane diffraction is used.

The conventional Bragg diffraction is used to determine the crystallographic orientation, morphology, particle size and lattice parameters of thin films and the lattice mismatches and strain between the thin films and substrates. But grazing incidence diffraction (GIXD) provides in-plane quasi-two dimensional surface and interface structures [63].

In this technique, the beam is incident at a grazing angle. This results in the penetration depth of the X-rays to be smaller than 100 nm from the surface. The path length of the incident X-ray beam through the film is increased and so, the intensity from the film is increased also.

When the incident beam is close or below the critical angle for total external reflection, a Bragg reflection is excited from planes perpendicular to the surface [64]. Figure 3.5 shows the in-plane grazing incidence XRD geometry.

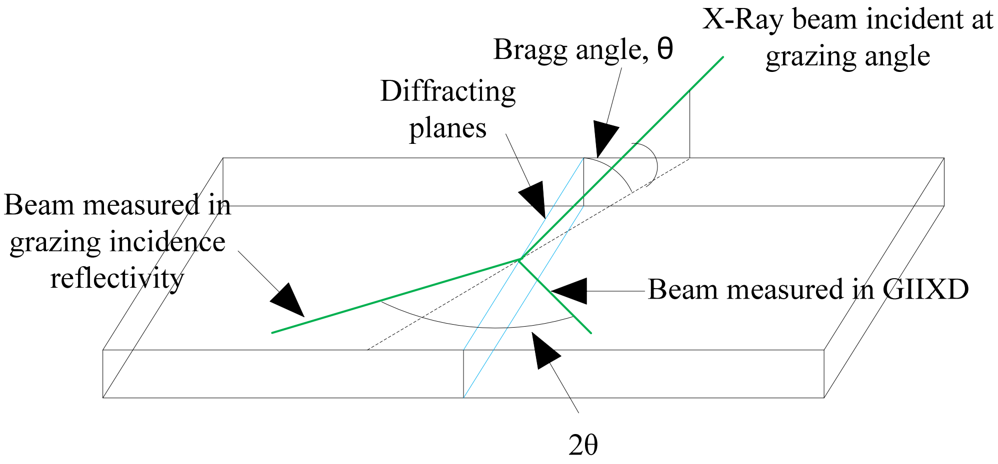

Figure 3.5 In-plane grazing incidence XRD geometry setup [65].

In the Figure 3.6 and 3.7, grazing incidence XRD schematic representation can be seen. In the one-beam case; the incident beam with the wave vector $\overrightarrow{k_O}$ is impinging on a crystal at a grazing angle α. If there are no atomic planes which satisfy Bragg's diffraction condition; only the forward diffracted beam of the wave vector $\overrightarrow{K_O}$ transmits through the crystal. This diffracted beam is reflected by the crystal surface along the wave vector, $\overrightarrow{k_O^S}$. In the two-beam case; the intensity of the $\overrightarrow{k_G^S}$ beam is measured while α - 2α scan (or θ -2θ scan) continuing. If the rotation of the crystal by α angle, together with the rotation of the detector by 2α angle is handled, this is called as reflectivity measurement. If the crystal is aligned in such a way that a given set of atomic planes (G) of the crystal is in position to diffract the grazing incident beam, the reflected beam by the atomic planes G along the wave vector $\overrightarrow{K_G}$ is generated inside the crystal. The accompanied beam of the wave vector $\overrightarrow{k_G^S}$ is specularly reflected by the crystal surface toward the exterior of the crystal. In the three beam case, the diffracted beams inside the crystal along the $\overrightarrow{K_O}$, $\overrightarrow{K_G}$, $\overrightarrow{K_L}$ are specularly reflected in the $\overrightarrow{k_O^S}$, $\overrightarrow{k_G^S}$, $\overrightarrow{k_L^S}$ directions, respectively. In all cases the intensities of the specularly reflected beams are measured [63].

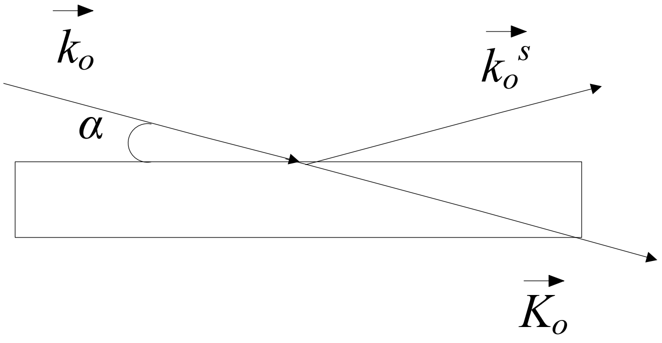

Figure 3.6 One-beam case [63].

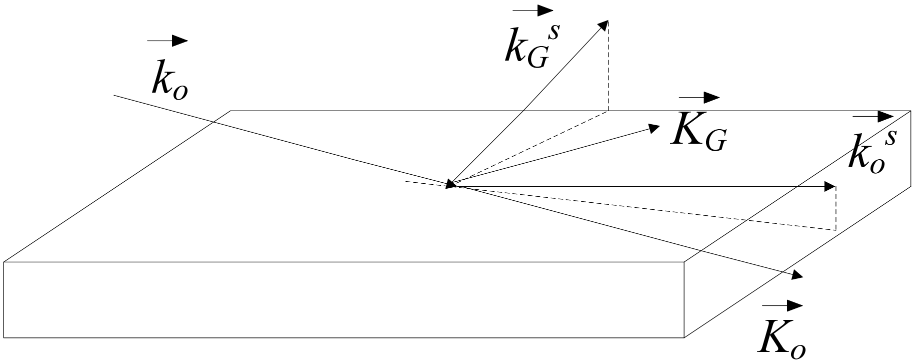

Figure 3.7 Two-beam case [63].

In the conventional method; X-ray source and the detector slit are at the focal points of the incident and diffracted beams, respectively. In the thin film arrangement, the incident and diffracted beams are made nearly parallel. This is made by using a narrow slit on the incident beam and a long soller slit on the detector side. Also, incident beam makes a very small angle with the film surface. This increases the path length of the X-ray beams through the film, which results an increase in diffracted intensity and a reduction in diffracted intensity from film. During the collection of diffraction spectrum, only the detector rotates through the angular range. So incident angle, beam path length and irradiated area are keep constant [66].

Chemical, microstructural analysis, thickness and surface of the magnetite thin films were investigated by JEOL JSM-6400 Scanning Electron Microscope (SEM) equipped with an Energy Dispersive Spectrometer (EDS analyser) and by FEI Quanta 400 FEG Field Emission Scanning Electron Microscope (FESEM). Composition analyses were carried out from the surface of the films and thickness measurements were done by using the cross-section view of the samples. The morphology of the films was investigated by atomic force microscopy (AFM) (Nanosurf easy scan 2).

Electron diffraction studies were done by using a JEOL 2100 HRTEM Transmission Electron Microscopy (TEM).

3.4.2. Optical Analysis

Optical transmittance of the films was measured in Department of Chemistry at METU by Shimadzu 160 UV-VIS Spectrometer and in Metallurgical and Materials Engineering Department at METU by UV-1900 UV-VIS Spectrometer. Transmittance (%)-Wavelength (nm) curves were drawn in the range of 300 nm-1100 nm.

3.4.3. Magnetic Analysis

VSM measurements were done by using ADE Magnetics Model EV9 and Quantum Design Vibrating Sample Magnetometers. Hysteresis M-H curves were recorded at room temperature. In these measurements, specimen with a surface area 10 x 10 mm^2 was used and results were presented in terms of emu/g and emu/cm^3.

CHAPTER 4

RESULTS AND DISCUSSION

Aim of this study was to prepare crack-free and homogenous Fe_3O_4 thin films on glass substrates and investigate the experimental parameters. The adhesion of the film to the substrate, surface properties and crystalline phase of the films were taken into account to obtain best properties. Sintering temperature, sintering time and thickness of the films were taken as experimental variables. The solution preparation and its properties were carefully taken into account because crack-free and homogenous film production is favored only in stable and homogenous solutions. DTA (Differential Thermal Analysis) and viscosity measurements were used in order to investigate solution properties.

After the investigation of solution properties, thin film properties were extensively studied. XRD of both in-plane and out-of-plane measurements were done in order to structurally characterize the thin films. SEM (Scanning Electron Microscopy), FESEM (Field Emission Scanning Electron Microscopy) and TEM (Transmission Electron Microscopy) were used to characterize thin films chemically and also microstructural analysis, thickness and surface of magnetite thin films were investigated by these methods. For optical analysis; UV-VIS spectroscopy was used and VSM (Vibrating Sample Magnetometer) was used for magnetic property characterizations. Thin film morphology was investigated by AFM (Atomic Force Microscopy).

Experimental details of the samples prepared in this study were given in Table 4.1.

Table 4.1 Experimental details of the sample preparations used in this study.

Spin Coating Speed	Solution	Drying	Heat Treatment Applied	No. of Layers	Atmosphere	Sample no.
4000 rpm	S1	110 °C 15 min	300 °C for 2 h	6	Nitrogen	5
4000 rpm	S1	110 °C 15 min	300 °C for 2 h	3	Nitrogen	7
4000 rpm	S1	110 °C 15 min	350 °C for 2 h	3	Nitrogen	9
4000 rpm	S1	110 °C 15 min	380 °C for 2 h	1	Nitrogen	18
4000 rpm	S1	110 °C 15 min	450 °C for 2 h	1	Nitrogen	20
4000 rpm	S1	110 °C 15 min	300 °C for 2 h	15	Nitrogen	24
4000 rpm	S1	110 °C 15 min	300 °C for 2 h	20	Nitrogen	25
4000 rpm	S1	110 °C 15 min	400 °C for 2 h	1	Nitrogen	30
5000 rpm	S1	110 °C 15 min	300 °C for 2 h	1	Nitrogen	31
5000 rpm	S5	-	300 °C for 1 h	1	Air	32
5000 rpm	S1	110 °C 15 min	300 °C for 3.5 h	1	Nitrogen	33
4000 rpm	S5	-	300 °C for 1 h	1	Air	37
5000 rpm	S5	-	300 °C for 2 h	1	Air	41
2000 rpm	S5	-	300 °C for 1 h	1	Air	42
2000 rpm	S1	110 °C 15 min	300 °C for 2 h	1	Nitrogen	43
1500 rpm	S5	-	300 °C for 1 h	1	Air	44
2000 rpm	S1	110 °C 15 min	300 °C for 2 h	10	Nitrogen	45
2000 rpm	S1	110 °C 15 min	450 °C for 2 h	1	Nitrogen	47
2000 rpm	S1	110 °C 15 min	300 °C for 2 h	3	Nitrogen	50
2000 rpm	S1	110 °C 15 min	450 °C for 2 h	2	Nitrogen	51
5000 rpm	S1	110 °C 15 min	350 °C for 2 h	1	Nitrogen	52
2000 rpm	S1	110 °C 15 min	300 °C for 2 h	2	Nitrogen	53
2000 rpm	S1	110 °C 15 min	400 °C for 2 h	1	Nitrogen	54
5000 rpm	S1	110 °C 15 min	400 °C for 2 h	1	Nitrogen	55
5000 rpm	S1	110 °C 15 min	350 °C for 2 h	1	Nitrogen	56
2000 rpm	S1	110 °C 15 min	350 °C for 2 h	1	Nitrogen	57

4.1. Solution Properties

Solution preparation is the main step in thin film formation process, because if the prepared solution is homogenous, prepared thin films will also be homogenous, crack free and will have smooth surfaces. Therefore preparing homogenous solution is crucial for this study.

For the preparation of solutions there are many steps and many parameters which affect the solution quality. Atmospheric conditions such as the ambient atmosphere and pressure are important because if there are any undesired reaction between the gases in the atmosphere and precursors in the solution, undesired phases can be formed. Precursor selection is also important, because obtaining desired phases in the films is directly related to the precursor choice. Choosing compatible solvent with right solutes and solubility of solute in that solvent are important parameters for the precursor selection. Heating temperature is also an important parameter for solution preparation.

Viscosity of the solution is related to the homogenous thin film formation. It directly affects the homogeneity of the thin films. Viscosity of the main solution (S1) with respect to shear rate is given in Figure 4.1.

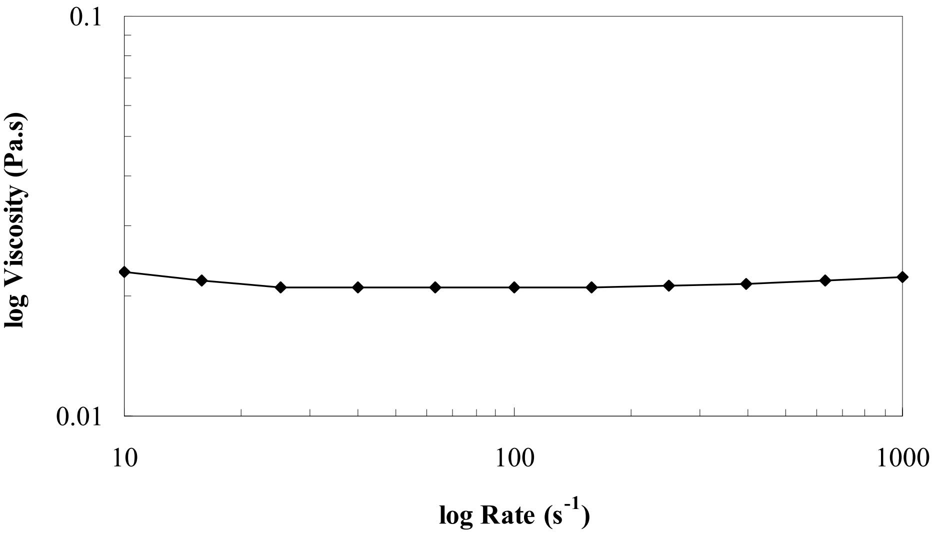

Figure 4.1 Viscosity change of main solution (S1) with respect to shear rate.

For the observation of main solution (S1) behavior, Power Law index value was calculated by using the Equation 2.9. Power Law index value was found as 1.0000007 between 10 and 10^3 shear rate values. Power Law index value is very close to 1, so the solution can be accepted as a Newtonian solution. Viscosity of this solution was found as approximately 0.0215 Pa.s.

For comparison of other solution behavior, viscosity of solution S5 was also discussed. The viscosity of solution S5 with respect to shear rate graph was given in Figure 4.2.

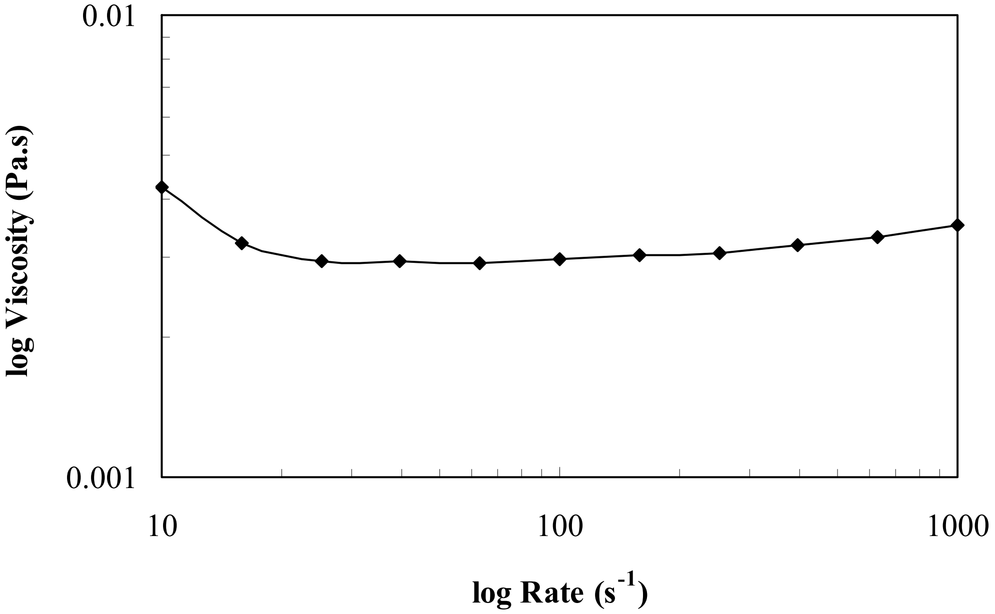

Figure 4.2 Viscosity change of solution S5 with respect to shear rate.

By applying the same procedure with (S1) power law index value was found to be as 1.0000002 and again it is very close to 1, so this solution can also be accepted as a Newtonian solution. Viscosity of this solution was around 0.0032 Pa.s.

Shear rate directly affects the spin coating process. In this thesis, spin coating process was performed at room temperature. So viscosity measurements must also be performed at room temperature. By viscosity measurements, it was found that viscosity of the main coating solution and also viscosity of solution S5 do not change with varying shear rate. So during spin coating process, viscosity of the solution does not change. Consequently, homogenous films can be obtained by using these solutions [35].

For observing the thermal properties of the coating solution, powder samples were obtained by drying the solution at 110 ºC for 24 h in a drying furnace. DTA analysis was performed from room temperature up to 500 ºC with a heating rate of 3 ºC/min. DTA curve for the coating solution is given in Figure 4.3. DTA curve shows 4 exothermic peaks. First exothermic peak at 179 ºC shows the decomposition of organometallic precursors. The second exothermic peak which is at 291 ºC shows the crystallization of magnetite phase. The third and the fourth exothermic peaks are observed at 369 ºC and 402 ºC respectively. These peaks show the phase transitions from magnetite to maghemite at 369 ºC and magnetite to hematite at 402 ºC.

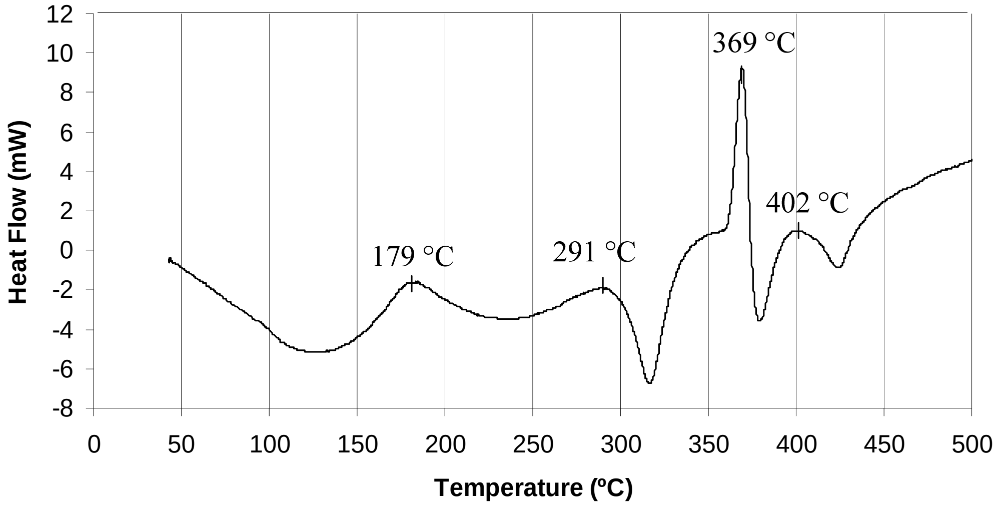

Figure 4.3 DTA curve of the powder sample from main solution (S1) which was obtained after drying at 110 °C for 24 h in air.

4.2. XRD Study of Powder Samples

Powder samples were obtained from main solution (S1) by drying at 110 ºC for 24 h in an ambient atmosphere followed by heat treatment and they were examined by XRD in order to investigate the magnetite and other phase formations at different sintering temperatures in nitrogen and air atmospheres.

XRD results of powders sintered at different temperatures but in the same atmosphere are shown in Figure 4.4. From the figure, it can be seen that at 250 ºC, no crystalline phase was observed. But when temperature was increased to 300 ºC, magnetite peaks were detected in X-ray spectrum. This result complies with DTA result which indicates that magnetite crystallization does not occur below 291 ºC. Up to 350 ºC, magnetite peaks continue to exist as the only phase in the structure. When the temperature was increased to 400 ºC, some maghemite peaks were observed with magnetite peaks and when the temperature was increased further to 450 ºC, hematite phase was also observed in the system together with maghemite.

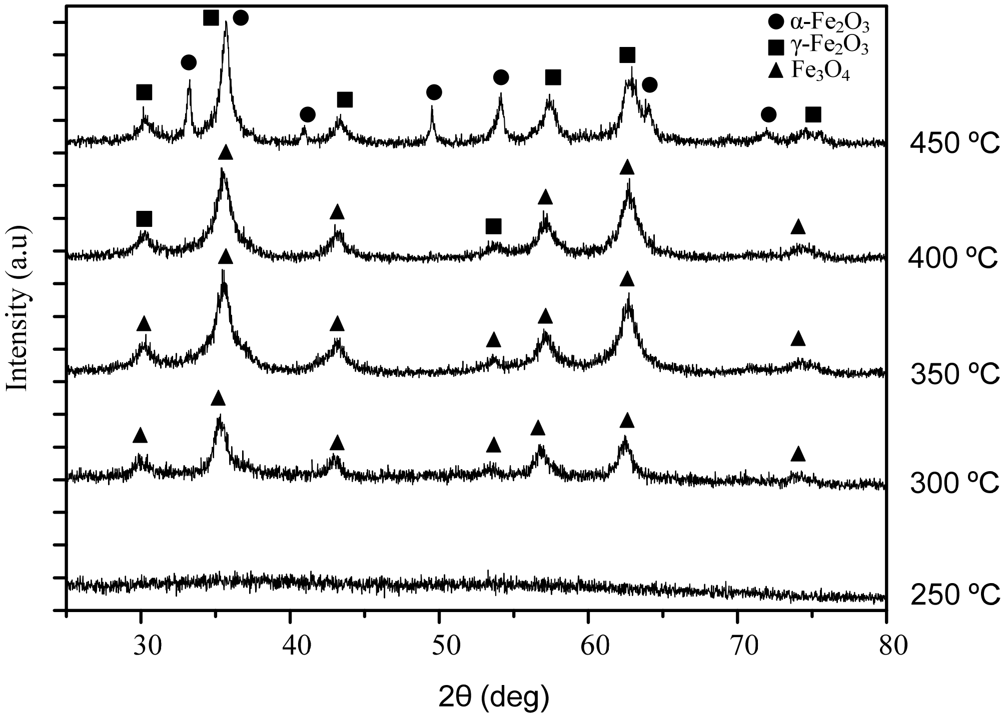

Figure 4.4 XRD patterns of iron oxide powders sintered at different temperatures.

In Figure 4.5; effect of sintering atmosphere on the phase formation is shown. Experimental parameters were kept constant as an sintering temperature of 300 ºC and sintering time of 2 h. The powders prepared in nitrogen atmosphere consist of only magnetite whereas only maghemite phase exist for the powders which were sintered in air.

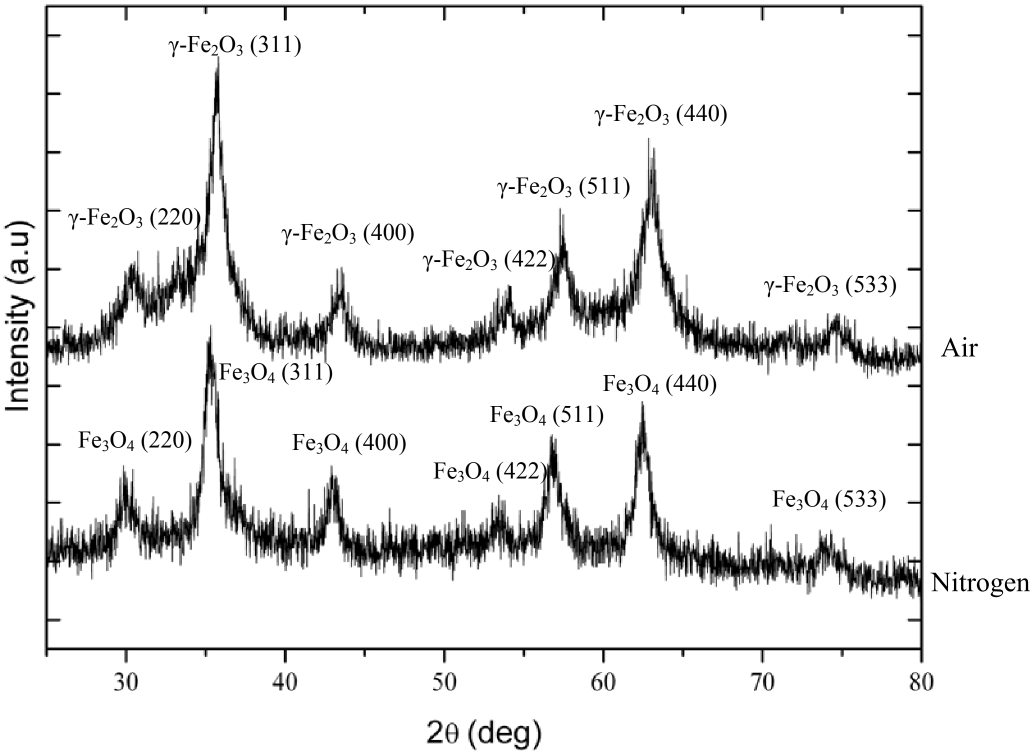

Figure 4.5 Effects of sintering atmosphere on XRD patterns of iron oxide powders sintered at 300 ºC for 2 h.

Particle size of the powder samples was calculated by using Scherrer's formula. It is a technique based on measuring the full width of X-ray diffraction peaks at the half maximum height of the peak.

$$t = \frac{0.94x\lambda}{Bx\cos\theta} \qquad \text{Eq. [4.1]}$$

In the Equation 4.1, t is the average particle size, λ is the wavelength of radiation of the X-ray beam used, B is the width of the peak at half of the maximum intensity (in radians) and θ is the half of the diffraction angle 2θ [35]. For the particle size determination, magnetite (311) peak, which was the most intense peak, was used.

In Table 4.2, calculated particle sizes for 300 ºC and 350 ºC sintering temperatures and 2 h of sintering time in nitrogen atmosphere, are shown.

Table 4.2 Approximate particle sizes of iron oxide powders obtained at different sintering temperatures.

$t = \dfrac{0.94x\lambda}{Bx\cos\theta}$	**Powder sintered at 300 ºC for 2 h in nitrogen atmosphere**	**Powder sintered at 350 ºC for 2 h in nitrogen atmosphere**
Approximate Particle Size	18.5 nm	51.6 nm

These results show that smaller particle sizes were obtained at lower sintering temperatures.

4.3. Thin Film Preparation

Preparation of the substrates is the main step in the thin film preparation. Substrates must be clean and active in order to be coated. Adhesion of the films on the substrates is one of the main criteria on the film formation. In this study, ordinary soda lime glasses were chosen as substrates. These substrates have many advantages over the other substrates used in the literature. Mainly it is simple and easy to obtain and use. It has also many benefits in magnetic data storage technology.

SEM image of the cleaned substrates prepared by different cleaning techniques are shown in the figures below. In Figure 4.6, SEM image of as-received glass substrate is given. As shown, the surface of this substrate contains many defects and dirts on the surface.

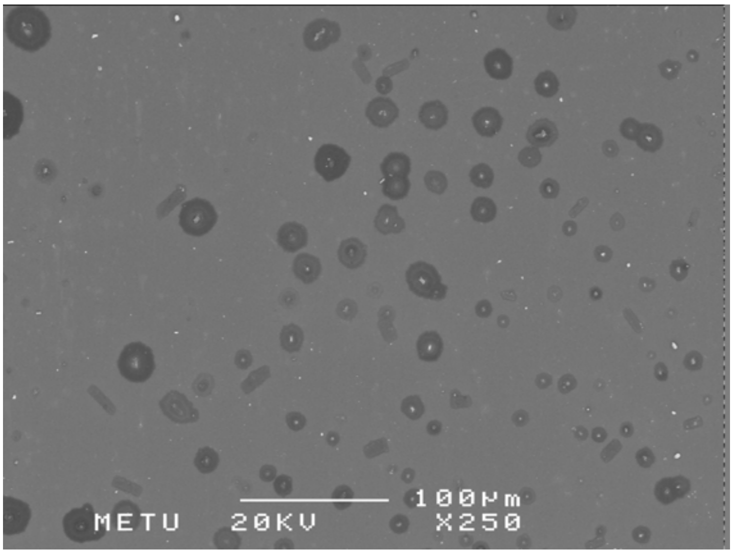

Figure 4.6 SEM image of as-received glass substrate.

In Figure 4.7, SEM image of substrates prepared and cleaned with AC cleaning method was given. Surface of this substrate is very smooth, free of dirts and other defects.

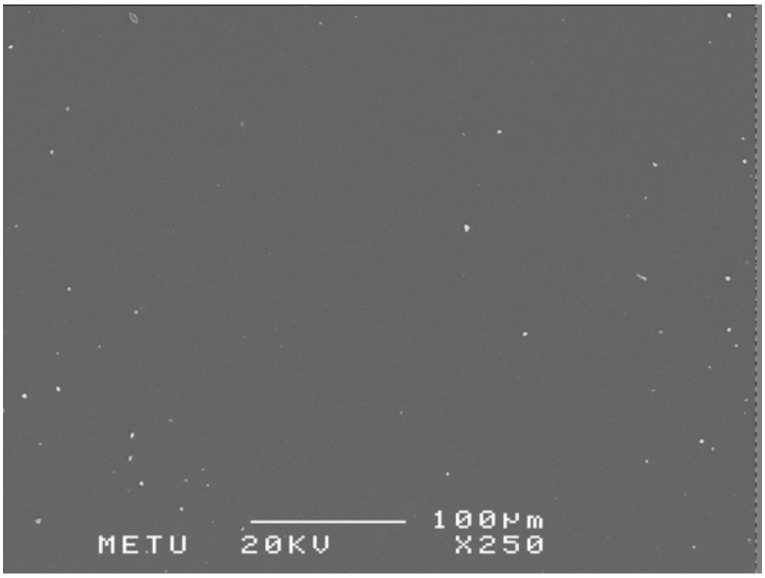

Figure 4.7 SEM image of cleaned substrate (with AC method).

Within the cleaned and prepared substrates, smoothest surface was obtained using DC cleaning method. In Figure 4.8, SEM image of this substrate was shown. There are less number of defects or dirts on this substrate.

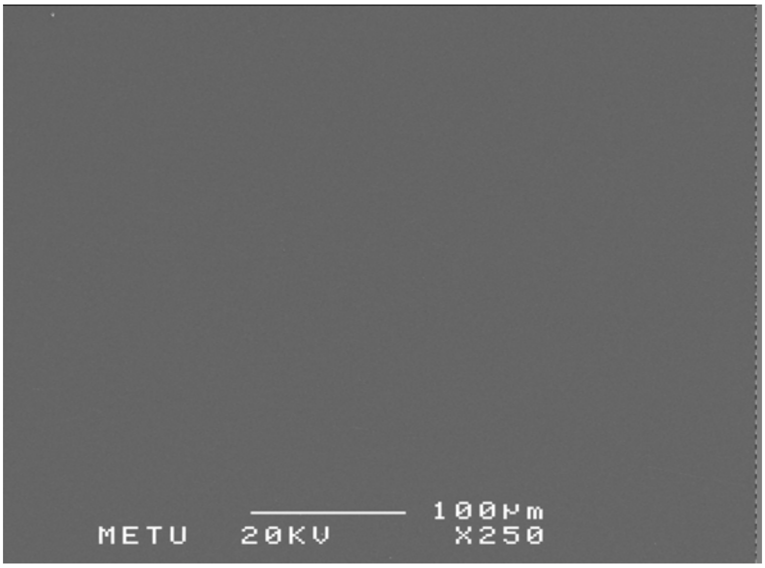

Figure 4.8 SEM image of cleaned substrate (with DC method).

As a result, smoothest surface is obtained using DC cleaning method. So, in this study, substrates were cleaned by using DC cleaning method. The EDS analysis of a substrate prepared by using DC cleaning method was shown in Figure 4.9. As it can be seen from EDS analysis, there is no unwanted chemicals left after cleaning process.

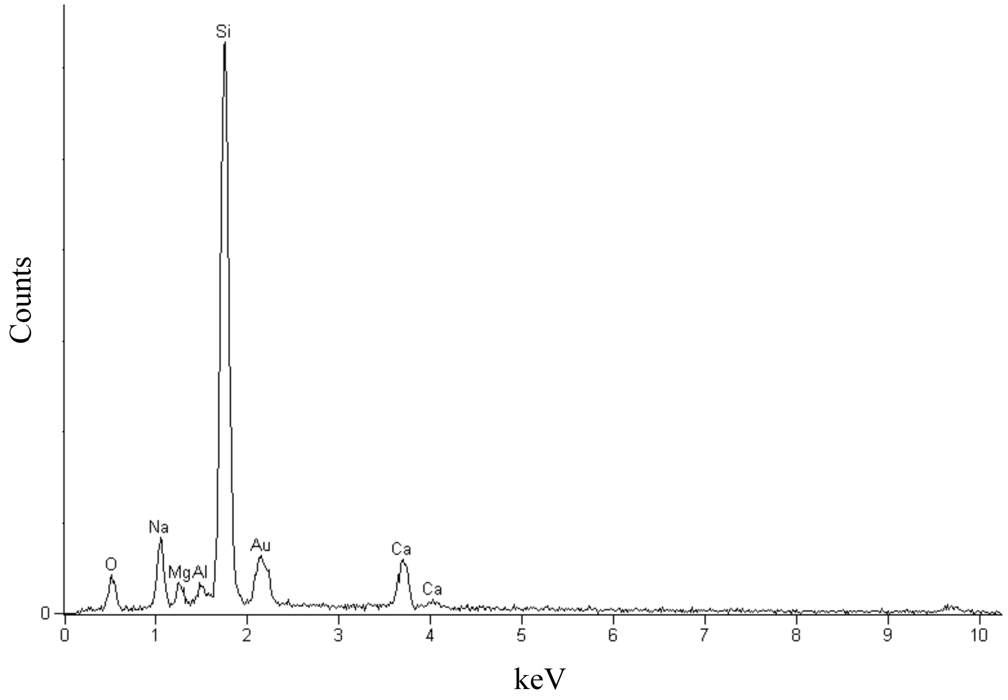

Figure 4.9 EDS analysis of cleaned glass substrate (with DC method).

4.4. Morphology of the Films

Surface morphology of thin films was studied by using SEM and AFM. Most of the deposited thin films have crack free and homogenous surfaces. Two different deposited films were shown in Figures 4.10 and 4.11. Figure 4.10 shows a film surface coated at 2000 rpm and sintered at 300 ºC for 3.5 h in nitrogen atmosphere and Figure 4.11 shows a film surface coated at 5000 rpm and sintered at 300 ºC for 2 h in nitrogen atmosphere. As it can be seen in these two figures, crack free and homogenous thin films were deposited by main solution (S1) in the study. In order to compare the film surfaces coated by using different solutions, SEM micrographs of thin films coated by solution S5 was shown in Figure 4.12. As it can be seen in the figure, surface of the film is not smooth and cracks can be observed. The film shown in Figure 4.12 was prepared at 5000 rpm and sintered at 300 ºC for 1 h in air.

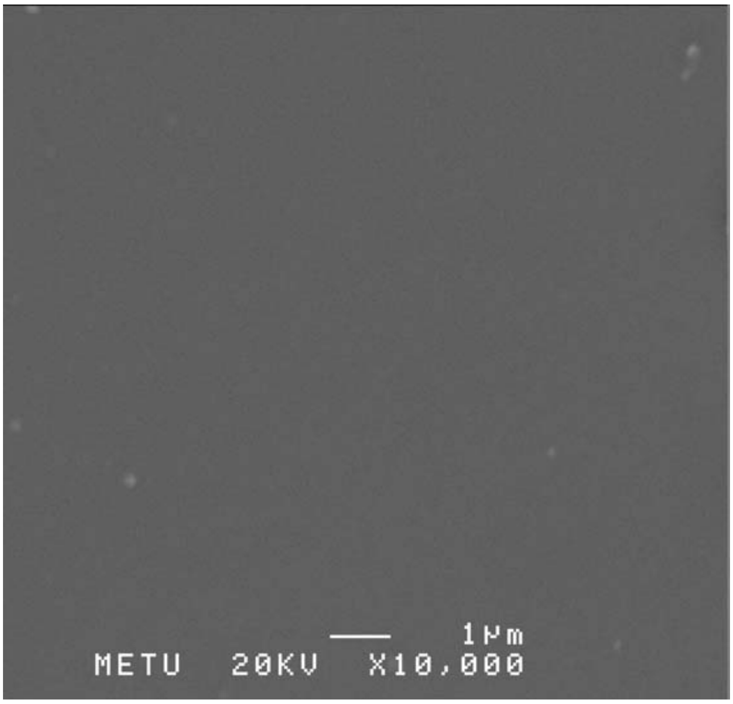

Figure 4.10 SEM image of a thin film prepared by main solution (S1) at 2000 rpm and sintered at 300 ºC for 3.5 h in nitrogen atmosphere.

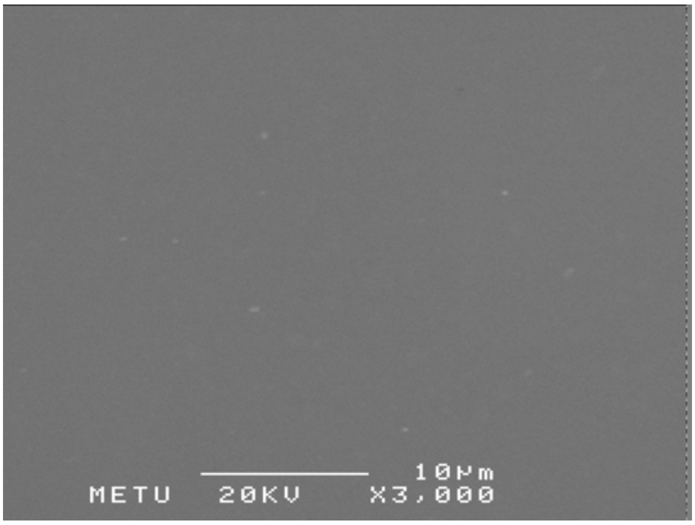

Figure 4.11 SEM image of a thin film prepared by main solution (S1) at 5000 rpm and sintered at 300 ºC for 2 h in nitrogen atmosphere.

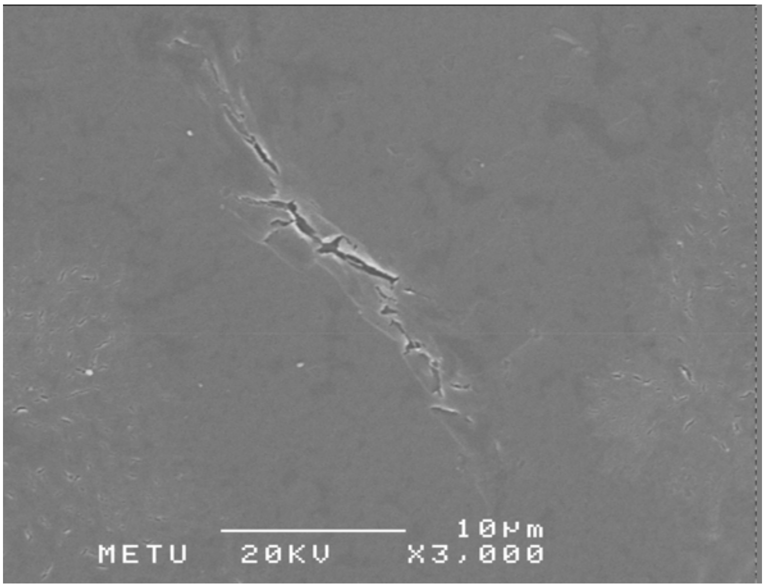

Figure 4.12 SEM image of a thin film prepared by solution S5 at 5000 rpm and sintered at 300 ºC for 1 h in air.

The sample shown in Figure 4.12 is prepared in air atmosphere and no drying step was performed for it. Observed crack may occur because of this reason [35].

By FESEM images, the homogeneity and crack freeness of the films were proven. FESEM image of a sample prepared at 1500 rpm and sintered at 300 ºC for 2 h in nitrogen atmosphere by main solution (S1) is given in Figure 4.13.

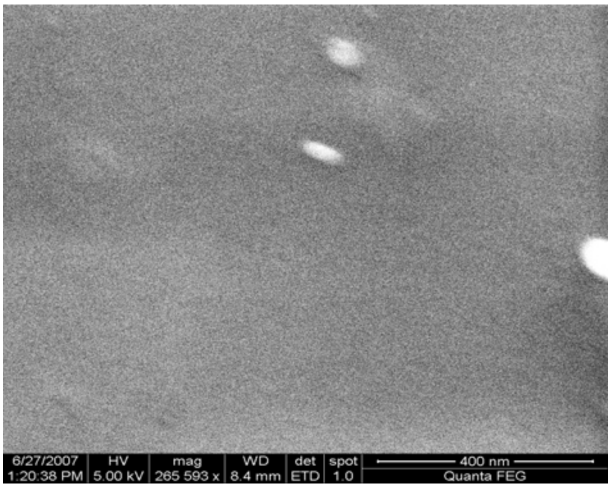

Figure 4.13 FESEM image of a thin film which was prepared by main solution (S1) at 1500 rpm and sintered at 300 ºC for 2 h in nitrogen atmosphere.

For the main solution (S1), the thicknesses of the thin films were estimated by using cross-sectional SEM images. Thickness of a one layered film prepared at 2000 rpm and sintered at 300 ºC for 2 h in nitrogen atmosphere, was estimated as ~100 nm. Cross sectional view of this sample is shown in Figure 4.14.

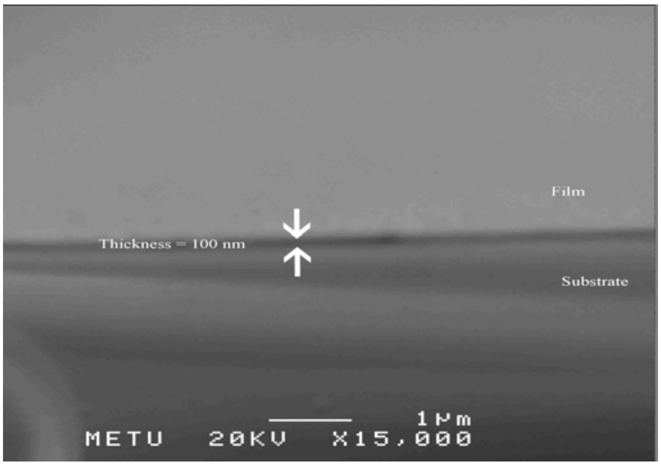

Figure 4.14 Cross sectional SEM image of a thin film prepared by main solution (S1) at 2000 rpm and sintered at 300 ºC for 2 h in nitrogen atmosphere.

Cross sectional SEM micrograph of the film prepared at 1500 rpm and sintered at 300 ºC for 2 h in nitrogen atmosphere is given in Figure 4.15. From the figure, it can be estimated that, thin films prepared at this condition have a thickness of ~180 nm.

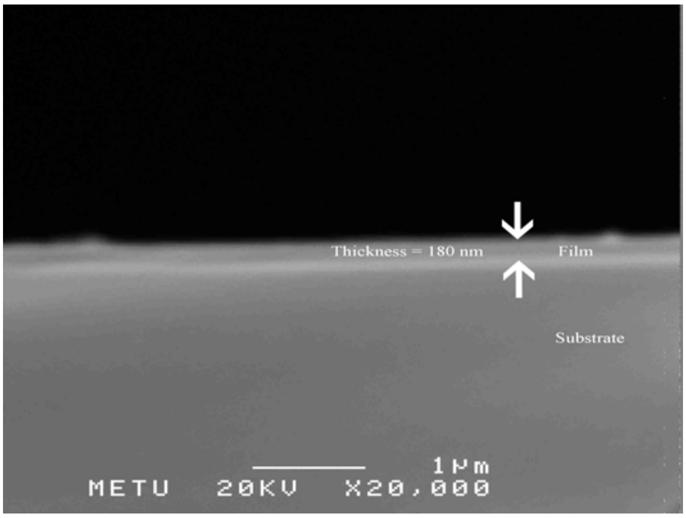

Figure 4.15 Cross sectional SEM image of a thin film prepared by main solution (S1) at 1500 rpm and sintered at 300 ºC for 2 h in nitrogen atmosphere.

Thicknesses of the thin films were also determined by taking cross sectional FESEM images. Thickness of a thin film prepared at 1500 rpm and sintered at 300 ºC for 2 h in nitrogen atmosphere was found approximately as 200 nm by using FESEM. In Figure 4.16, cross-sectional FESEM image of the film prepared at these conditions is given.

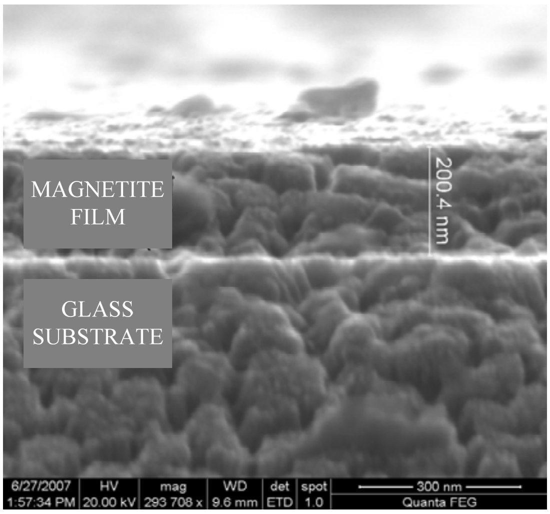

Figure 4.16 Cross-sectional FESEM image of a thin film which was spin coated at 1500 rpm and sintered at 300 °C for 2 h in nitrogen atmosphere.

For the solution S5, thicknesses of the thin films were also estimated by using SEM images. In Figure 4.17, SEM image of a sample prepared by using solution S5 at 2000 rpm and sintered at 300 ºC for 1 h in air is given. Thickness of this sample was found as 35 nm.

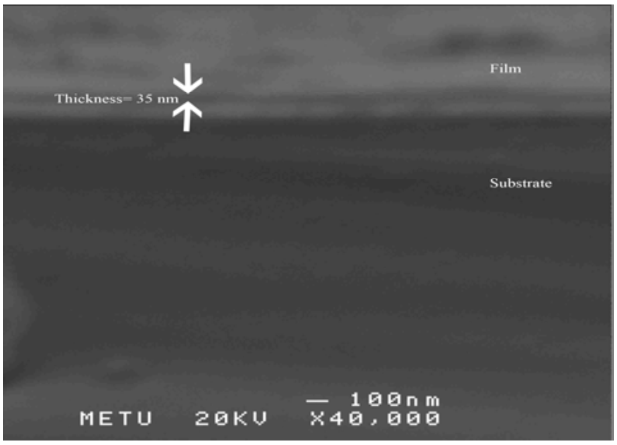

Figure 4.17 Cross sectional SEM image of a thin film which was prepared by solution S5 at 2000 rpm and sintered at 300 ºC for 1 h in air.

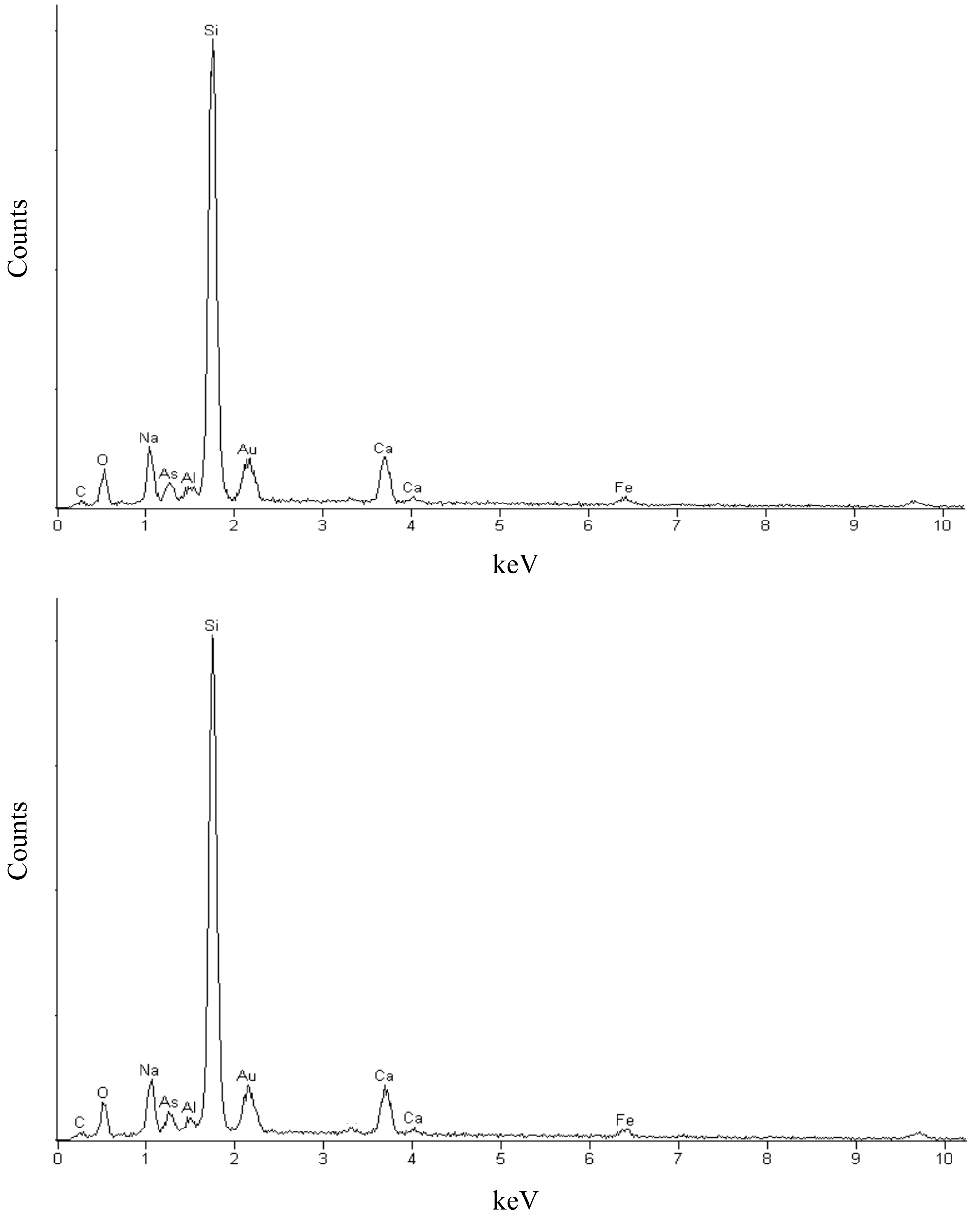

Figure 4.18 EDS analysis of a thin film having a thickness of ~100 nm prepared at 2000 rpm, sintered at 300 ºC for 2 h in nitrogen atmosphere. Each graph shows EDS analysis of different areas of the same film surface.

EDS analysis of the samples were taken at different positions on the film surface. The results show that chemical composition is the same all over the film surface indicating the chemical homogeneity throughout the film (Figure 4.18).

To compare the EDS analysis of different samples with different thicknesses, EDS analysis of a ~10 nm thick film and a ~100 nm thick film is compared. Both films were prepared at the same conditions except spinning rate values. Figure 4.19 shows EDS analysis of a sample prepared at 5000 rpm and Figure 4.20 shows EDS analysis of a sample prepared at 2000 rpm. Other parameters were fixed as an sintering temperature of 300 ºC for 2 h in nitrogen atmosphere using main solution (S1).

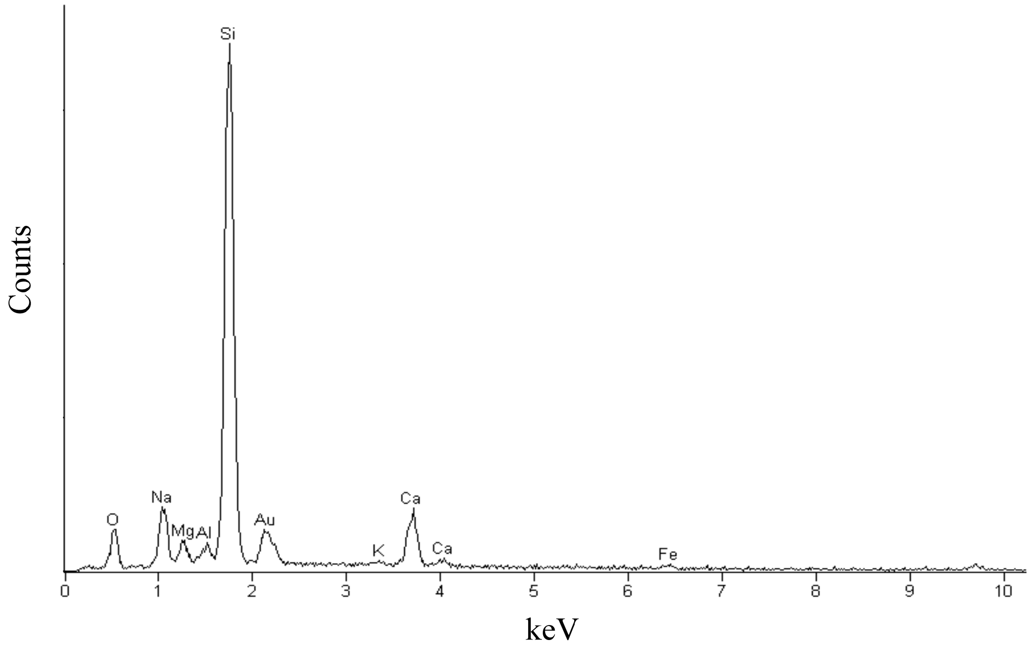

Figure 4.19 EDS analysis of a ~10 nm thick film.

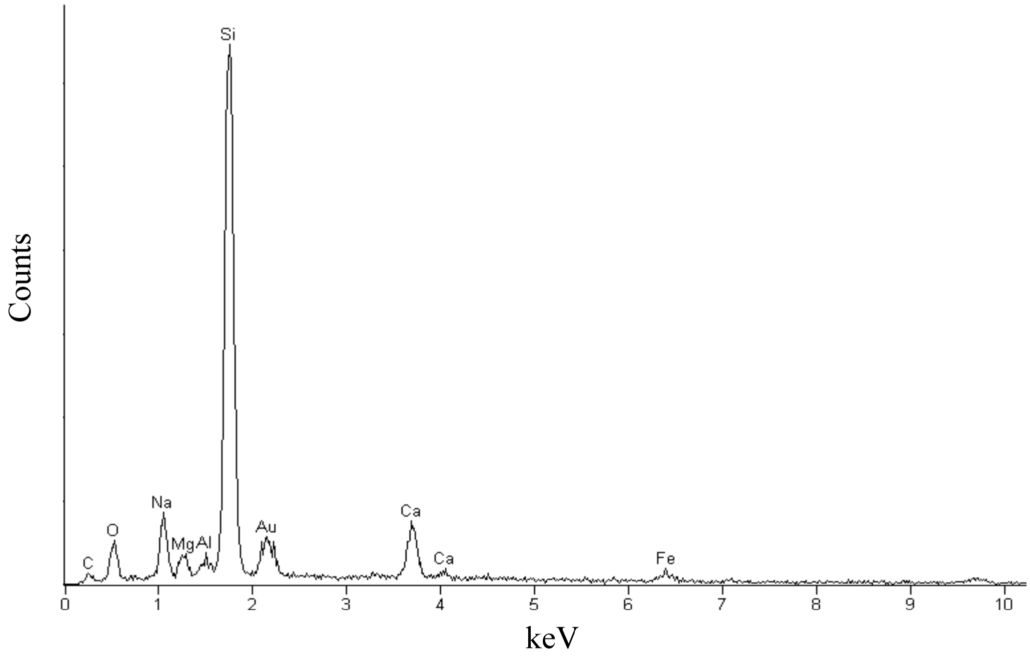

Figure 4.20 EDS analysis of a ~100 nm thick film.

From the EDS analysis of these thin films, it was seen that ~100 nm thick sample showed more intense Fe peak compared to that for ~10 nm thick sample. This can be explained by the substrate effect. The chemical species present in the substrate are more dominant in the EDS spectra for thinner films compared to thicker ones.

4.5. AFM of Thin Films

Surface morphology of the thin films was also characterized by using AFM. AFM images showed that no cracks or any other defects on the film surface were present. AFM image (Figure 4.21) of the film having a thickness of ~10 nm prepared by main solution (S1) at 5000 rpm and sintered at 300 ºC for 3.5 h in nitrogen atmosphere indicates the presence of nanoscale spherical grains.

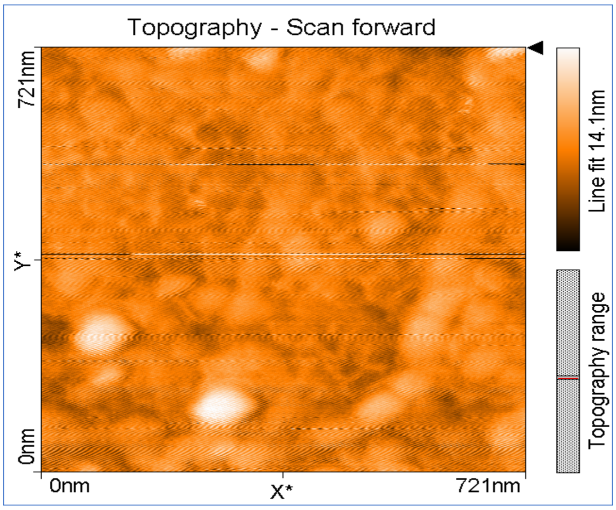

Figure 4.21 AFM image of a sample having a thickness of ~10 nm prepared at 5000 rpm and sintered at 300 ºC for 3.5 h in nitrogen atmosphere.

Another AFM image was taken from a thicker film. In Figure 4.22, an AFM image of a sample prepared using the main solution (S1) at 2000 rpm and sintering at 300 ºC for 3.5 h in nitrogen atmosphere was shown.

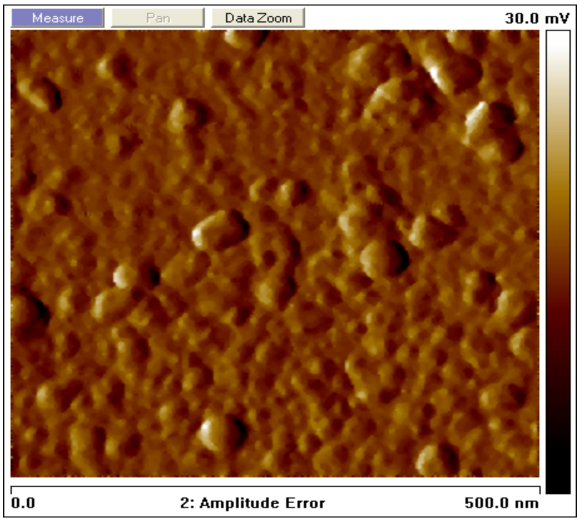

Figure 4.22 AFM image of a sample having a thickness of ~100 nm prepared at 2000 rpm and sintered at 300 ºC for 3.5 h in nitrogen atmosphere.

AFM results of samples prepared by different solutions were also compared. An AFM image of a sample prepared by solution S5 at 4000 rpm and sintered at 300 ºC for 1 h in air was given in Figure 4.23.

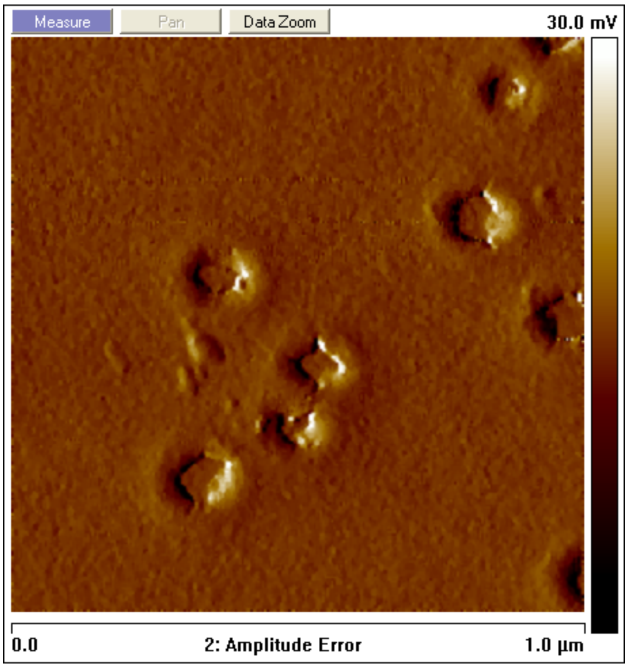

Figure 4.23 AFM image of a sample prepared by solution S5 at 4000 rpm and sintered at 300 ºC for 1 h in air.

As it can be seen from the figure, films which are obtained by using solution S5 gives some cavities and hills all over the surface. These are maybe the result of sintering the films in air and they were not observed in samples sintered in nitrogen atmosphere.

4.6. XRD of Thin Films

In order to obtain crack free, homogenous and crystalline films, heat treatment step is extremely important. The drying step performs removal of water without any crack formation and sintering step crystallize the thin film into the desired phase. For the thin film formation, using correct parameter values for these two steps is crucial.

In order to study the magnetite formation, different sintering temperatures were used. For XRD analysis of these films, two diffraction methods were employed; conventional diffraction and grazing incidence diffraction. The differences between the two methods were explained in chapter 3.

Several different iron oxide films were studied using conventional diffraction method. For these films, variable parameters were sintering time, sintering temperature, spinning rate, coating layer number and sintering atmosphere.

In Figure 4.24, conventional XRD patterns of iron oxide thin films with respect to increasing number of coating layers were given. All the films were coated at 4000 rpm and sintered at 300 ºC for 2 h in nitrogen atmosphere.

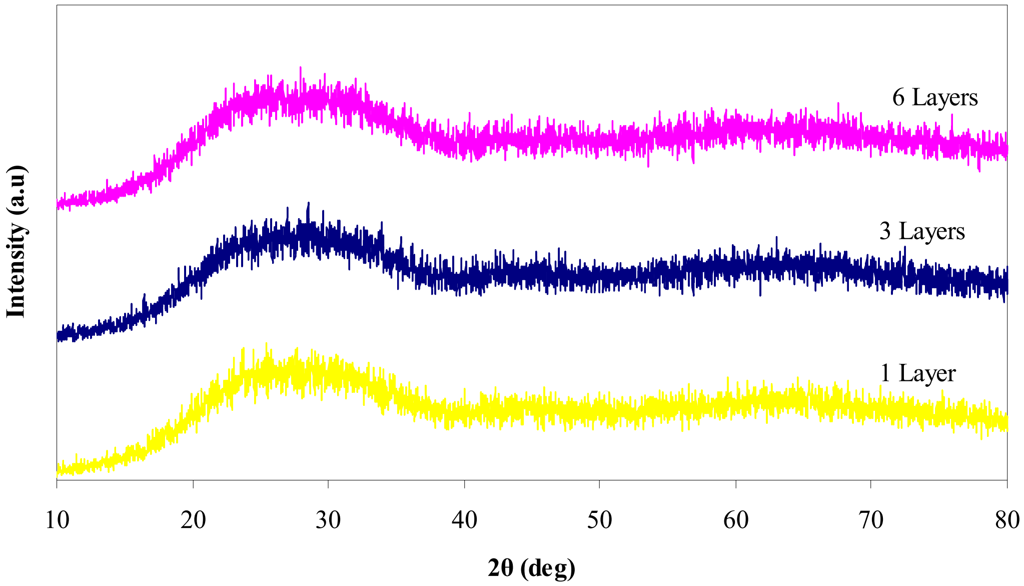

Figure 4.24 XRD pattern of iron oxide thin films prepared by main solution (S1) at 4000 rpm and sintered at 300 ºC for 2 h in nitrogen atmosphere.

In the figure, no crystalline phase was observed even if the coating layer number was increased to 6 layers. As it was discussed by Karakuşcu et al. [35], conventional powder XRD method fails in the detection of nanoscale phases.

The second reason of not observing any crystalline phase in the diffraction patterns is the thickness of the films. Although 6 layered film was investigated, it is still so thin and any diffraction from the film cannot be observed. Instead of film, diffraction from the substrate dominates the X-ray diffraction patterns.

In Figure 4.25, conventional XRD patterns of iron oxide thin films with respect to increasing sintering temperatures were given. All the films were 3 layered and they were coated at 4000 rpm and sintered in nitrogen atmosphere for 2 h. Again, it can be seen in the figure that no diffraction peaks were observed. The broad diffraction peak comes from the substrate and it masked the possible diffracted peaks from the film. Therefore no peaks can be observed using conventional methods in these films.

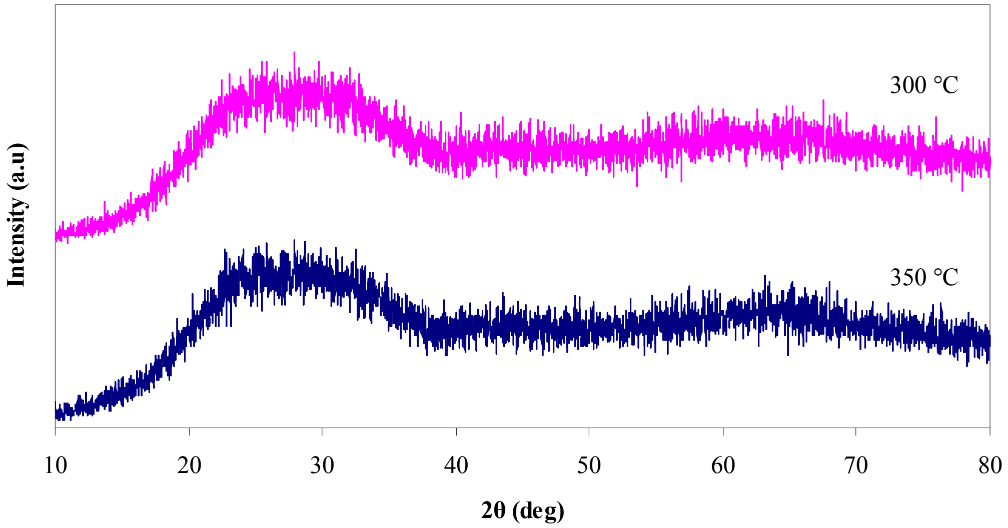

Figure 4.25 XRD patterns of iron oxide thin films which are 3 layered and prepared by main solution (S1) at 4000 rpm and sintered at different temperatures for 2 h in nitrogen atmosphere.

In order to prevent the broad diffraction peak coming from substrate, 15 and 20 layered thin films were produced. In Figure 4.26, comparison of conventional XRD patterns of 1, 15 and 20 layered iron oxide thin films were given. All the films were coated at 4000 rpm and sintered in nitrogen atmosphere for 2 h. Drying step was performed between each layer. For numerous number of coatings, this multiple drying steps can produce new phases in the film and at the substrate-film interface which is an undesired event in this study. Another drawback of producing multi-layered thin films is that cracks on the films can be seen on the film surface even by naked eye. Hence, in the study multi-layered thin films were not investigated in detail and they were not taken into account.

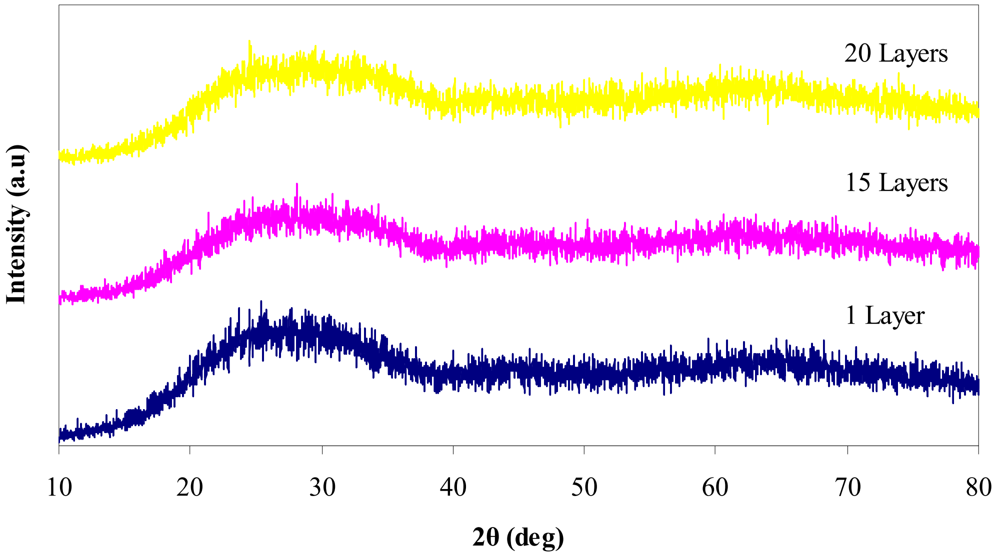

Figure 4.26 XRD patterns of iron oxide thin films prepared by main solution (S1) at 4000 rpm and sintered at 300 ºC for 2 h, with respect to increasing coating layers.

In Figure 4.27, conventional XRD patterns of iron oxide thin films using different sintering periods were given. All the films were coated at 5000 rpm and sintered in nitrogen atmosphere at 300 ºC and they are all single layered. As it can be seen from the figure, increasing sintering time also does not yield any diffraction peaks.

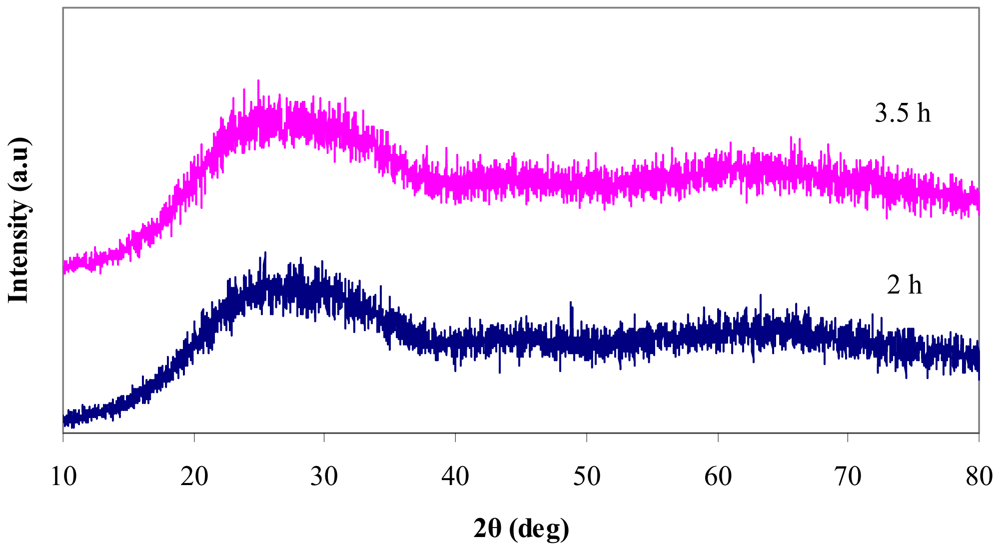

Figure 4.27 XRD patterns of iron oxide thin films having a thickness of ~10 nm, prepared by main solution (S1) at 5000 rpm and sintered at 300 ºC for 2 h, with respect to increasing sintering time.

In order to by-pass the extra drying steps while producing thicker films, film thickness was adjusted by changing the spinning rate. Films between 10-100 nm were produced (10 nm at 5000 rpm and 100 nm at 2000 rpm) and they were characterized by X-ray diffraction. From the XRD patterns shown in Figure 4.28, it can be seen that no diffraction peaks were observed.

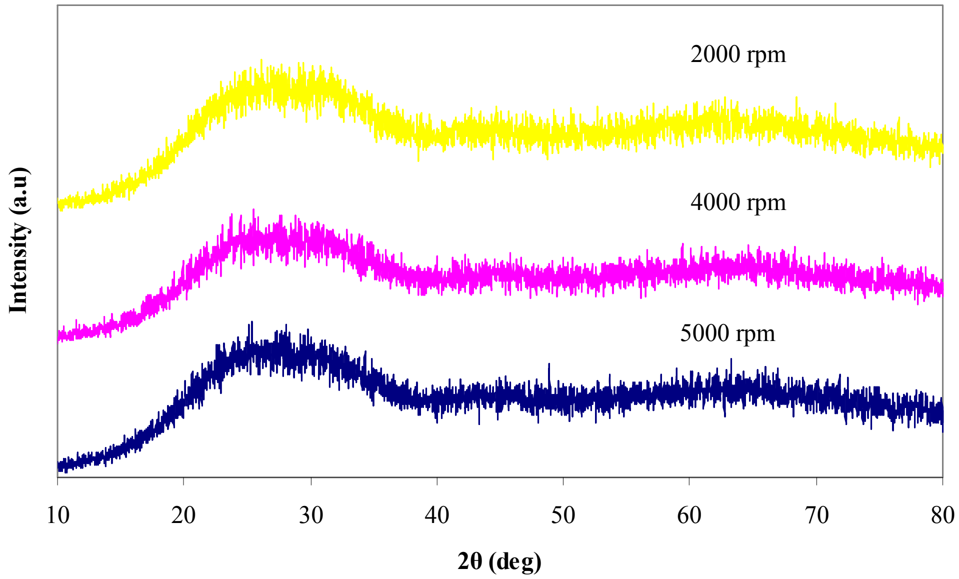

Figure 4.28 XRD patterns of iron oxide thin films coated at different spinning rates and prepared by main solution (S1) and sintered at 300 ºC for 2 h in nitrogen atmosphere.

Magnetite films were also investigated by grazing incidence X-ray diffraction method. In Figure 4.29, in-plane grazing incidence XRD pattern of a thin film having a thickness of ~10 nm coated at 5000 rpm and sintered in nitrogen atmosphere at 300 ºC for 3.5 h was given. The peaks belong to magnetite (311) and (440) planes. In-plane grazing incidence XRD technique measures diffracted beams, which are scattered nearly parallel to the film surface and therefore it reveals lattice planes that are perpendicular to the film surface. These planes are inaccessible by other methods. This is the real reason why no diffraction peaks were observed in the conventional Bragg's diffraction method.

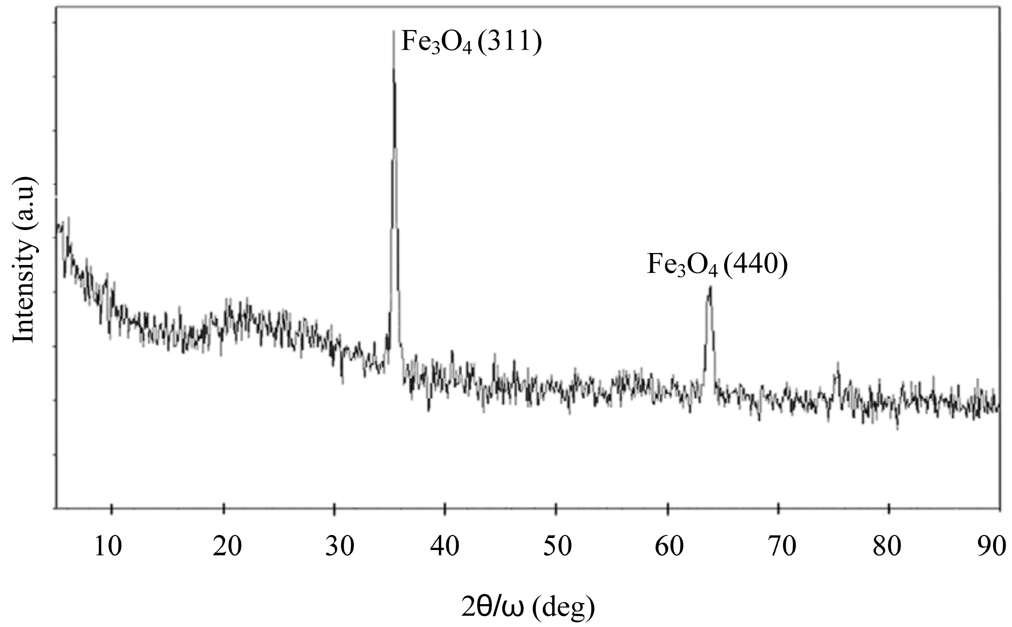

Figure 4.29 In-plane grazing incidence XRD pattern of a thin film having a thickness of ~10 nm prepared by main solution (S1) at 5000 rpm, sintered at 300 °C for 3.5 h in nitrogen atmosphere.

In order to compare and show the differences between conventional diffraction and in-plane grazing incidence diffraction, diffraction pattern difference for the same sample is given in Figure 4.30. In the conventional method, incident beam penetrates deep in the substrate, so most of the diffraction comes from the glass substrate suppressing the magnetite peaks resulting from the film of ~10 nm thickness.

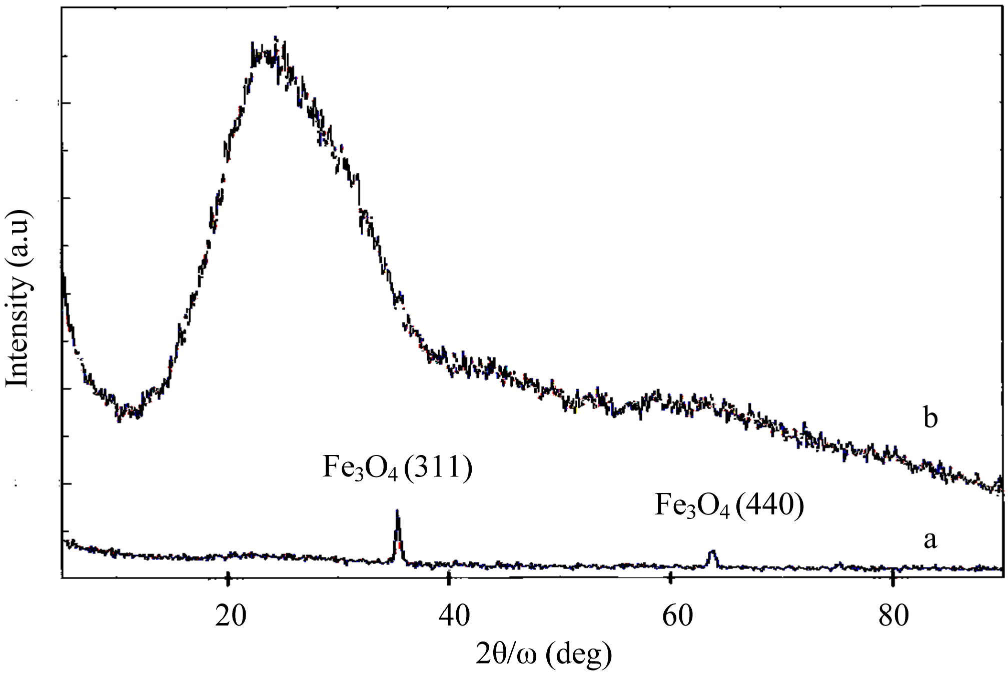

Figure 4.30 a) In-plane grazing incidence and **b)** Conventional XRD patterns of a thin film having a thickness of ~10 nm prepared at 5000 rpm, sintered at 300 °C for 3.5 h in nitrogen atmosphere.

In the in-plane grazing incidence XRD pattern, there are no other peaks observed, which belong to ferric nitrate or α-Fe_2O_3 or γ- Fe_2O_3. This means that, all of the resultant film is Fe_3O_4. By using the Scherrer's Formula (Equation 4.1), grain size of this film was found approximately as 15 nm.

From the X-ray reflectivity profile (Figure 4.31), roughness of the single layered film produced at 5000 rpm and sintered at 300 °C in nitrogen atmosphere for 2 h was found as 2.4 nm and the thickness of this sample was found as ~8 nm.

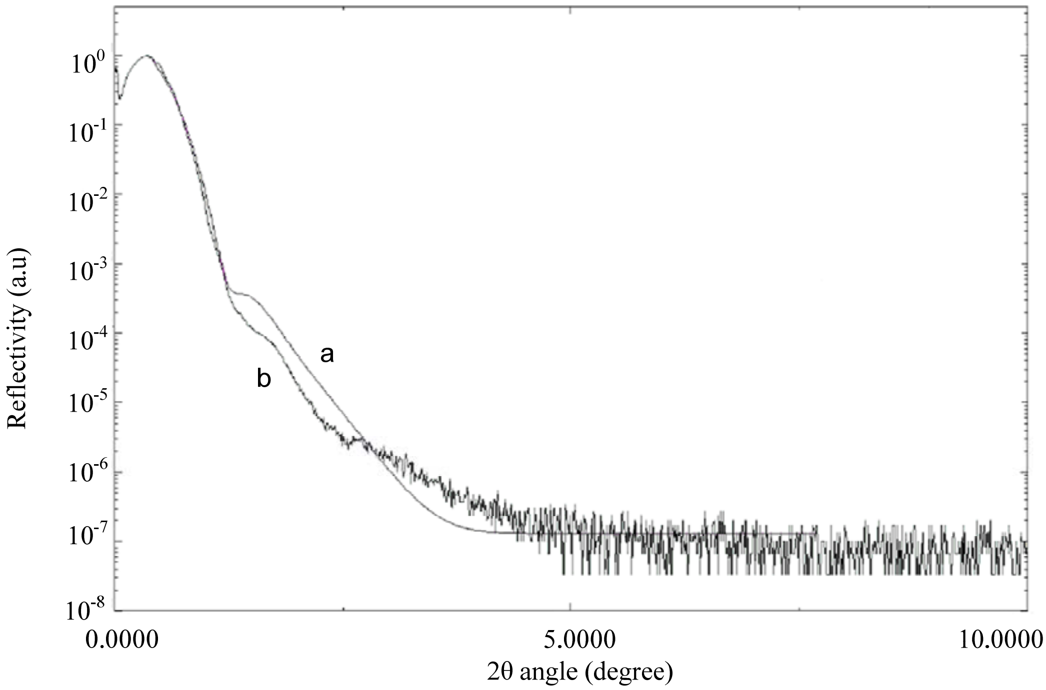

Figure 4.31 X-ray reflectivity profile of a thin film having a thickness of ~10 nm which is produced by main solution (S1) at 5000 rpm and sintered at 300 °C for 2 h in nitrogen atmosphere. **a)**simulation, **b)**measured data

4.7. Transmission Electron Microscopy (TEM)

TEM samples were prepared by scraping the film off the surface and attaching onto the carbon coated copper grids. The morphology of a single-layered thin film having a thickness of ~10 nm which is produced by main solution (S1) at 5000 rpm and sintered at 300 °C for 3.5 h in nitrogen atmosphere is shown in Figure 4.32 and corresponding electron diffraction pattern of this film is given at the inset.

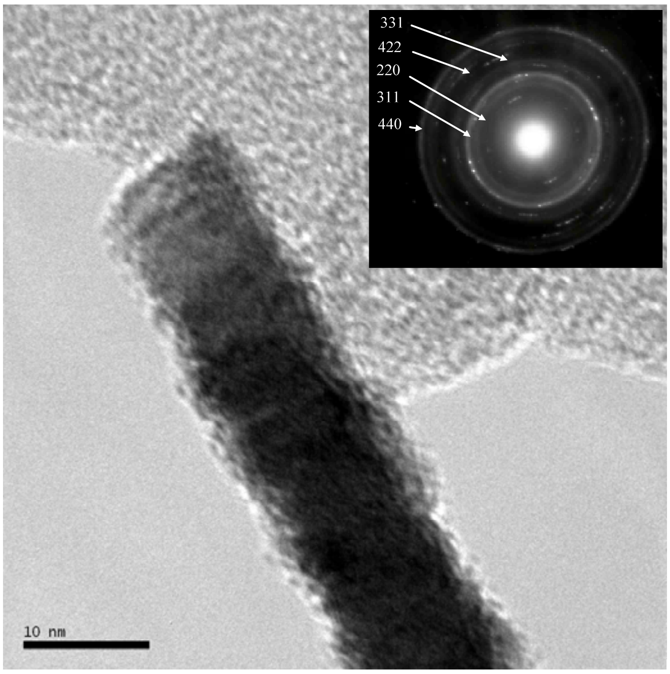

Figure 4.32 TEM micrograph and electron diffraction pattern of the single-layered magnetite thin film (~10 nm) which is produced by main solution (S1) at 5000 rpm and sintered at 300 °C for 3.5 h in nitrogen atmosphere.

TEM constants for the sample characterization was λ=0.02510 Å for 200 kV and the camera constant is given as 298.8 pixels. By using the radii in the diffraction pattern, the interplanar spacings of the sample were calculated from Equation [4.4]. This equation is obtained by using Bragg Law and simple geometric equations given in Equations [4.2] and [4.3], respectively which were discussed by Williams et al. [67]. For very small angles, Bragg law can be written as;

$$\lambda = 2d\theta \qquad \text{Eq. [4.2]}$$

Geometrically;

$$\frac{R}{L} = 2\theta \qquad \text{Eq. [4.3]}$$

By combining equations [4.2] and [4.3];

$$\frac{R}{L} = \frac{\lambda}{d} \qquad \text{Eq. [4.4]}$$

Table 4.3 Measured radii and calculated d_{hkl} of the magnetite thin film (~10 nm) which is produced by main solution (S1) at 5000 rpm and sintered at 300 °C for 3.5 h in nitrogen atmosphere.

Measured Radius	**d_{hkl}**
R_1=100 pixels	d_1= 2.98 Å
R_2=116.7 pixels	d_2= 2.56 Å
R_3=155.62 pixels	d_3= 1.92 Å
R_4=168.81 pixels	d_4= 1.77 Å
R_5=197.88 pixels	d_5= 1.51 Å

Table 4.3 shows the measured interplanar spacing values of the sample. Magnetite has cubic structure and for cubic structures, interplanar spacing can be calculated theoretically from Equation 4.5.

$$d_{hkl} = \frac{a_0}{\sqrt{h^2 + k^2 + l^2}} \qquad \text{Eq. [4.5]}$$

Magnetite is known to have a FCC structure. For the FCC structure, possible $h^2+k^2+l^2$ values are 3, 4, 8, 11, 12, 16…

Comparison between the observed and theoretical interplanar spacings is given in Table 4.4.

Table 4.4 The observed and theoretical interplanar spacings of the magnetite thin film (~10 nm) which is produced by main solution (S1) at 5000 rpm and sintered at 300 °C for 3.5 h in nitrogen atmosphere.

d_{hkl}	hkl (magnetite)	d_{hkl} (evaluated)
2.98 Å	220	2.96 Å
2.56 Å	311	2.53 Å
1.92 Å	331	1.92 Å
1.77 Å	422	1.71 Å
1.51 Å	440	1.48 Å

The theoretical and measured interplanar spacings were matched for magnetite. Therefore it can be said that the observed ring pattern belongs to the magnetite phase with [001] zone axis. Ring pattern reveals finer grain size for the investigated sample which supports the XRD results. Since the grains are small, all the reciprocal lattice points will be broadened by the shape effect, so will the sphere or circles [67].

Another TEM micrograph for the same sample is given in Figure 4.33. From these figures it can be seen that in the sample both rod-like and spherical particles were observed.

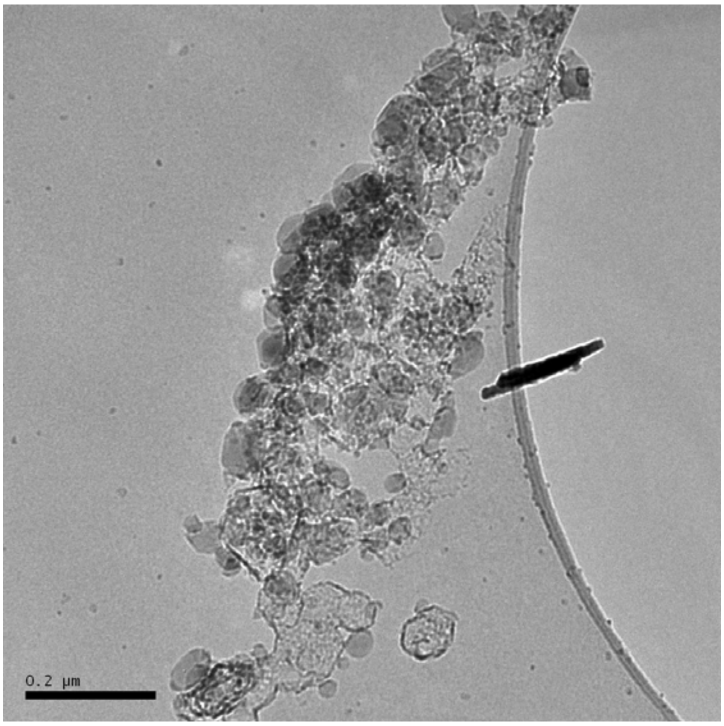

Figure 4.33 TEM micrograph of a single-layered magnetite thin film (~10 nm) which is produced by main solution (S1) at 5000 rpm and sintered at 300 °C for 3.5 h in nitrogen atmosphere.

TEM micrograph for a magnetite thin film (~10 nm) which is produced by main solution (S1) at 5000 rpm and sintered at 350 °C for 2 h in nitrogen atmosphere is given in Figure 4.34 and corresponding electron diffraction is shown inset.

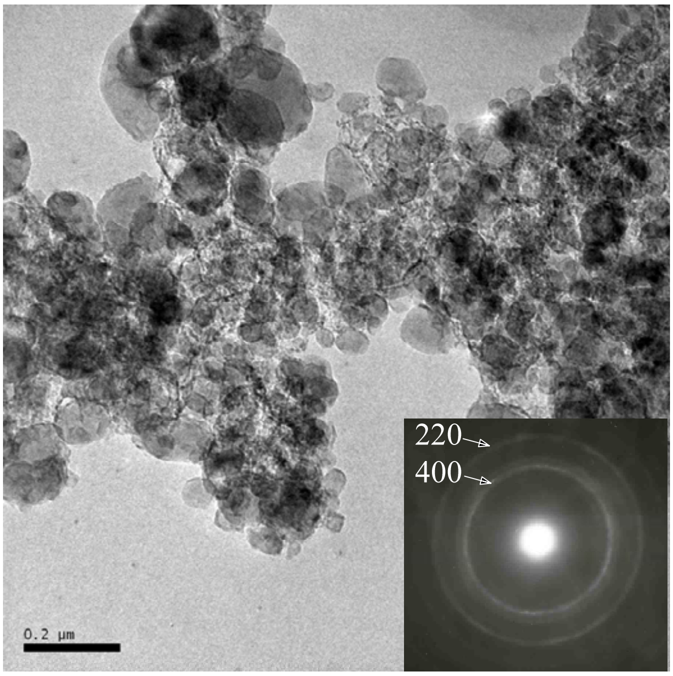

Figure 4.34 TEM micrograph and electron diffraction pattern of the single-layered magnetite thin film (~10 nm) which is produced by main solution (S1) at 5000 rpm and sintered at 350 °C for 2 h in nitrogen atmosphere.

The calculated and theoretical interplanar spacings of this sample are given in Table 4.5.

Table 4.5 The observed and theoretical interplanar spacings of the magnetite thin film (~10 nm) which is produced by main solution (S1) at 5000 rpm and sintered at 350 °C for 2 h in nitrogen atmosphere.

d_{hkl}	hkl (magnetite)	d_{hkl} (evaluated)
2.98 Å	220	2.96 Å
2.08 Å	400	2.09 Å

Another TEM micrograph for the same sample is given in Figure 4.35. As it was seen in the previous sample, this sample also consists of both rod-like and spherical particles.

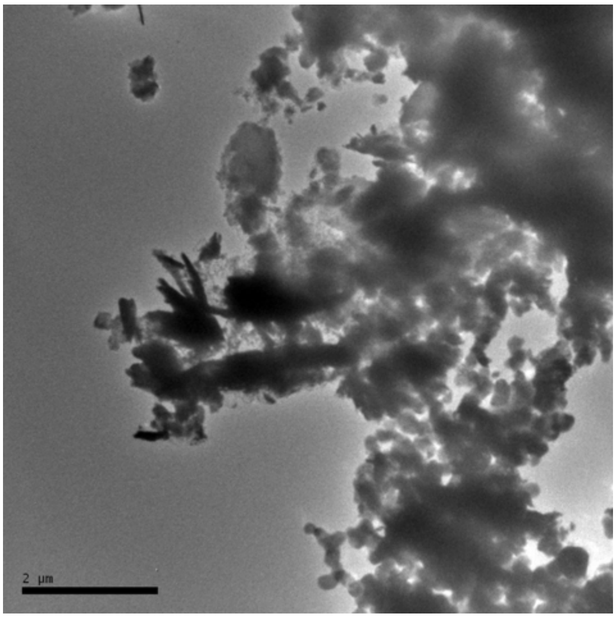

Figure 4.35 TEM micrograph of a single-layered magnetite thin film (~10 nm) which is produced by main solution (S1) at 5000 rpm and sintered at 350 °C for 2 h in nitrogen atmosphere.

The interplanar spacing values of both samples match with the theoretical interplanar spacing values of magnetite. Therefore, both samples were proved to be single phased magnetite. This result matches with the previous DTA results which showed that between 291 °C and 369 °C magnetite phase can be obtained. Previous XRD results also showed that at 300 °C, magnetite phase was obtained.

TEM micrograph of a magnetite thin film (~100 nm) which is produced by main solution (S1) at 2000 rpm and sintered at 300 °C for 2 h in nitrogen atmosphere is shown in Figure 4.36.

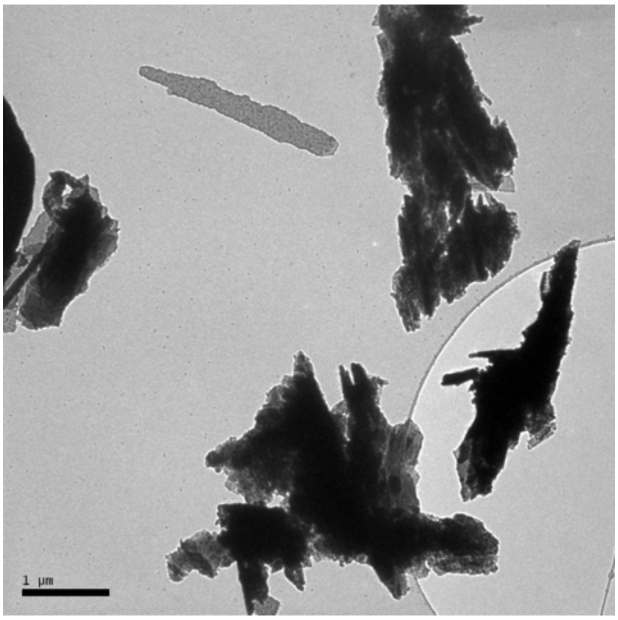

Figure 4.36 TEM micrograph of a single-layered magnetite thin film (~100 nm) which is produced by main solution (S1) at 2000 rpm and sintered at 300 °C for 3.5 h in nitrogen atmosphere.

Another TEM micrograph for the same sample is given in Figure 4.37. It can be seen from these figures that this sample also consists of both rod-like and spherical particles just like the previous samples.

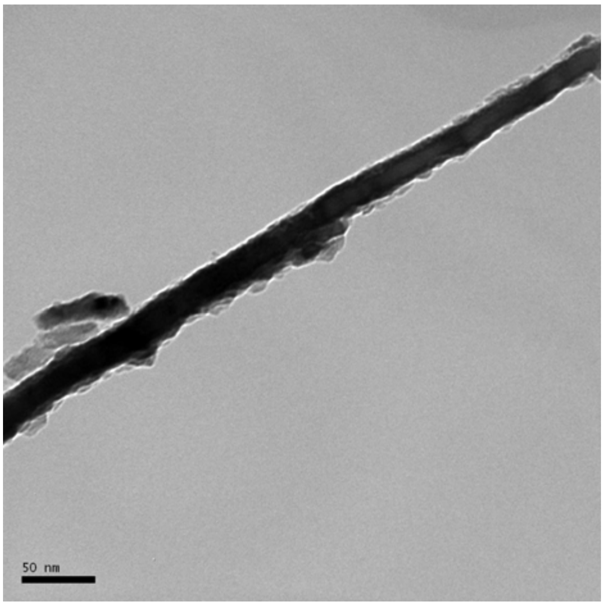

Figure 4.37 TEM micrograph of a single-layered magnetite thin film (~100 nm) which is produced by main solution (S1) at 2000 rpm and sintered at 300 °C for 3.5 h in nitrogen atmosphere.

Electron diffraction pattern of this sample is shown in Figure 4.38.

As it can be seen from the figure, rings are made up of discrete spots. The previous samples gave continuous ring patterns. This phenomenon can be explained by the grain size effect; finer grain size produces more continuous ring pattern whereas larger grain size produces a ring that is made up of discrete spots [67]. Probably the sample shown in Figure 4.38 (~100 nm) is thicker than the previous samples (~10 nm) has larger grain size and therefore exhibited a ring pattern consisting of discrete spots. In the sol-gel derived nanocrystalline thin films, the crystallization process starts from an amorphous material and proceeds through the development of nanocrystals. In such films, the lack of long-range order may lead to some amount of disorder in the detected electron diffraction patterns [68].

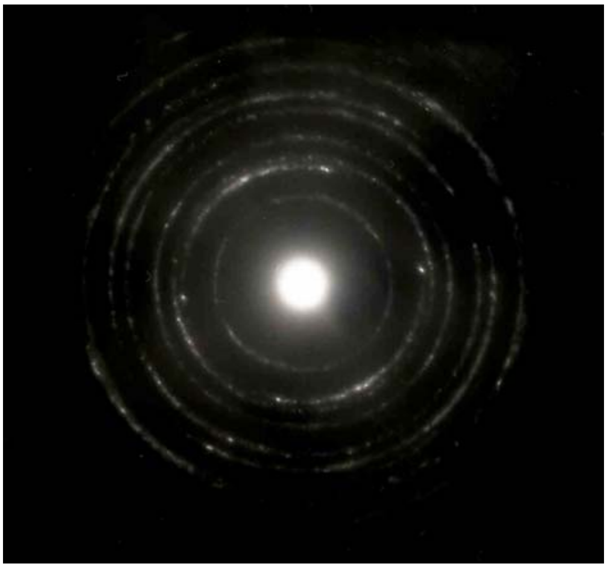

Figure 4.38 Electron diffraction pattern of a single-layered magnetite thin film (~100 nm) which is produced by main solution (S1) at 2000 rpm and sintered at 300 °C for 3.5 h in nitrogen atmosphere.

4.8. Transmittance of Magnetite Thin Films

Magnetite thin films are highly transparent. By using this property, they can be used in many applications in the industry. For example in the computer memory applications and in magneto-optical devices, magnetite thin films can be used. Therefore optical characterization of these films was also conducted.

Figure 4.39 shows transmission spectra of one-layered magnetite thin films prepared by main solution (S1) at 2000 rpm and sintered at 300 ºC for 3.5 h in nitrogen atmosphere in the wavelength range of 300-1100 nm. Only difference between the two samples is the sintering period. From the figure, it can be seen that no significant difference between the optical transmissions of two samples exist. Samples gave maximum 90% transmittance between wavelength range of 900 and 1100 nm.

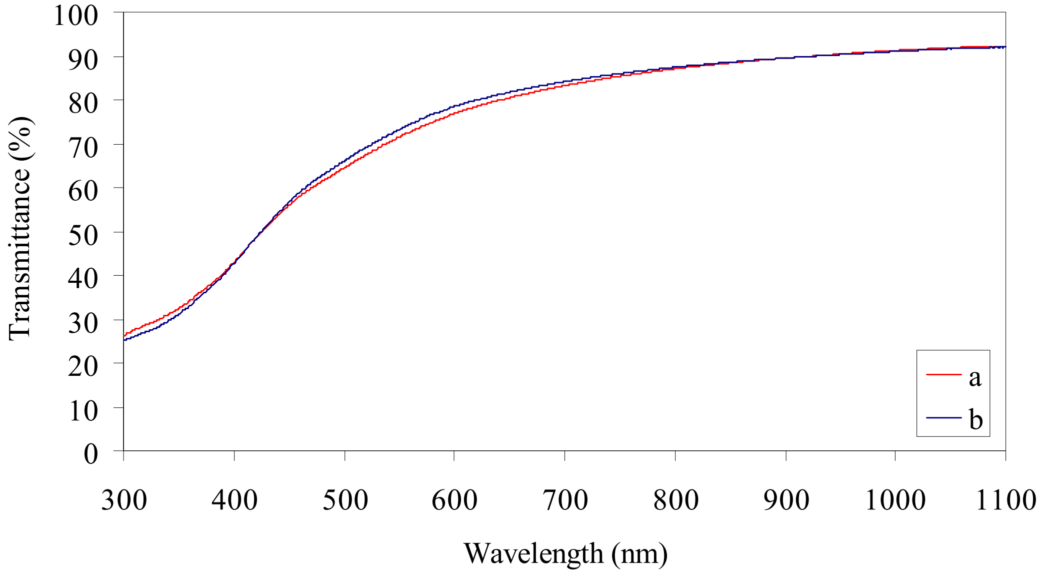

Figure 4.39 UV-Vis spectra of iron oxide thin films sintered for different periods; **a)** Sample prepared by main solution (S1) at 2000 rpm and sintered at 300 °C for 3.5 h, **b)** Sample prepared by main solution (S1) at 2000 rpm and sintered at 300 °C for 2 h.

Figure 4.40 shows transmission spectra of one-layered magnetite thin films prepared at different sintering temperatures. Other parameters like spinning rate, sintering time and sintering atmosphere were kept constant. Spinning rate was 2000 rpm, sintering time was 2 h and sintering atmosphere was nitrogen for the both samples. The wavelength range of the transmission spectra is between 300-1100 nm. From the figure, it can be seen that the optical transmittance of the sample prepared at lower temperature is greater than the sample prepared at higher temperature. The sample prepared at 380 ºC gives a maximum transmittance of 80 % between wavelengths of 900-1100 nm whereas the sample prepared at 300 ºC gives about 10% higher transmittance all over the spectrum.

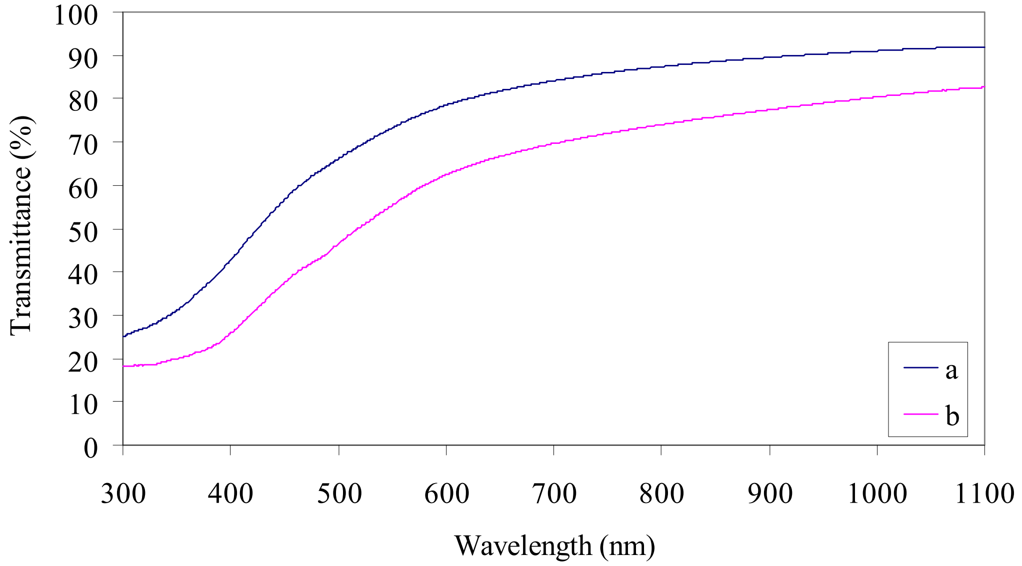

Figure 4.40 UV-Vis spectra of iron oxide thin films sintered at different temperatures; **a)** Sample prepared by main solution (S1) at 2000 rpm and sintered at 300 ºC for 2 h, **b)** Sample prepared by main solution (S1) at 2000 rpm and sintered at 380 ºC for 2 h.

Figure 4.41 shows transmission spectra of one-layered magnetite thin films prepared by different spinning rates. Other parameters like sintering temperature, sintering time and sintering atmosphere were kept constant. Sintering temperature was 300 ºC, sintering time was 2 h and sintering atmosphere was nitrogen for both samples. The wavelength range of the transmission spectra is between 300-1100 nm. From the figure, it can be seen that the optical transmittance of the sample prepared at lower spinning rate is lower than the sample prepared at higher spinning rate. The sample prepared at 5000 rpm gives a maximum transmittance of 95% between wavelengths of 900-1100 nm whereas the sample prepared at 2000 rpm gives only a transmittance value of 90% within this spectrum.

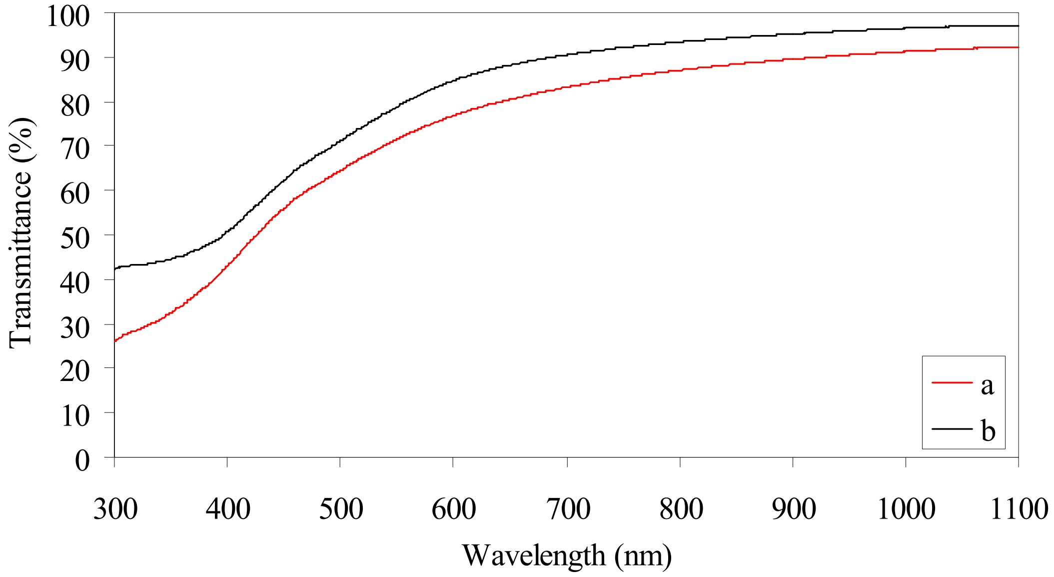

Figure 4.41 UV-Vis spectra of iron oxide thin films prepared at different spinning rates; **a)** Sample prepared by main solution (S1) at 2000 rpm and sintered at 300 ºC for 3.5 h **b)** Sample prepared by main solution (S1) at 5000 rpm and sintered at 300 ºC for 3.5 h.

In order to compare the optical transmissions of samples prepared by different solutions, transmission spectra between the wavelengths of 300-1100 nm for two different samples has given in Figure 4.42. The first sample was prepared by main solution (S1). It was spin coated at 2000 rpm and sintered at 300 ºC for 2 h in nitrogen atmosphere. The second sample was prepared by solution S5. It was sintered at 300 ºC for 1 h in air. Between the wavelength range of 300-350 nm and 550-1100 nm, optical transmission of the sample prepared by solution S5 is greater. Between the wavelength range of 350-550 nm there is no significant transmission difference between these two samples.

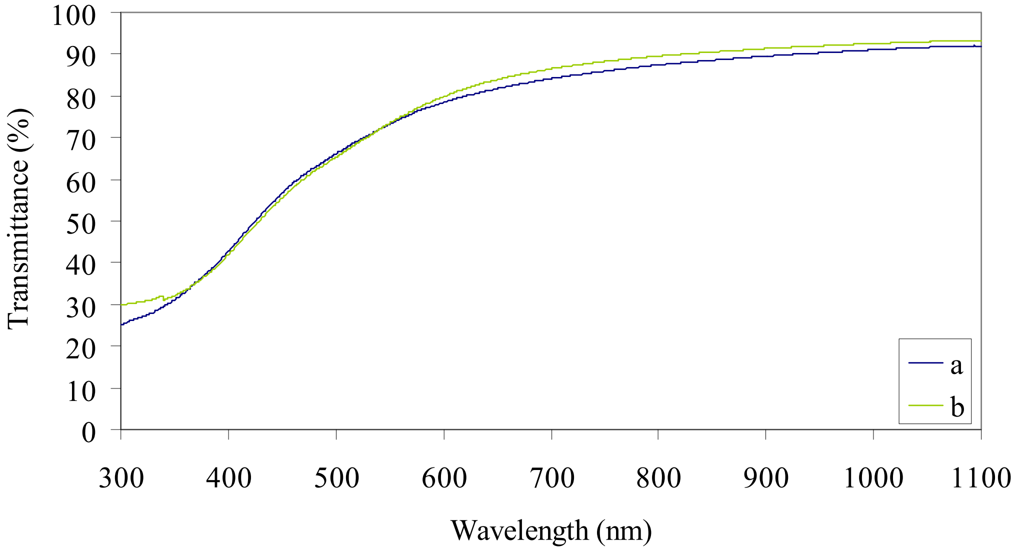

Figure 4.42 UV-Vis spectra of iron oxide thin films prepared by different solutions; **a)** Sample prepared by main solution (S1) at 2000 rpm and sintered at 300 ºC for 2 h in nitrogen atmosphere. **b)** Sample prepared by solution S5 at 2000 rpm and sintered at 300 ºC for 1 h in air.

From the figures above, it can be concluded that increasing sintering time of the thin films does not significantly affect the transmission values over the measured wavelength range but increasing sintering temperature has a significant effect on transmission values. Increasing sintering temperature decreases the transmission values. This may be due to the presence of mixed phases in the sample (magnetite and maghemite). Lower sintering temperatures for the same film thickness yielded highly transparent films due to the presence of single magnetite phase. Decreasing spinning rate decreases the transmittance values which can be explained by the thickness effect of the films. Larger thicknesses are obtained at low spinning rates and transmittance values decreases in thicker films. Finally, films obtained from different solutions at the same rpm values yield nearly same transmittance values. At same rpm values, films obtained from main solution (S1) will be expected to be thicker than the films obtained from solution S5. It can be concluded that for the same thickness value, main solution (S1) yield more transparent films than solution S5.

As it can be seen in Figure 4.43, highly transparent films were obtained at lower sintering temperatures and at lower thicknesses. Highly transparent nature of the magnetite thin films leads itself to be a candidate for magneto-optical applications. It is known that when the magnetite nanocrystals are deposited on a noble metal surface such as gold, the magneto-optical effects significantly increase. This effect can be useful for novel-optical data storage media [69]. High transparency of the films is the result of the high quality (fewer vacancies, holes or cracks) of the film and homogenous dispersion of finely divided particles [70].

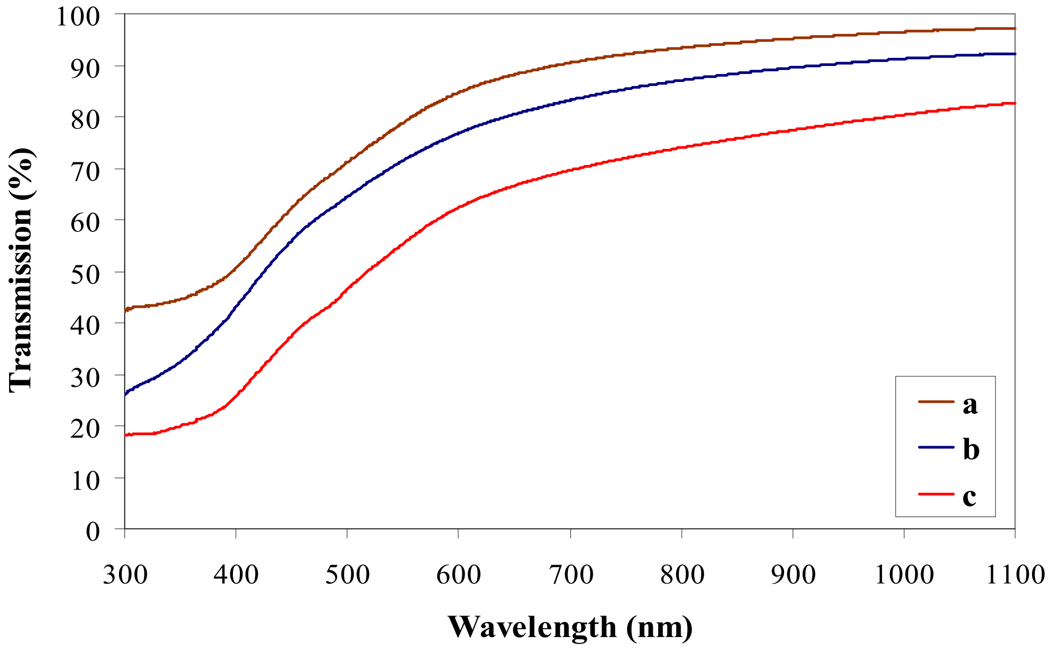

Figure 4.43 UV-Vis spectra of iron oxide thin films prepared by main solution (S1) at different spinning rates and sintered at different temperatures; **a)** Sample sintered at 300 °C for 3.5 h and coated at 5000 rpm, **b)** Sample sintered at 300 °C for 3.5 h and coated at 2000 rpm, **c)** Sample sintered at 380 °C for 2 h and coated at 2000 rpm.

4.9. Magnetic Properties of Magnetite Thin Films

As Zhu et al. [25] implies, as a magnetic material, the magnetic property of Fe_3O_4 thin films is greatly important to its applications. Figure 4.44 and 4.45 displays the magnetization curves and partial magnified hysteresis behaviors at the inset, measured at room temperature for a magnetite thin film having a thickness of ~10 nm sintered at 300 °C for 3.5 h and coated at 5000 rpm. The saturation magnetization (M_s) of this thin film was found as ~35 emu/cm^3. Our reported saturation magnetization value is between the reported values in the literature. In the literature, many different magnetization values ranging from 32 emu/cm^3 to 458 emu/cm^3 were reported so far [15, 21, 29, 30, 45, 71]. These values are smaller than the reported bulk saturation magnetization value (471 emu/cm^3) [45]. There exist several possible reasons for this reduction. Nanocrystalline magnetite particles and defects on the film surface may be the reasons for this behavior. Another possible reason were discussed by Mi et al. [15]; amorphous Fe_3O_4 phase at the grain boundaries should be nonmagnetic or lattice defects in the grains can also decrease magnetization. Therefore, magnetization values in the polycrystalline magnetite films decreases as compared to bulk samples.

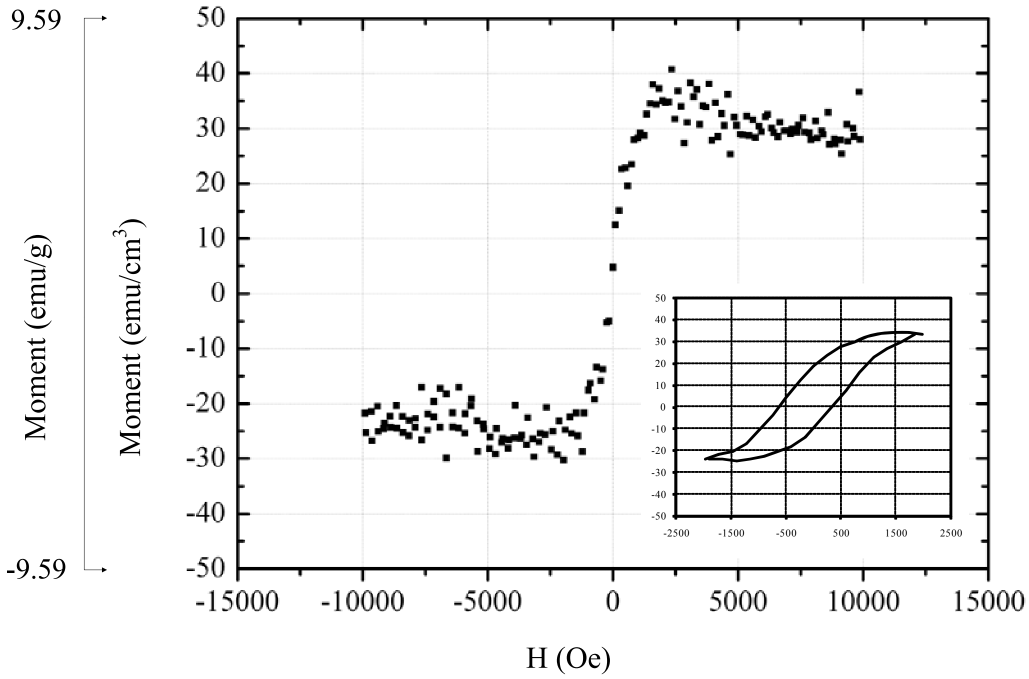

Figure 4.44 Room temperature magnetization curve of a sample prepared by main solution (S1) at 5000 rpm and sintered at 300 ºC for 3.5 h in nitrogen atmosphere (thickness ~10 nm).

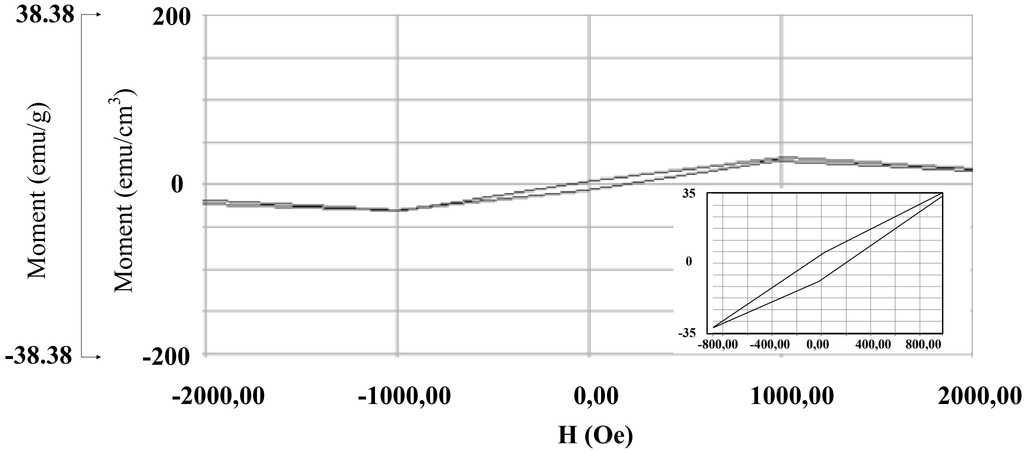

Figure 4.45 Room temperature magnetization curve of a sample prepared by main solution (S1) at 5000 rpm and sintered at 300 ºC for 3.5 h in nitrogen atmosphere (thickness ~10 nm).

CHAPTER 5

CONCLUSIONS AND FURTHER SUGGESTIONS

In this chapter main results obtained from this study will be declared.

From the results it can be concluded that, magnetite film formation depends on different parameters. These parameters can be listed by means of process sequence in the film formation. Spinning rate affects the thickness of thin films, sintering temperature effects the magnetite phase formation and sintering time affects the grain size of the films.

The coating solution used in this study showed Newtonian behavior. It indicated that thin films produced by using this solution will be homogenous. Viscosity of the solution was found as 0.0215 Pa.s.

Magnetite phase obtained in a narrow temperature range. Between 300 °C and 350 °C, magnetite phase was observed. Above 350 °C, maghemite and hematite formation was observed. Magnetite thin films are obtained in single layered films. Increasing number of layers will result in phase transformation because of heat treatment procedure applied between each layer. Therefore phase transformation probability increases in multilayered thin films. Thickness of single layered thin films was found between 10-200 nm. The variation in this value depends on the variation in spinning rates and low spinning rates yield higher thickness values.

Magnetite phase was proved by in-plane grazing incidence X-ray diffraction. Diffraction spectrum obtained by conventional methods did not give any result. The reason for this behavior was explained by thickness effects of the films. Diffraction obtained from substrate masked possible diffraction peaks coming from thin film. Grain size of the samples was calculated by Scherrer's equation and found as approximately 15 nm. Thickness of the thin films was also found by using X-ray reflectivity measurements.

TEM results proved the existence of single magnetite phase in the films which were sintered between 300 ºC and 350 ºC. This result is parallel with the results that were found by DTA and in-plane grazing incidence XRD. Particles that were seen in TEM micrographs are both spherical and rod-like.

From optical measurements, it was seen that transparency of the films increases as thickness and sintering temperature decreases. Between 900-1100 nm wavelengths, prepared thin films gave a maximum transmittance of 95%. As a conclusion, highly transparent films were obtained in this study.

The saturation magnetization (M_s) of the magnetite thin film was found as 35 emu/cm^3. In the literature, a bulk value of 471 emu/cm^3 was reported. There are several reasons for this reduction. Very small (few nanometers) particle size and defects on the film surface and strain on the film surface were considered as the possible reasons. It was also seen that our reported saturation magnetization value is between the reported values in the literature.

In this study many different characterization techniques were used. Prepared thin films were structurally, morphologically, optically and magnetically characterized. To verify the magnetite phase formation, many further characterization techniques could be used. It is difficult to distinguish magnetite and maghemite phases. Spectroscopic characterization techniques give valuable information about this problem. X-ray Photoelectron Spectroscopy (XPS) and Raman Spectroscopic analyses could be used to understand the stability of magnetite phase. But they still have some limitations such as thickness effect restrictions of Raman Spectroscopy. In order to overcome this restriction, micro-Raman spectroscopy should be used.

As a final suggestion, giant magnetoresistance of the prepared magnetite thin films could be investigated. Because of 100% spin polarization, magnetite is very important for future spintronic device applications.

REFERENCES

1. J. D. Desai, et al., Nanocrystalline hematite thin films by chemical solution spray. Semiconductor Science and Technology, 2005. 20: p. 705-709.
2. N. Ozer and F. Tepehan, Optical and electrochemical characteristics of sol-gel deposited iron oxide films. Solar Energy Materials and Solar Cells, 1999. 56: p. 141-152.
3. M. Aronniemi, J. Lahtinen, and P. Hautojärvi, Characterization of iron oxide thin films. Surface and Interface Analysis, 2004. 36: p. 1004-1006.
4. T. Tepper, F. Ilievski, and C.A. Ross. The microstructure and magneto-optical properties of pulsed laser deposited maghemite films. in Magnetics Conference IEEE International. 2003.
5. P. Chauhan, S. Annapoorni, and S.K. Trikha, Preparation, characterization and optical properties of α-Fe_2O_3 films by sol-spinning process. Bulletin of Materials Science, 1998. 21(5): p. 381-385.
6. E. L. Miller, et al., Low-temperature reactively sputtered iron oxide thin film devices. Thin Solid Films, 2004. 466: p. 307-313.
7. G. Zhang, et al., Magnetic and transport properties of magnetite thin films. Journal of Magnetism and Magnetic Materials, 2005. 293: p. 737-745.
8. A. Iljinas, et al., Synthesis of Fe_3O_4 thin films by solid state reactions. Materials Science and Engineering: C, 2005. 25(5-8): p. 590-594.
9. Q. Wang, et al., Synthesis of Nanocrystalline Magnetite (Fe3O4) Films by Self-Reduction Sol-Gel Route. Materials Science Forum, 2003. 423-425: p. 569-572.
10. R. M. Cornell and U. Schwertmann, The Iron Oxides: Structure, Properties, Reactions, Occurences and Uses. 2nd ed.: WILEY-VCH GmbH & Co. KGaA, Weinheim, 2003.

11. S. P. Sena, et al., Investigation of Magnetite Thin Films Produced by Pulsed Laser Deposition. Journal of Magnetism and Magnetic Materials, 1997. 176: p. 111-126.
12. S. Mathur, et al., Phase selective Deposition and microstructure control in iron oxide films obtained by single-source CVD. Chemical Vapor Deposition, 2002. 8(6): p. 277-283.
13. N. T. H. Kim-Nygan and W. Soszka, Low Energy Ion Scattering From Fe_3O_4 Thin Film Surfaces. Nuclear Instrumentation and Methods in Physics Research B, 2002. 193: p. 391-395.
14. S. Oh and I. Yu, Electrical Conduction Noise in Magnetite Thin Films. Journal of the Korean Physical Society, 1997. 31(4): p. 621-624.
15. W. B. Mi, et al., Microstructure, magnetic and magneto-transport properties of polycrystalline Fe3O4 films. Acta Materialia, 2007. 55: p. 1919-1926.
16. X. L. Tang, et al., Study of the buffer-layer and annealing-temperature impact on fabrication of polycrystalline Fe3O4 film for the application of spintronic devices The Journal of Vacuum Science and Technology B, 2005. 23(6): p. 2314-2318.
17. Z. L. Lu, et al., Large Low-Field Magnetoresistance in Nanocrystalline Magnetite Prepared by Sol-Gel Method. Journal of Physical Chemistry B, 2006. 110: p. 23817-23820.
18. W. Kim, et al., Fabrication and Magnetoresistance of Tunnel Junctions Using Half-Metallic Fe_3O_4. Journal of Applied Physics, 2003. 93(10): p. 8032-8034.
19. W. Eerenstein, et al., Magneto-resistance and superparamagnetism in magnetite films on MgO and $MgAl_2O_4$. Journal of Magnetism and Magnetic Materials, 2003. 258-259: p. 73-76.
20. D. Reisinger, et al., Hall effect, magnetization, and conductivity of Fe_3O_4 epitaxial thin films. Applied Physics Letters, 2004. 85(21): p. 4980-4982.
21. Y. Peng, C. Park, and D.E. Laughlin, Fe_3O_4 thin films sputter deposited from iron oxide targets. Journal of Applied Physics, 2003. 93(10): p. 7957-7959.

22. Y. K. Kim and M. Oliveria, Magnetic properties of reactively sputtered $Fe_{1-x}O$ and Fe_3O_4 thin films. Journal of Applied Physics, 1994. 75(1): p. 431-437.
23. D. T. Margulies, et al., Anomalous moment and anisotropy behavior in Fe_3O_4 films. Physical Review B, 1996. 53(14): p. 9175-9186.
24. T. Furubayashi, Magnetite films prepared by reactive evaporation. Journal of Magnetism and Magnetic Materials, 2004. 272-276: p. e781-e783.
25. H. Zhu, D. Yang, and L. Zhu, Hydrothermal growth and characterization of magnetite (Fe_3O_4) thin films. Surface & Coatings Technology, 2007. 201: p. 5870-5874.
26. I. Nedkov, et al., Microstructure and Magnetic Behavior of Nanosized Fe_3O_4 Powders and Polycrystalline Films. Monatshefte für Chemie, 2002. 133: p. 823-828.
27. C. Y. Oh, J. H. Oh, and T. Ko, The microstructure and characteristics of magnetite thin films prepared by ultrasound-enhanced ferrite plating. IEEE Transactions on Magnetics, 2002. 38(5): p. 3018-3020.
28. N. J. Tang, et al., Nanostructured magnetite (Fe_3O_4) thin films prepared by sol–gel method. Journal of Magnetism and Magnetic Materials, 2004. 282: p. 92-95.
29. K. Tanaka, et al., Preparation of Fe_3O_4 thin film by the sol-gel method and its magnetic properties. Journal of Materials Science Letters, 1989. 8: p. 83-85.
30. H. S. W. Chang, C.-C. Chiou, and Y.-W. Chen, Synthesis, Characterization, and Magnetic Properties of Fe_3O_4 Thin Films Prepared via Sol-Gel Method. Journal of Solid State Chemistry, 1997. 128: p. 87-92.
31. S. N. Malchenko, et al., Formation of iron oxide films from stabilized magnetite sols-magnetic liquids. Thin Solid Films, 1993. 227: p. 128-132.
32. M. Sedlář and V. Matějec, Preparation of Fe_3O_4 thin film by the sol-gel method and its magnetic properties. Journal of Sol-Gel Science and Technology, 1994. 2: p. 587-589.

33. T. Hashimoto, T. Yamada, and T. Yoko, Third-order nonlinear optical properties of sol–gel derived α-Fe_2O_3, γ-Fe_2O_3, and Fe_3O_4 thin films. Journal of Applied Physics, 1996. 80(6): p. 3184-3190.

34. T. Hashimoto and T. Yoko, Sol-Gel Preparation and Nonlinear Optical Properties of Transition Metal Oxide Thin Films. Materials Transactions, JIM, 1996. 37(3): p. 435-441.

35. A. Karakuşcu, Characterization of maghemite thin films prepared by sol-gel processing, M.S. Thesis, Supervisor Prof. Dr. Macit Özenbaş, Middle East Technical University, Turkey, 2006

36. C. Cao, M. Luo, and H. Zhu, PLZT films prepared by sol-gel process. Journal of Non-Crystalline Solids, 1999. 254: p. 146-150.

37. Hard disk drives / Library / Higher reliability with IBM glass substrate disks, http://www.hgst.com/hdd/library/whitepap/glassdisk/whiteglass.htm, "Last accessed date": January 2008.

38. N. Agarwal, Characterization of Lithographically Patterned Magnetic Nanostructures, Arizona State University, USA, 2007.

39. U. Schwertmann and R.M. Cornell, Iron Oxides in the Laboratory: Preparation and Characterization, Weinheim, New York, VCH, 1991.

40. W. Xu, et al. Pressure-Induced Coordination Crossover in Magnetite; the Breakdown of the Verwey-Mott Localization Hypothesis in ERICE 2003. 2003.

41. Q. Song, Size and Shape Controlled Synthesis and Superparamagnetic Properties of Spinel Ferrites Nanocrystals, Georgia Institute of Technology, USA, 2005.

42. N. Poudyal, Synthesis and Characterization of Magnetic Nanoparticles, The University of Texas at Arlington, USA, 2005.

43. G. Salazar-Alvarez, Synthesis, Characterization and Applications of Iron Oxide Nanoparticles, KTH, Sweden, 2004.

44. M. L. Paramês, et al., PLD of Fe_3O_4 Thin Films: Influence of Background Gas on Surface Morphology and Magnetic Properties. Applied Surface Sciences, 2006. 252: p. 4610.

45. G. Q. Gong, et al., Magnetoresistance and magnetic properties of epitaxial magnetite thin films Physical Review B, 1997. 56(9): p. 5096-5099.

46. M. Ziese, et al., Magnetic and Magnetotransport Properties of Magnetite Films with Step Edges. Journal of Magnetism and Magnetic Materials, 2004. 279: p. 331-342.

47. J. M. De Teresa, et al., Magnetotransport Properties of Fe_3O_4 Thin Films for Applications in Spin Electronics. Microelectronic Engineering, 2007. 84: p. 1660-1664.

48. S. Sakka, Handbook of Sol-Gel Science and Technology; Processing, Characterization and Applications. Applications of Sol-Gel Technology. Vol. 3: Kluwer Academic Publishers, New York, Boston, Dordrecht, London, Moscow, 2005.

49. H. Kozuka, Handbook of Sol-Gel Science and Technology; Processing, Characterization and Applications. Sol-Gel Processing. Vol. 1: Kluwer Academic Publishers, New York, Boston, Dordrecht, London, Moscow, 2005.

50. E. J. A. Pope, S. Sakka, and L.C. Klein, Sol-Gel Science and Technology, The American Ceramic Society, Westerville, Ohio, 1995.

51. F. A. Yıldırım, PZT Films on Stainless Steel by Chemical Solution Deposition, M.S. Thesis, Supervisor Prof. Dr. Macit Özenbaş, Middle East Technical University, Turkey, 2002

52. Novel Materials from Solgel Chemistry, http://www.cmls.llnl.gov /?url=science_and_technology-chemistry-solgel_chemistry, "Last accessed date": January 2008

53. M. Izaki and O. Shinoura, Advanced Materials, 2001. 13(2): p. 142-145.

54. Ö. Kaya, Characterization of Titanium Dioxide Thin Films Prepared by Sol-Gel Processing, M.S. Thesis, Supervisor Prof. Dr. Macit Özenbaş, Middle East Technical University, Turkey, 2002.

55. D. E. Bornside, C. W. Macosko, and L.E. Scriven, On Modeling of Spin Coating, Journal of Imaging Technology, 1987. 13: p. 122-129.

56. E. İzgi, Characterization of Superconductiong Bi-Sr-Ca-Cu-O System Prepared by Sol-Gel Processing, M.S. Thesis, Supervisor Prof. Dr. Macit Özenbaş, Middle East Technical University, Turkey, 1996.

57. John. D. Wright and N.A.J.M. Sommerdijk, Sol-Gel Materials: Chemistry and Applications, Gordon and Breach Science Publishers, Amsterdam, 2001.

58. nonnewtonian.pdf, http://www.clarkson.edu/subramanian/ch301/notes/nonnewtonian.pdf, "Last accessed date": January 2008.

59. N. Uekawa and K. Kaneko, Journal of Materials Research, 1999. 14(5): p. 2002-2006.

60. D. Bersani, P. P. Lottici, and A. Montenero, Micro-Raman Investigation of Iron Oxide Films and Powders Produced by Sol-Gel Syntheses. Journal of Raman Spectroscopy, 1999. 30: p. 355-360.

61. G. M. da Costa, et al., Synthesis and Characterization of Some Iron Oxides by Sol-Gel Method. Journal of Solid State Chemistry, 1994. 113: p. 405-412.

62. Rheometric Ares Rheometer, http://felix.metsce.psu.edu/rheology/Research/ares.html , "Last accessed date": February 2008

63. S.-L. Chang, Thin-Film Characterization by Grazing Incidence X-ray Diffraction and Multiple Beam Interference. Journal of Physics and Chemistry of Solids, 2001. 62: p. 1765-1775.

64. M. S. Goorsky and B.K. Tanner, Grazing Incidence In-Plane Diffraction Measurement of In-Plane Mosaic with Microfocus X-ray Tubes. Crystal Research and Technology, 2002. 37(7): p. 645-653.

65. B. K. Tanner, et al., Grazing Incidence In-Plane X-ray Diffraction in the Laboratory. International Centre for Diffraction Data 2004, Advances in X-ray Analysis, 2004. 47.

66. H & M Analytical Services, I., Grazing Incidence Angle Thin Film Analysis, http://www.h-and-m-analytical.com/pdfs/grazing_incidence.pdf, "Last accessed date": January 2008.

67. D. B. Williams and C.B. Carter, Transmission Electron Microscopy: A Textbook for Materials Science 1996: Plenum Press, New York and London.

68. A. Karakuscu and M. Ozenbas, Characterization of Iron Oxide Thin Films Prepared by Sol-Gel Processing. Journal of Nanoscience and Nanotechnology, 2007. 8(2).

69. Research Interests, http://www.tau.ac.il/~gilgroup/research_interests.htm, "Last accessed date": January 2008.

70. N. Takahashi, et al., Characterization of Iron Oxide Thin Film Prepared by the Sol-Gel Method. Journal of Materials Science, 1991. 26: p. 497-504.

71. H. Liu, et al., Large Room-Temperature Spin-Dependent Tunneling Magnetoresistance in Polycrystalline Fe_3O_4 Films Applied Physics Letters, 2003. 83(17): p. 3531-3533.